
Of Resonances and Radicals – Hydrate Studies for Benchmarking

DISSERTATION

for the award of the degree

"Doctor rerum naturalium"

of the Georg-August-Universität Göttingen

within the doctoral program chemistry

of the Georg-August University School of Science (GAUSS)
as part of the BENCh Research Training Group (RTG 2455)

submitted by

TAIJA LENA FISCHER

from Braunschweig

Göttingen, 2023

Thesis Advisory Committee:

Prof. Dr. Martin A. Suhm, Institut für Physikalische Chemie,
Georg-August-Universität Göttingen

Prof. Dr. Jörg Behler, Center for Theoretical Chemistry,
Ruhr-Universität Bochum

Prof. Henrik Grum Kjærgaard, Department of Chemistry, University of
Copenhagen

Members of the Examination Board**Reviewer:**

Prof. Dr. Martin A. Suhm, Institut für Physikalische Chemie,
Georg-August-Universität Göttingen

Second Reviewer:

Prof. Dr. Jörg Behler, Center for Theoretical Chemistry,
Ruhr-Universität Bochum

Further Members of the Examination Board:

Jun.-Prof. Dr. Daniel Obenchain, Institut für Physikalische Chemie

Jun.-Prof. Dr. Anna Krawczuk, Institut für Anorganische Chemie

PD Dr. Oliver Bünermann, Institut für Physikalische Chemie

Dr. Tim Schäfer, Institut für Physikalische Chemie

Date of the Oral Examination: 02.06.2023

Acknowledgements

As I could not have achieved everything alone, I would like to thank a lot of people for their contributions. First, I want to thank my first supervisor Martin A. Suhm for his ideas, quick feedback, and the whole thesis committee for the fruitful discussions. I would like to thank my graduate school, BENCH (RTG 2455) for kick starting collaborations, funding my work and conference travels, as well as the PostDoc startup funding. I am also grateful that BENCH gave me the opportunity to organize a workshop in Berlin and Finn Kraft and Lukas Haseke for helping me.

Gratitude is also owed to my numerous collaborators without I would not have been able to achieve all the projects. I would like to especially thank my two students, Till Wagner and Margarethe Bödecker, who did not only work for and with me, but also were good company during the pandemic. I would also like to thank my predecessor, Hannes Gottschalk, for patiently introducing me to the topic and novel *gratin* jet setup. Elisa Brás, Martijn Tepaske and Robin Dohmen, with whom I had the chance to share my laboratory with. My colleagues, who helped me when I had questions and provided me a lot of feedback for my numerous talks.

I would also like to thank the team organizing the HyDRA blind challenge with me and all participating groups. Appreciation also belongs to my friends and family who supported me throughout my studies and PhD. Last but not least, I would like to thank the examination board and the DFG for funding and the chemistry workshops for their quick help with the experimental setup.

Abstract

Theory experiment benchmarks are a valuable tool to improve quantum numerical methods. To provide experimental data suitable for benchmarking, this work focuses on the investigation of jet cooled hydrate clusters using fourier transform infrared spectroscopy at a novel recycling setup. A universal resonance in ketone water complexes is reported for 10 systems, where the O-H stretching vibration of the bound water (OH_b) couples to the bending overtone and libration motion of the bridging H atom (b2lib). The first jet cooled spectra of the hydrate of the stable TEMPO ((2,2,6,6-tetramethylpiperidin-1-yl)oxyl) radical are measured and the first solvation steps are examined. The so called HyDRA (hydrate donor red shift anticipation) blind challenge, focusing on the OH shift of water when it binds to an organic compound, was launched and evaluated. As follow up project different benzaldehyde species were investigated. The published data alone reports 44 OH_b wavenumbers (OH and OD) of 25 different organic molecules, which will be provided to the community in a data base (all reported shifts are summarized in Tables 7.1 and 7.2 in Chapter 7).

Contents

1	Introduction	1
1.1	Interpretation of Experimental Data	3
1.1.1	Hydrate Spectra	3
1.1.2	Concentration Series	5
1.1.3	Determining Relative Intensities	7
2	Experimental Setup	9
2.1	<i>gratin</i> Jet Spectroscopy	9
2.2	Testing and Optimization	14
2.2.1	Explaining <i>NOTCH</i> and <i>RMSE</i>	14
2.2.2	Gas Pulses	15
2.2.3	Double Detection and Varying the Optics	18
2.2.4	Internal Detector Settings	22
2.2.5	Higher Resolution	27
2.2.6	Future Work	29
3	A Rather Universal Resonance	31
3.1	Theory - Energy Flow and Resonances	31
3.1.1	Theory Data Evaluation	32
3.2	Experimental Results	34
3.2.1	Outlook	45
4	Radicals	47
4.1	Investigation of Stable Radicals in the Gas Phase	47
4.1.1	Hydrates of TEMPO and TEMCO	47
4.1.2	Hydrates of DTBN and HMA	57
4.1.3	TEMPO-H + TEMPO Hydrogen Transfer	62
5	The HyDRA Blind Challenge	71
5.1	Implementation of the Blind Challenge	71

5.2	Experimental Results	76
5.2.1	Formaldehyde - BC02	77
5.2.2	Pyridine - BC16	80
5.2.3	2,2,2-Trifluoroacetophenone - BC18	82
5.2.4	Tetrahydrofuran - BC20	84
5.2.5	Cyclooctanone - BC22	86
5.2.6	1,3-Dimethyl-2-imidazolidinone - BC27	88
5.2.7	Tetrahydrothiophene - BC29	90
5.2.8	Methyl lactate - BC30	92
5.2.9	1-Phenylcyclohexane-cis-1,2-diol - BC36	95
5.2.10	2,2,2-Trifluoroethan-1-ol - BC38	97
5.2.11	Statistics	99
5.2.12	Summary and Outlook	100
6	Benzaldehyde Hydrates - an IR Study	103
6.1	Motivation	103
6.2	IR Investigation	104
6.2.1	Signal Integration	110
7	Summary and Outlook	111
8	Supplement	115
8.1	Energy Consumption <i>Gratin</i> Jet Spectroscopy Setup	115
8.2	Experimental Details	116
8.2.1	A Rather Universal Resonance	116
8.2.2	Radicals	117
8.3	Unpublished Hydrate Spectra	118
8.3.1	Additional Data on Acetophenone Hydrates	118
8.3.2	1,4-diazabicyclo[2.2.2]octane (DABCO) Hydrate	124
8.3.3	Cyclopentanone	125
8.3.4	Methyl 2-Hydroxyacetate Hydrate	132
8.3.5	<i>tert</i> -Butylalcohol Hydrate	134
8.3.6	2,2,4,4-Tetramethyl-3-pentanone Hydrate	137
8.4	Data Collected for the HyDRA Blind Challenge	139
	Literature	141

1 Introduction

Solvation processes are important in many fields and a better understanding is of interest for numerous reasons. Modeling hydration processes is difficult and challenging, as water provides some chemical specialties/exceptions due to its strong intermolecular interactions. Life on earth is highly dependent on water and most reactions in nature and our own body involve water and solvation processes[1]. In order to understand the complex mechanisms simulations and theory predictions become more and more important, but they share a problem. In many cases the values derived from novel computational methods are rather compared to the ones from more costly and/or already established methods instead of experimental values. This has two main reasons. On one hand it is easier to derive the same properties, on the other some properties cannot be determined experimentally as they are not accessible or the error is too high. For these reasons the BENCH Research Training Group (RTG2455) focuses on designing suitable experiments for benchmarking.

To provide experimental values which are comparable to theory, the same conditions need to be matched. For higher level calculation methods these are isolated molecules or small clusters at low temperatures. One way of obtaining these conditions experimentally are super sonic jet expansions. In this work the novel, so called *gratin* jet spectroscopy setup, is used. It is introduced in the first chapter and has the main advantage, that the expanded gas mixture can be reused, which lowers the substance consumption by at least one order of magnitude (and up to three orders of magnitude for favourable cases) allowing the usage of pricier chemicals and carrier gases. The recycling setup comes with the disadvantage, that water keeps accumulating inside during the measurements. The most probable reason for water impurities is the desorption of water from the walls of the setup.[2] This disadvantage was tackled by studying hydrate clusters.

As water and its fundamental OH stretching vibrations are sensible to its chemical environment, the shifts of the OH stretching vibration when forming a complex with an organic molecule can be used for benchmarking and assigning the structure of the complex.

One way of benchmarking theoretical predictions are so called blind challenges in which a prediction for a yet unknown property is requested and the experiment is conducted later on. Afterwards the experimental results are compared to the theory predictions. This might be the only way to get an unbiased theory prediction as a literature known experimental value is easier to match - but not necessarily for the right reason. Blind challenges are established in some fields like protein[3] and crystal structures[4], but not yet in vibrational spectroscopy. With this work, and the blind challenge presented, we want to start a series of blind challenges for vibrational shifts as they deserve an unbiased benchmark as well.[5–8] In a previous blind challenge organized in Göttingen in which the energy differences between the docking preferences of methanol to furan derivatives (oxygen lone pair or π system) were requested from theory groups, some experimental challenges were faced. One of them is that the requested property cannot be measured directly.[9, 10] This was changed in the presented follow up project in which the requested property is a vibrational shift. In Chapter 5 the process and experimental data of the so called HyDRA (Hydrate Donor Redshift Anticipation) is discussed.

1.1 Interpretation of Experimental Data

1.1.1 Hydrate Spectra

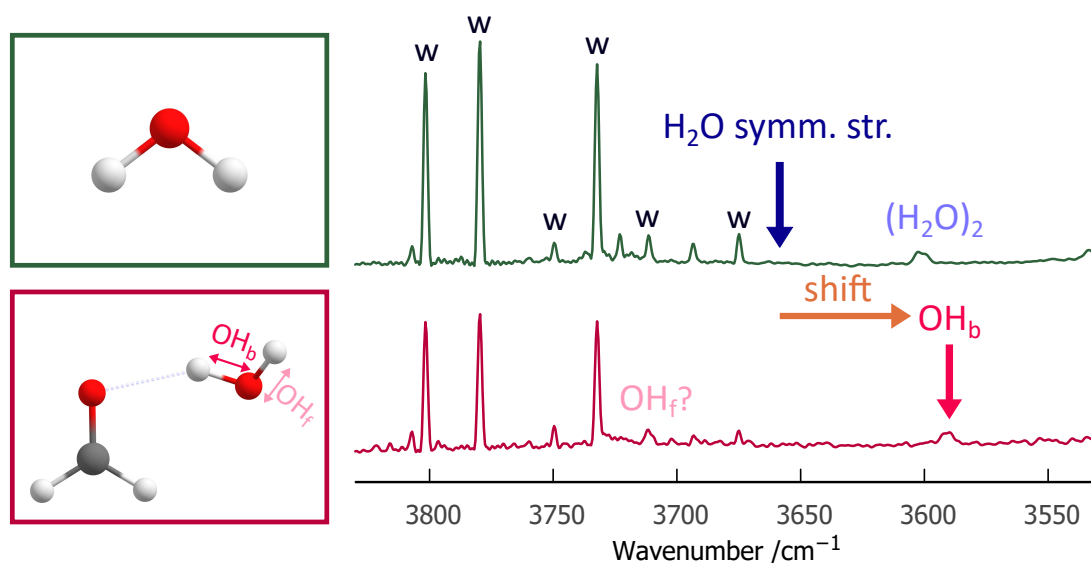


Fig. 1.1: On the left the molecular structures of water monomer and the water-formaldehyde minimum structure on B3LYP (BJD3) def-2 TZVP level of theory are depicted. On the right the FTIR spectra of water in neon (green, upper trace) and water with formaldehyde in helium (lower, dark red trace) are shown. Water monomer is labeled w, water dimer $(\text{H}_2\text{O})_2$, mixed dimers $\text{OH}_{b/f}$.

Before diving deeper into the topic, here a few words to the interpretation of hydrate spectra. In Figure 1.1 molecular structures obtained by B3LYP (BJD3) def-2 TZVP level of theory using ORCA 4.2.1 and FTIR (Fourier-transform infrared) spectra of water expanded in Ne and a mixture of formaldehyde and water in He are depicted. As commonly known water monomer has two stretching vibrations, a more IR active antisymmetric and a less IR active symmetric one. In the upper spectrum of pure water (green) water monomer signals are labeled with w and all visible w signals belong to rotational lines of the asymmetric stretching vibration. The three most dominant signals lie at 3732, 3780 and 3801 cm^{-1} and their rotational quantum numbers are given in table 1.1. The band center lies at 3756 cm^{-1} .^[11] The band center of the symmetric stretching vibration however, would be positioned at 3657 cm^{-1} (blue arrow in Fig. 1.1).^[11] When a second molecule, like formaldehyde or another water, is added, the water fundamentals shift and new signals become visible in the spectrum. The water homo dimer is visible in the upper spectrum and labelled $(\text{H}_2\text{O})_2$ (light blue). In the lower spectrum one can find new signals of mixed species. Here a distinction between OH stretching vibrations is made, the more strongly shifted vibration including the hydrogen forming the hydrogen bond is

Tab. 1.1: Rotational transitions of rovibrational excitation of the water OH stretching vibrations in the jet cooled spectrum.[12] The assigned spectral lines are divided into the three main signals at 3732, 3780 and 3802 cm^{-1} , and the minor, assigned signals. The letters in brackets indicate whether the corresponding transition can be assigned to the symmetric (s) or the antisymmetric (a) water stretching vibration.

$\tilde{\nu} / \text{cm}^{-1}$	J'	K'_a	K'_c	J''	K''_a	K''_c
main signals						
3732 (a)	0	0	0	1	0	1
3780 (a)	1	0	1	0	0	0
3801 (a)	2	0	2	1	0	1
minor signals						
3693 (s)	1	1	1	0	0	0
3750 (a)	1	1	1	1	1	0
3807 (a)	2	1	1	1	1	0

called OH_b . And the signal which is less shifted compared to the water monomer of the free hydrogen is called OH_f . In this work mostly OH_b and its corresponding shift from the symmetric stretching vibration is investigated (orange arrow).

1.1.2 Concentration Series

As the *gratin* spectroscopy setup does not include size selectivity for complexes another method to distinguish between different cluster sizes is applied - a concentration series. This method was for example used in [2] to confirm the position of water dimer and trimer as controversial results were published recently.[13] In Figure 1.2 three spectra with water expanded in Ne are shown in blue. The darker the blue shade, the higher the water concentration. The water cluster size $((\text{H}_2\text{O})_n)$ is labelled using $n = 2,3,4,5$. As different cluster sizes scale differently when more substance is added to the expansion, the cluster sizes can be distinguished by how they scale relative to each other. In Fig. 1.2 the water spectra are scaled to the homo dimer signal of the intermediate spectrum (m). A factor of 0.7 is needed for the spectrum with the highest concentration (h) and a factor of 1.8 for the spectrum with the lowest water concentration (l). To confirm the positions of water dimer the subtraction spectrum of the highest and lowest concentration spectrum is formed, first both are scaled in a way, that the trimer signal vanishes when subtracted (upper gray spectrum). And for the lower gray spectrum both are scaled in a way that the dimer signal vanishes. The scaling factors are given on top of the corresponding spectrum.

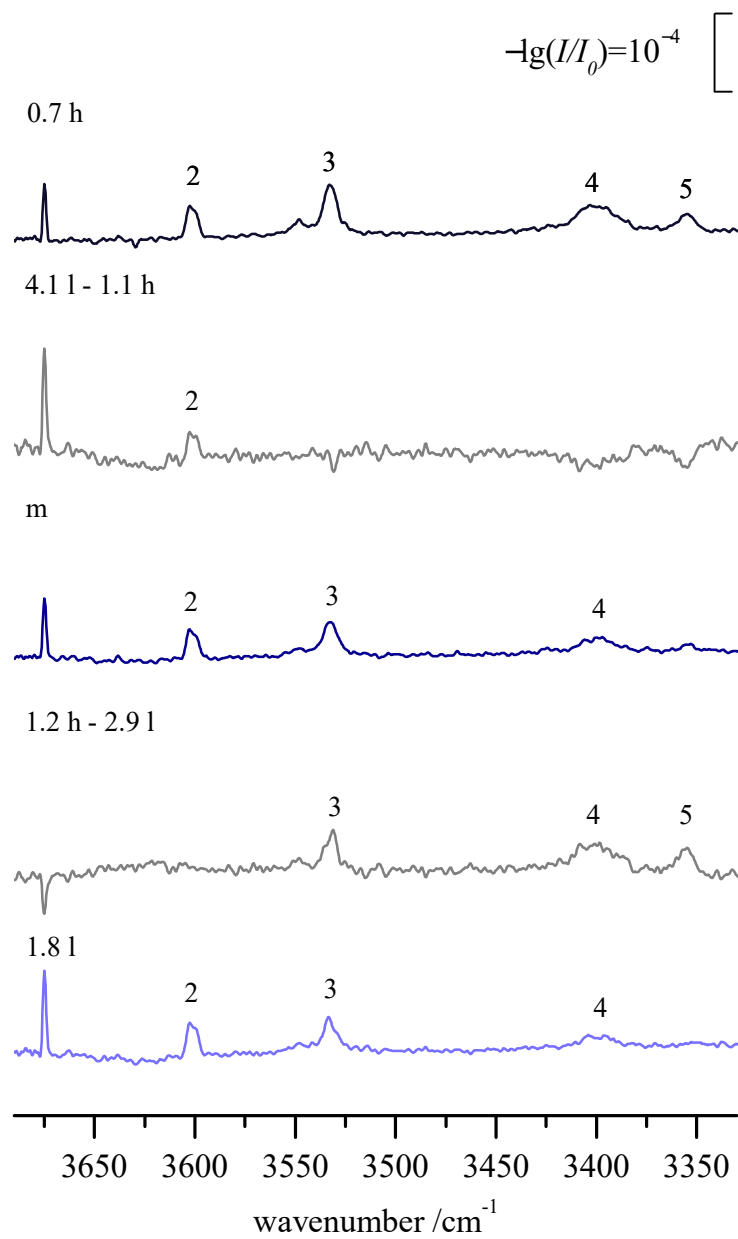


Fig. 1.2: FTIR spectra at different water concentrations expanded in neon (shades of blue) and subtraction spectra (gray). [2]

1.1.3 Determining Relative Intensities

In this work four different methods to obtain relative signal intensities were used. They are all briefly described and can also be found in the electronic supplement of [14].

Method A

In method A the median intensity between 3400–3600 cm^{-1} is determined and the height of the signals to the median is formed. The method only works for a wavenumber range in which only a small number of signals appear and a relatively straight baseline. The ratio between the two signal heights is called r .

Method B

A first order polynomial is fitted to the spectrum between 3400–3600 cm^{-1} as a baseline correction. Later a density function is applied whose maximum is considered as baseline. From this baseline the signal height is determined and an intensity ratio is formed. The density function is also used to estimate an error for the intensity ratio. A more detailed description can be found in the electronic supplement of [14].

Method C

In method C the absorbance spectra were evaluated using the built in integration method B of OPUS 7.8 (Bruker) in which wavenumber limits are picked and the area between these two points and the spectral line is integrated. The wavenumber limit is picked individually for each signal. Later the ratio of two areas is formed.

Method D

In method D a Julia package for uncertainty evaluation of numeric integrals NoisySignal-Integration.jl by Dr. N. Lüttschwager, which is introduced and used in [15] and can be found in [16]. It analyses the noise of an individually picked wavenumber range in the spectrum. This allows the script to simulate noise, which can be added to the spectrum. Additionally the signal position and a wavenumber range with a margin for variance can be given. The noise is added and the signal within the given margin is integrated n times. Later the integral distributions are regarded and the minimum and maximum integral

ratio using the 95% confidence interval is formed and taken as error margin. The value for r is then determined by taking the mean value of the error margin.

2 Experimental Setup

2.1 *gratin* Jet Spectroscopy

In this work FTIR (Fourier-transform infrared) spectroscopy is used to investigate solvation effects of small molecules. The obtained data can be used for benchmarking quantum numerical methods. The experiments for this work were mainly conducted using the novel recycling setup whose construction, planning and concept is described in more detail in [2, 18]. The working principle is comparable to [19] where a gas pulse is expanded through a slit nozzle with pre-expansion chamber into vacuum and molecular clusters are investigated in the resulting supersonic jet expansion using a FTIR spectrometer with a tungsten filament as light source. As the cluster concentration in the expansion is low, a long slit nozzle is used (700×0.2 mm) to create a long path in which the clusters can absorb light. Due to the nozzle size and the time of the gas pulse the method is rather substance consuming compared to other experimental setups. To address this issue the main idea for the novel setup was to recycle the gas mixture. Figure 2.1 shows the new experimental *gratin*-jet spectroscopy FTIR setup. *gratin* stands for *gas recycling atom-economic infrared*. It enables recycling of the gas mixture and lowers the substance consumption by at least one order of magnitude and up to three orders of magnitude in favourable cases [2, 18]. It allows the usage of pricier carrier gasses and isotopically labelled chemicals,[14, 20] but has the disadvantage of accumulating water impurities. In order to turn the water impurities into an advantage mainly water complexes were studied in this work.

During a measurement gas is expanded from the reservoir (0.2 m^3) through a $700 \times 0.2 \text{ mm}^2$ slit nozzle with pre-expansion chamber into the buffer volume (4 m^3). The clusters formed in the supersonic jet expansion are investigated using a BRUKER VERTEX 70V FTIR spectrometer and a liquid nitrogen cooled InSb/MCT sandwich detector. After the gas pulse the buffer volume is emptied by a series of roots pumps (PFEIFFER OKTA 500 and 2000) and the gas mixture is re-compressed and led back to the reservoir by a screw pump (BUSCH COBRA NS 0070 C).

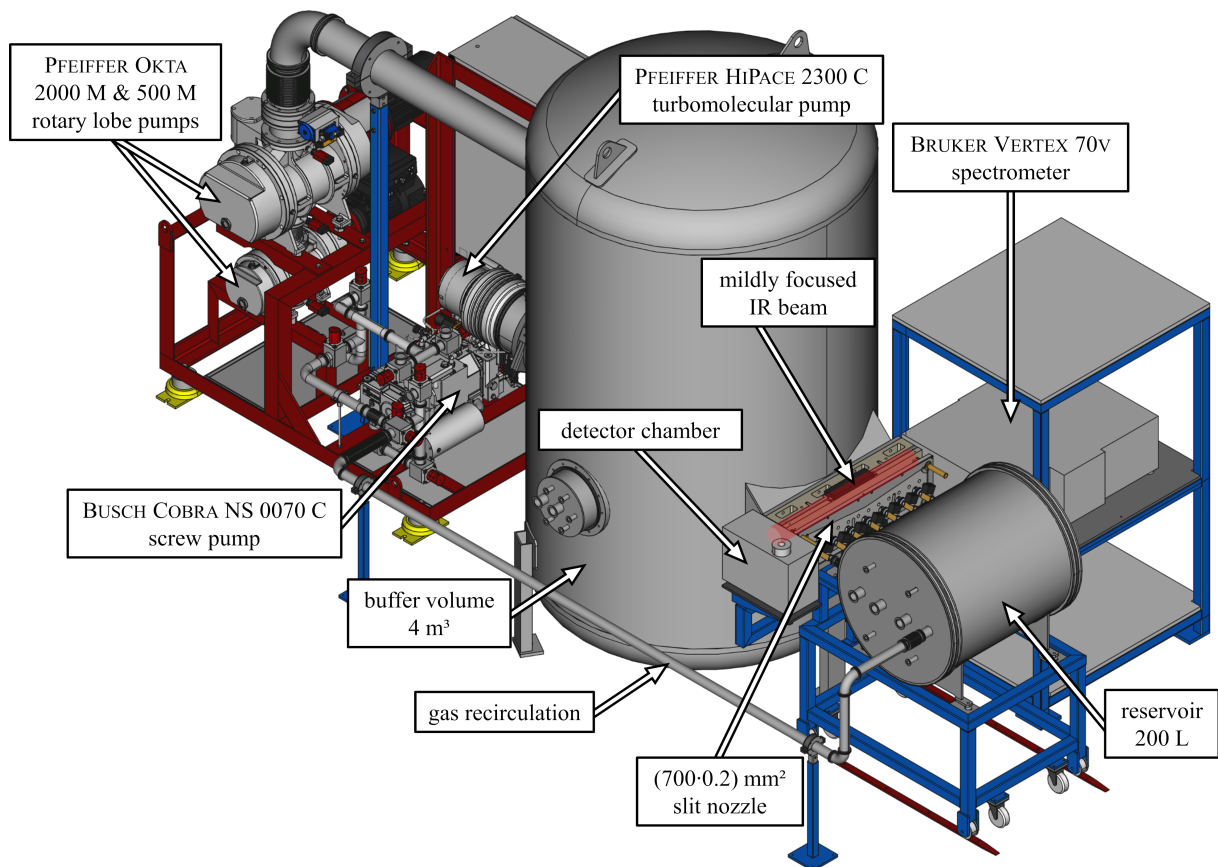


Fig. 2.1: The novel gas recycling IR spectroscopy setup. Gas is pulsed from the reservoir through a slit nozzle into the buffer volume, which is emptied by a series of roots pumps and led back to the reservoir using a screw pump. The supersonic expansion is investigated using a FTIR spectrometer and a sandwich detector. The figure is adapted from Ref. [17], licensed under CC BY 4.0 and was published in [2].

After the measurement, the setup can be emptied/evacuated using a PFEIFFER HIPACE 2300 C turbomolecular pump, with an ACP 40G as a dry pump. First a valve behind the screw pump needs to be closed in order to stop the gas flow back to the reservoir. Instead the gas mixture is lead to the exhaust. Then a bypass between the reservoir and buffer volume is opened cautiously to guide the remaining gas mixture from the reservoir to the exhaust by passing the buffer volume, to the roots pumps and the screw pump. When a certain pressure in the setup (buffer volume and reservoir) is reached, the screw pump is isolated from the system by closing valves towards the pump and opening a bypass, as it cannot be evacuated below 300 mbar on the high-pressure side. Then the turbomolecular pump and its dry pump are used to evacuate the system and the screw pump is flushed with helium three times for several seconds to remove remaining substances (5–10 s). After the roots pumps and the screw pump have been switched off, the screw pump is filled with helium to minimize leaking of air into the pump.

Another option to empty the setup is to close the valve behind the screw pump and use the dry pump of the turbomolecular pump to empty the reservoir. For that the dry pump is disconnected from the turbomolecular pump and can be connected to the reservoir to empty it. When a pressure of < 100 mbar in the reservoir is reached, the bypass between the reservoir and buffer volume can be opened and the remaining gas mixture is removed by the roots pumps and the screw pump. The remaining steps of isolating the screw pump and flushing it with helium remain the same.

Substance can be filled in by connecting the reservoir or buffer to a lock where Schlenk flasks with one substance each are attached. These can be opened successively starting with the less volatile substance which evaporates into the reservoir/buffer. The amount of substance is monitored using pressure gauges. Different gas bottles are also connected to the lock to add carrier gas to the gas mixture (usually neon and/or helium). As the maximum partial pressure of a substance that can be filled in the setup is limited by the corresponding vapor pressure, only sufficiently volatile compounds can be investigated.

The recycling concept already enabled studies using expensive isotopes and making expansions with pure neon and neon-helium mixtures more accessible in several studies that will be presented in the following chapters.

Unfortunately all spectra are showing traces of water, which drew the focus of this work on hydrate complexes. So far the main source of water has not fully been understood, but it is likely to be due to desorption of water from the walls of the setup. As the screw pump cannot be evacuated below 300 mbar it is the main suspect when it comes to traces of water. In order to tackle the problem a new pump ACP 40 CP is tested soon. Another limitation of the setup is that only volatile substances can be filled in. A possible project

Tab. 2.1: All available optical components and options of the *gratin* jet spectroscopy setup with the settings optimized for the OH- and CH-region by Hannes C. Gottschalk highlighted in magenta.[2, 18]

component/parameter	available options/values
light source	Globar (int.); tungsten filaments: 20 W (int.), 150 W (ext.)
beam splitter	broadband, KBr, CaF ₂
IR windows/lenses	KBr, CaF ₂
optical velocity / kHz	1.6, 2.5, 5, 7.5, 10, 20, 40, 60, 80, 120, 140, 160
max. resolution / cm ⁻¹	0.5
int. aperture / mm	0.25, 0.5, 1, 1.5, 2, 2.5, 3, 3.5, 4, 5, 6, 8
ext. aperture / mm	3, 3.5, 4, 6, 8, 10, 12, 14, 16, 18
detector	LN-InSb/MCT-SW, RT-DLaTGS (2x), InGaAs
filter mountings	∅25.4 mm, filter wheel (int.) & filter mounting (detector chamber)
acquisition modes	single sided, double sided

for the future is operating the setup consistently at higher temperatures and with less volatile compounds, as most parts of the setup are equipped with a heatable coat by HORST GMBH ($T_{\max}=370$ K) and the nozzle can also be heated. This has not yet been tested in a measurement, but the heatable coat is used for soft bake outs ($T=350$ K).

The spectrometer and detector chamber are evacuated using a EDWARDS NXDS dry pump. All optical components are listed in 2.1 and are depicted in figure 2.2. Hannes C. Gottschalk reported in his thesis that the settings marked in magenta in table 2.1 are best suited for measurements of the OH- and CH-region using the new *gratin* jet spectroscopy setup.[18]

Further, a spectral resolution of 2 cm^{-1} was found to be the best compromise in measurement time and resolution and a value for $t_{\text{delay}}=146$ ms and $t_{\text{on}}=133$ ms seemed to give the best synchronization of the spectrometer recording and the gas pulse (see figure 2.3 and chapter 2.2.2 for further details).

In addition to the options listed in table 2.1, the LN-InSb/MCT-SW detector preamplifier can be tuned by applying different resistors. In this way the output signal can be adjusted to the light intensity as KBr and CaF₂ are absorbing light more or less strongly at certain wavelengths.

Figure 2.2 shows the light path in the *gratin* jet spectroscopy setup. Normally the external light source (150 W tungsten filament) and the external detector (d3) are used, but the spectrometer also provides two internal light sources (20 W tungsten filament and globar) and two internal detectors (d1 and d2).

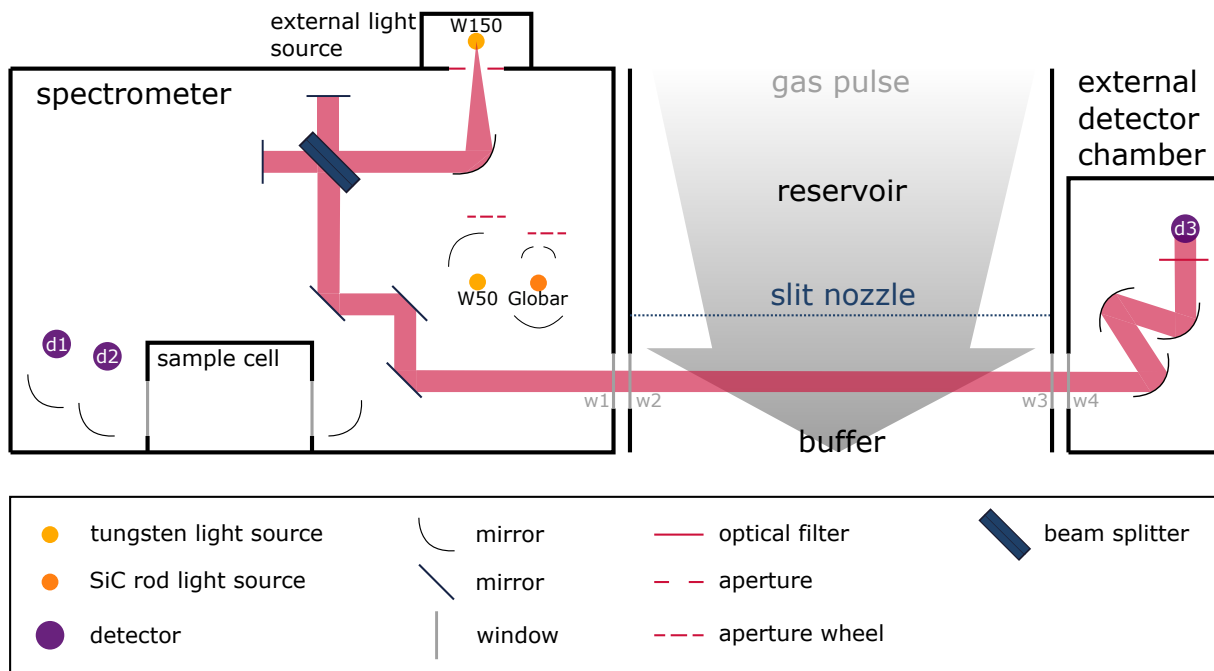


Fig. 2.2: Light path and optical components of the *gratin* jet spectroscopy setup. As default the external 150 W tungsten light source, the external InSb/MCT sandwich detector (d3) CaF₂ windows and the CaF₂ beam splitter are used.

More details on the *gratin* jet spectroscopy setup can be found in [2, 18] and a table with the energy consumption of individual components of the setup can be found in the Supplement (Chapter 8.1).

2.2 Testing and Optimization

2.2.1 Explaining *NOTCH* and *RMSE*

In order to compare different optical settings two methods were applied. The so-called *NOTCH*, “**Noise Test Challenge**”, in which background and sample spectra of the empty light path are recorded for one minute each and later on converted into a null absorbance spectrum. These *NOTCH*-spectra can further be analyzed by running an analysis of the *RMSE*, “**roote mean square error**”, of a quadratic fit of the baseline in a 50 cm^{-1} window.[21] The negative decadic logarithm of the *RMSE* can be used to evaluate the spectral quality, the higher the $-\log(RMSE)$ the lower the noise-level. As indicated in figure 2.2 the light passes a gap between the spectrometer and the nozzle, as well as between the nozzle and the external detector chamber, which is why atmospheric water and carbon dioxide are visible in the *NOTCH* spectra and the $-\log(RMSE)$ has a lower value in the OH stretching region of water (approximately $4000\text{--}3000\text{ cm}^{-1}$), the asymmetric stretching of CO_2 ($2450\text{--}2400\text{ cm}^{-1}$) and the water bending motion ($1900\text{--}1600\text{ cm}^{-1}$).

2.2.2 Gas Pulses

The synchronization of the gas pulse and the spectrometer settings during a measurement are shown in figure 2.3 and start with the signal of the mirror movement (t_{TTL} , orange) from the spectrometer. It is used as a trigger for the pulse generator and t_{delay} , which is set at the pulse generator, is started. After t_{delay} the magnetic valves are opened for the time t_{on} and the gas mixture is expanded into the buffer. It should be longer than the time the spectrometer is recording data t_{TKDA} to make sure the supersonic jet expansion has evolved until then and does not stop before t_{TTL} has finished. At the same time it should be as short as possible to keep the time the buffer volume needs to be emptied before the next gas pulse as short as possible. As there is a small gap between the time the spectrometer is recording data and the time the mirrors are moving (approximately 5 ms), the time starting with t_{TKDA} and ending with t_{TTL} is called t_{scan} . The time between t_{on} and t_{TKDA} starting is called t_{pre} and the time between t_{TTL} and t_{on} finishing is called t_{post} .

In order to test the usage of neon as carrier gas, instead of/as addition to helium, some tests regarding the pulse optimization were performed. In figure 2.4 the recorded spectra of a variety of different time settings, which are fully given in Table 2.2, of 2 mbar water in 500 mbar Ne are shown. For the spectra the KBr beam splitter and KBr windows, the 150 W tungsten light source with a 12 mm aperture and the InSb/MCT sandwich detector with filter F20 ($\tilde{\nu} \leq 4000 \text{ cm}^{-1}$), a resolution of 2 cm^{-1} and a scanning velocity of 140 Hz in double sided mode were used. In the figure water monomer is labeled w, water dimer D, water trimer T, water tetramer Q and water pentamer P.[22–28]

In [18] it is proposed, that using the single sided acquisition mode is beneficial due to the center burst occurring earlier in time which make it easier to recognize the gas pulse and the recording of the data by the spectrometer being asynchronous. In the double sided acquisition mode the negative t_{pre} values do not show artifacts until $t_{\text{pre}} = -55 \text{ ms}$ (red). In the pink ($t_{\text{pre}} = -35 \text{ ms}$) and light pink ($t_{\text{pre}} = -5 \text{ ms}$) spectrum only the signal intensities decrease. Nonetheless testing the settings later used in the experiment is also beneficial. This way an optimum of the desired cluster size can be addressed more easily. In most of the studies in this work dimers are the cluster size of interest, while higher clusters are less favored. The difference in the spectra with positive t_{pre} values are minor, but if one would have had the time and more scans would have been recorded the optimization could have been taken further. From the 50 scans recorded the second last spectrum ($t_{\text{pre}} = 55 \text{ ms}$) seems to show the sharpest dimer signal and could be used as starting point for further optimization steps. As a standard a $t_{\text{pre}} = 25 \text{ ms}$ is used (best

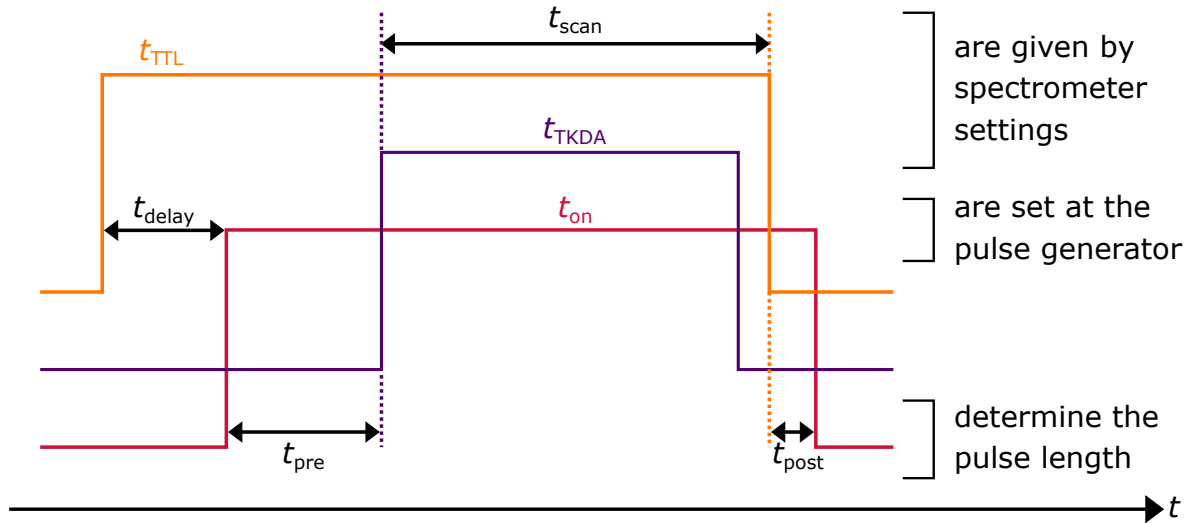


Fig. 2.3: Synchronization of the gas pulse and the scan of the spectrometer. t_{TTL} (orange, total time of mirror movement), t_{TKDA} (violet, time spectrometer is recording data, “take data”), t_{delay} (time that is waited after t_{TTL} starts before the magnetic valves are addressed/opened), t_{on} (red, time the magnetic valves are open), t_{pre} (time after t_{on} started and t_{TKDA} starts), t_{post} (time between t_{TTL} and t_{on} ending). Image adapted from [18].

Tab. 2.2: Time settings used for the pulse optimization for 500 mbar Ne gas pulse expanding 2 mbar water as a test substance.

measurement	a	b	c	d	e	f	g
t_{delay} /ms	106	126	146	166	186	206	226
t_{on} /ms	173	153	133	113	93	73	53
t_{pre} /ms	65	55	25	5	-5	-35	-55
t_{scan} /ms	105.5	105.5	105.5	105.5	105.5	105.5	105.5
t_{post} /ms	3	3	3	3	3	3	3

settings for 750 mbar He pulses).

When working without some of the pumps or with another carrier gas or stagnation pressure, the time between two scans needs to be adjusted. For that a description can be found in the safety folder in the laboratory and in the *gratin* folder of the group network drive.

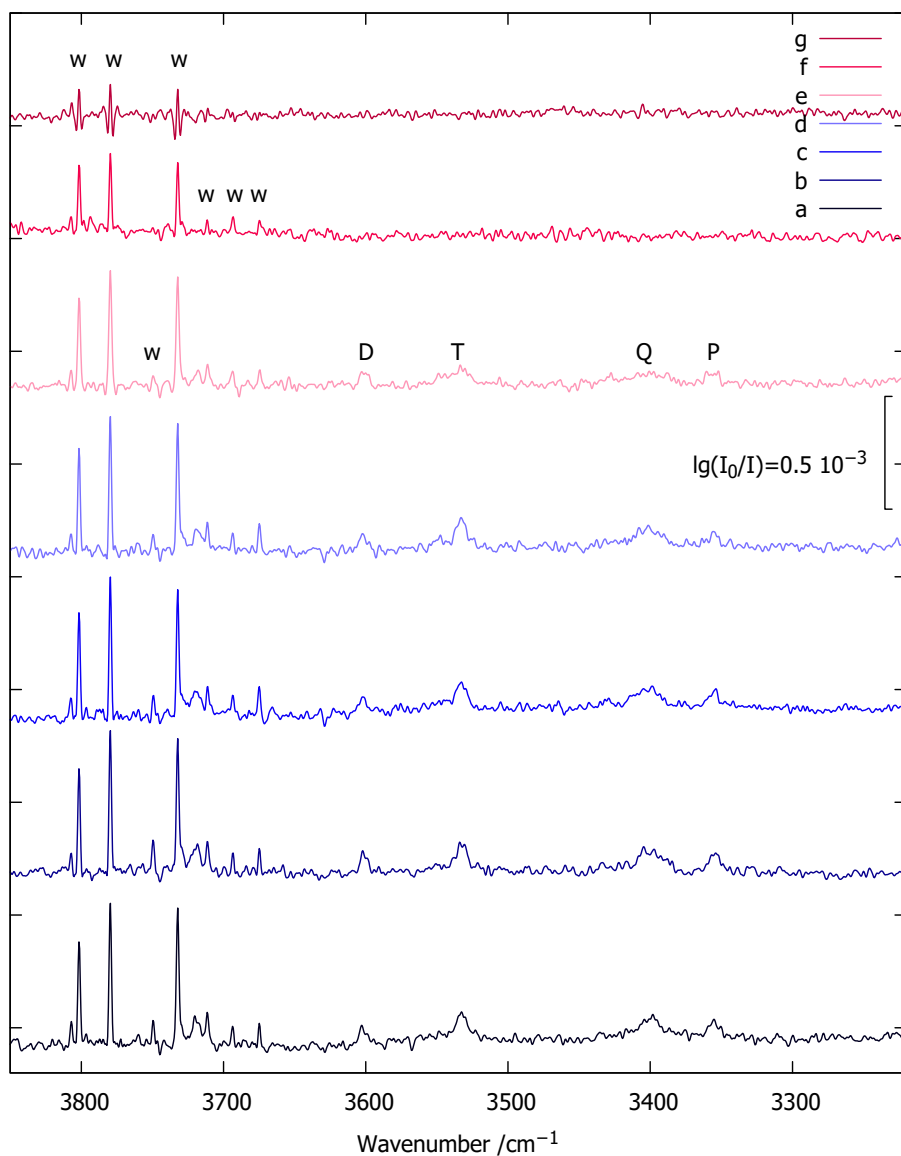


Fig. 2.4: Gas pulse optimization for 500 mbar neon. For the spectra 2 mbar water in 500 mbar neon were expanded and 50 scans were averaged. w labels water monomer, D dimers, T trimers, Q tetramers and P pentamers. Assignment taken from [22–28]. A similar figure for 750 mbar helium can be found in [2].

2.2.3 Double Detection and Varying the Optics

During the time of my PhD several tests with optics at the new *gratin* jet spectroscopy setup were performed. In order to test the double detection mode of the InSb/MCT sandwich detector, the CaF₂ beam splitter and windows (see figure 2.2 w1–4) were changed to KBr, which is absorbing less light in the MCT region (CaF₂: 4000–1250 cm⁻¹, KBr: 4000–500 cm⁻¹).

To test the double detection mode five *NOTCH* spectra were recorded and averaged and the $-\log(RMSE)$ was determined. For the test the external 150 W tungsten light source and filter F20 were used. The results are shown in Figure 2.5, the InSb-region is depicted in red and the MCT-region in blue. The upper panel shows the spectra and the lower panel the $-\log(RMSE)$. If impurities of atmospheric H₂O and CO₂ are neglected, the InSb-region has on average a higher $-\log(RMSE)$ and a lower noise level than the MCT-region.

To compare the performance of the double detection mode to the sole use of the InSb-region, again the average of five *NOTCH* spectra was formed (upper panel figure 2.6) and the $-\log(RMSE)$ determined (lower panel figure 2.6). The InSb-region using the double detection mode is shown in red and the single mode in orange. While the baseline of the orange spectrum shows a slope and a broad ice signal (3500–3000 cm⁻¹) the red curve has a straighter baseline. When the $-\log(RMSE)$ in areas without atmospheric H₂O or CO₂ are regarded, the performance between 3000–2500 cm⁻¹ behaves similarly, while for wavenumber < 2300 cm⁻¹ the double detection mode seems advantageous (higher $-\log(RMSE)$ value on average).

As figure 2.5 and 2.6 show, the double detection mode can be used for investigating molecular clusters with no loss in quality for the InSb-region where most of the signals of interest for this work are lying. So the additional data could be recorded as a new standard. Unfortunately, the software for the spectrometer, OPUS 7.8, is storing the different spectra as different data blocks (data block types) and channels. The InSb-stretching region is stored as channel 2, while the MCT-region is stored as channel 1. For channel 1 the data can be treated with all available tools, while some options are not available for channel 2. For example, to apply the *NOTCH* macro to determine the $-\log(RMSE)$ value of the InSb detector region, to compare the MCT and InSb detector regions, one needs to copy the recorded spectrum, click in the box of the measurement in OPUS labeled “2 CHN” and go to “Datei” “Datenblock-Typ ändern” and select “AB” as “Neuer Blocktyp”. This way the MCT spectrum, the block called “AB” earlier, is gone. Evaluating data this way is cumbersome and not suited for a large amount of data as an everyday-measurement.

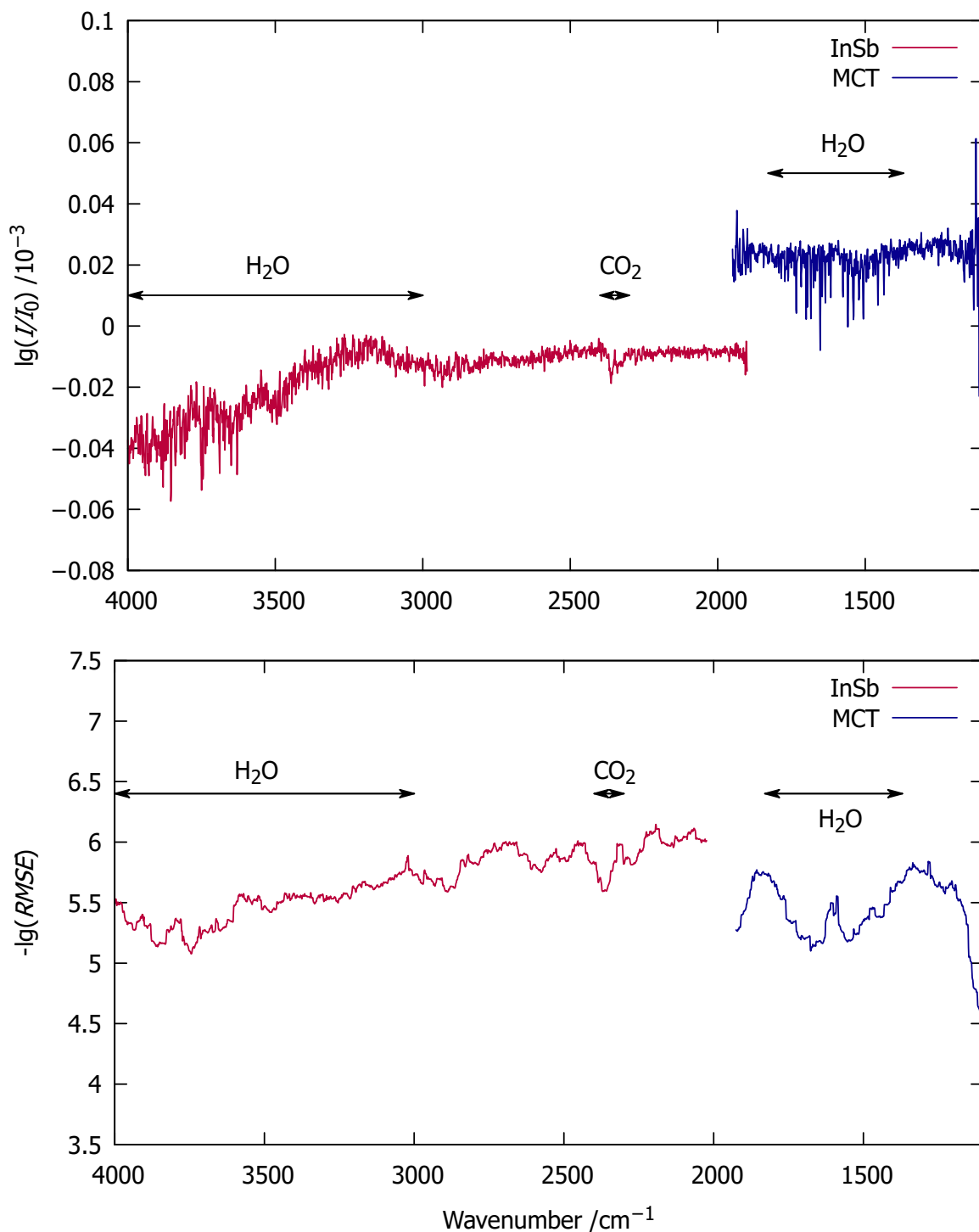


Fig. 2.5: The upper panel shows an average of 5 recorded *NOTCH* spectra of InSb (red) and MCT region (blue) and the lower panel the corresponding $-\log(\text{RMSE})$ values. A KBr beam splitter and KBr windows, a 150 W tungsten filament light source and resistance of $(0.47+51) \text{ k}\Omega$ at the detector were used.

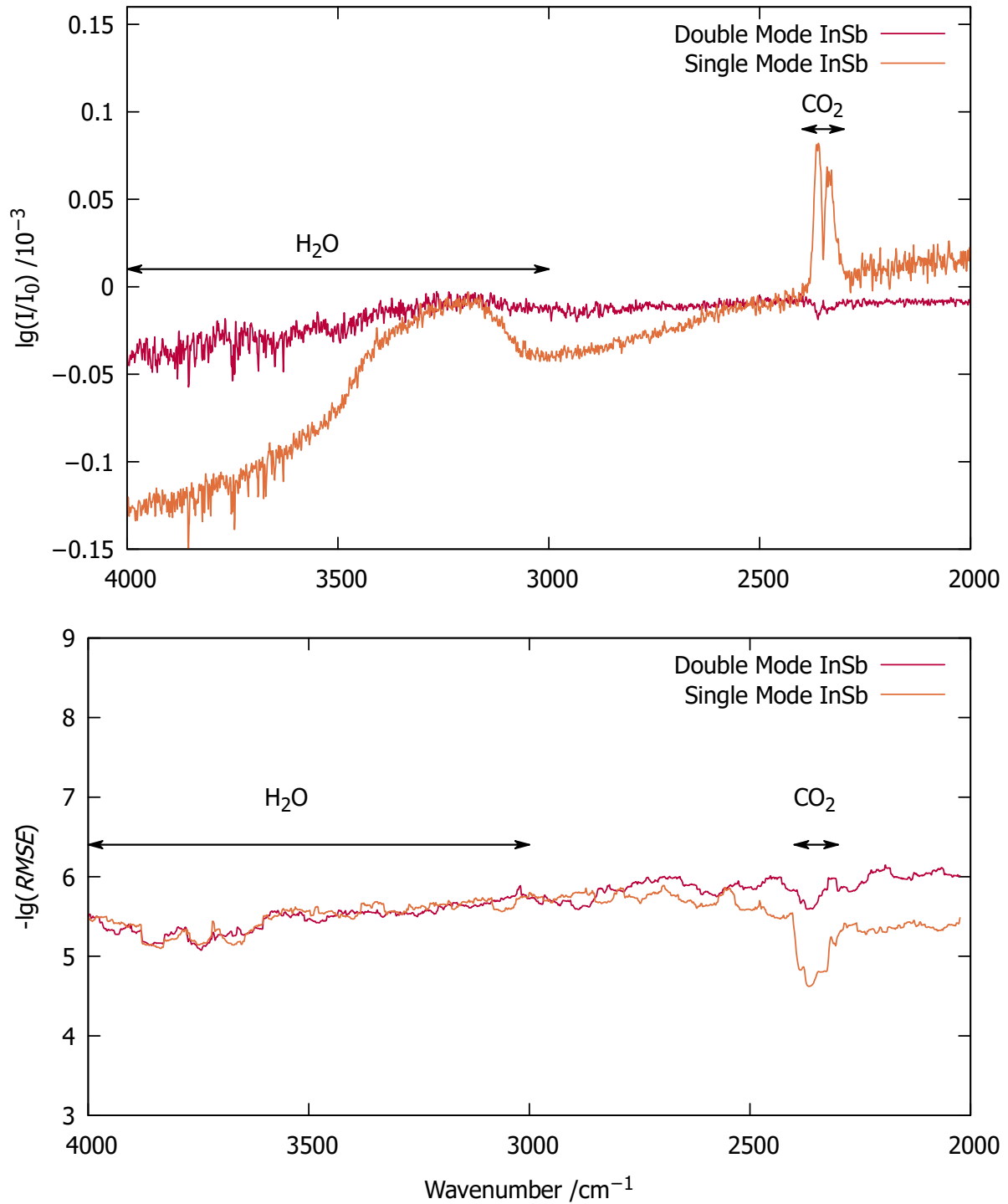


Fig. 2.6: Upper panel shows an average of 5 recorded *NOTCH* spectra of InSb region in single detection (orange) and double detection mode (red) and the lower panel the corresponding $-\log(RMSE)$ values. The spectra were recorded using a KBr windows and a KBr beam splitter, a 150 W tungsten filament as light source and a resistance of $(0.47+51) \text{ k}\Omega$.

Efforts to link the InSb detector to channel 1 and the MCT detector to channel 2 have not been successful yet. For this reason the double detection mode is not used as default.

2.2.4 Internal Detector Settings

To further tune the signal to noise ratio (S/N ratio) for the double detection mode, different detector and optical settings were tested. The software to run the spectrometer, OPUS, offers some internal detector settings, which are listed in table 2.3. For testing the options the settings of the sample and reference were kept identical, as picking different detector options does not seem reasonable. In Figure 2.7 the amplification options are varied and the pre-amplification options are kept at the default “Ref”. For the optics the double detection mode with the internal SiC rod light source (Globar in Figure 2.2), an aperture size of 6 mm of the internal apertures and resistors at the detector with (0.47+51) k Ω are used. Two slots for resistors can be modified at the detector, the numbers in brackets are giving the strengths of the individual resistors used. In the upper panel the average of 4 *NOTCH* spectra is depicted and the InSb- and MCT-region are plotted. In the lower panel the corresponding $-\log(RMSE)$ is shown. When evaluating the $-\log(RMSE)$ in the regions with no substance impurities, the different settings in OPUS do not make a large difference. The same test was performed for the pre-amplification settings, they were varied while the amplification settings were kept at the default (“Automatic”). The results are shown in figure 2.8, in the upper panel and average of 5 *NOTCH* spectra was formed, in the lower panel the corresponding $-\log(RMSE)$ is depicted. Again no large difference between the settings is visible. As a conclusion the default settings were kept.

As the overall spectral quality in measurements of the InSb-region seemed to be lowered by the usage of the KBr beam splitter and window, and double-detection was not found to be practical, the optics were changed back to CaF₂ (windows and beam splitter). While switching back the optics *NOTCH* spectra of different settings were recorded. The results are shown in Figure 2.9, for each spectrum 3 *NOTCH* spectra were averaged. As a first step a reference with KBr optics was recorded (orange). In a next step the settings were kept the same unless the windows and the beam splitter were changed to CaF₂ (red). Because of the intensity at the detector being at the limit to saturation, the resistors were changed from (0.47+51) k Ω to (0.56+51) k Ω (green). In the lower panel in the region between 3000 and 2500 cm⁻¹ the $-\log(RMSE)$ of the green curve is on average slightly above the other curves, indicating a lower noise level. The settings of the green curves were used as standard measurement settings in the following.

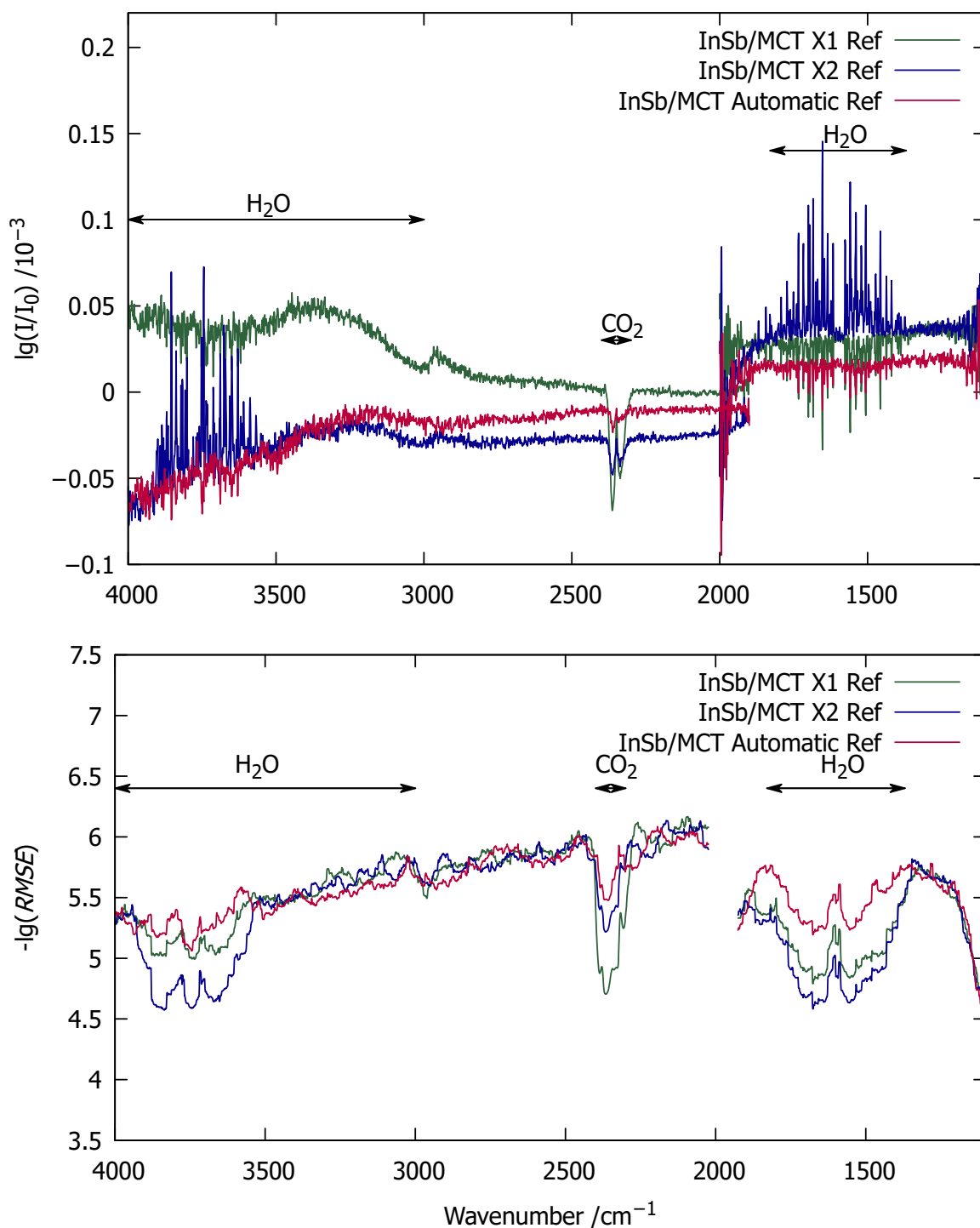


Fig. 2.7: Upper panel shows an average of 4 recorded *NOTCH* spectra of the InSb- and MCT-region in double detection mode using different OPUS detector settings for the amplification with KBr beam splitter and mirrors, the SiC rod light source, an aperture size of 6 mm and a resistor at the InSb sandwich detector of $(0.47+51) \text{ k}\Omega$. The lower panel shows the corresponding $-\log(\text{RMSE})$ values.

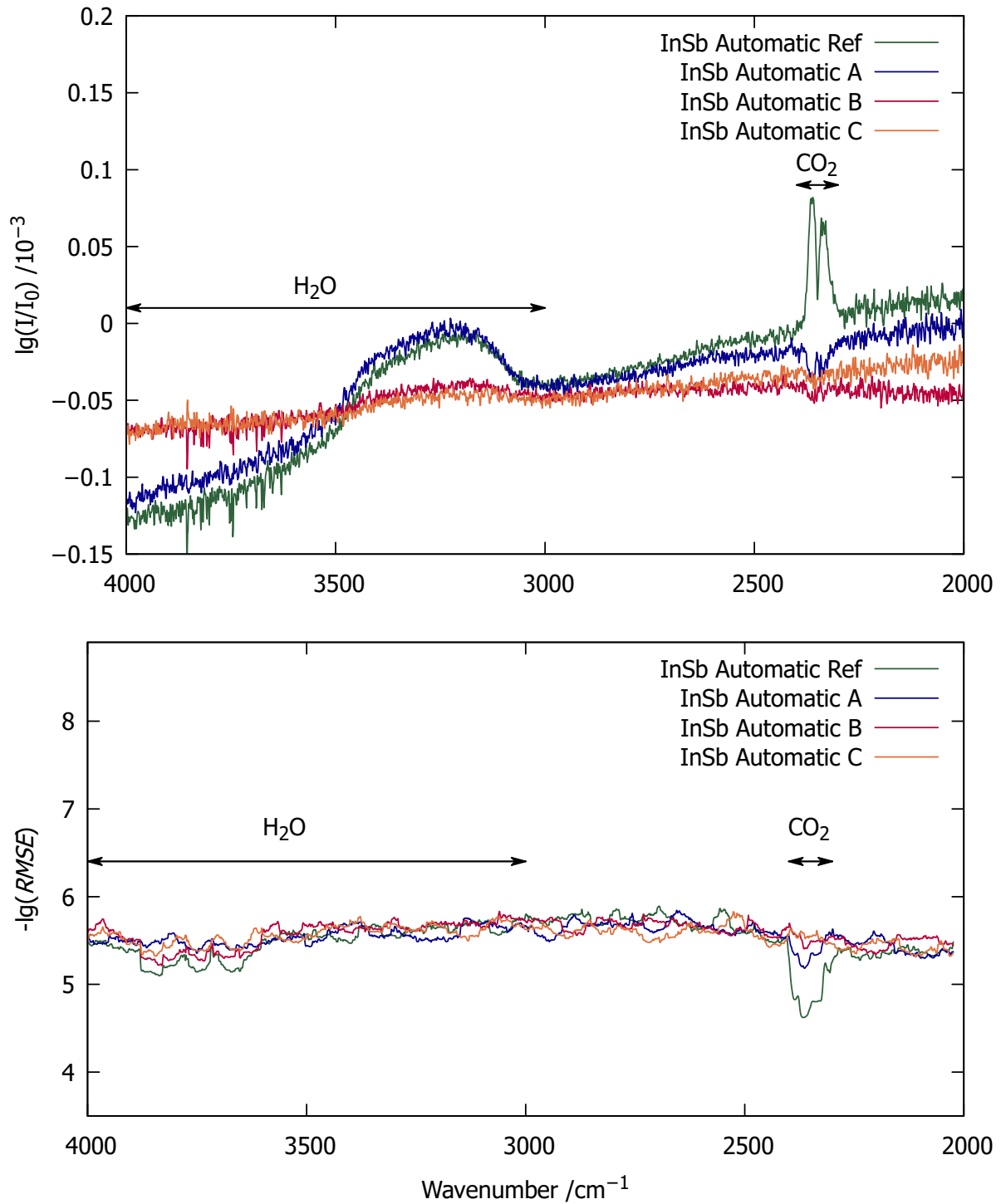


Fig. 2.8: Upper panel shows an average of 5 recorded *NOTCH* spectra of the InSb region in single detection mode using different OPUS detector settings for the pre-amplification. The KBr beam splitter, KBr mirrors double detection mode, the 150 W tungsten filament light source, an aperture size of 6 mm and a resistor at the InSb sandwich detector of $(0.47+51) \text{ k}\Omega$ were used. The lower panel shows the corresponding $-\log(\text{RMSE})$ values.

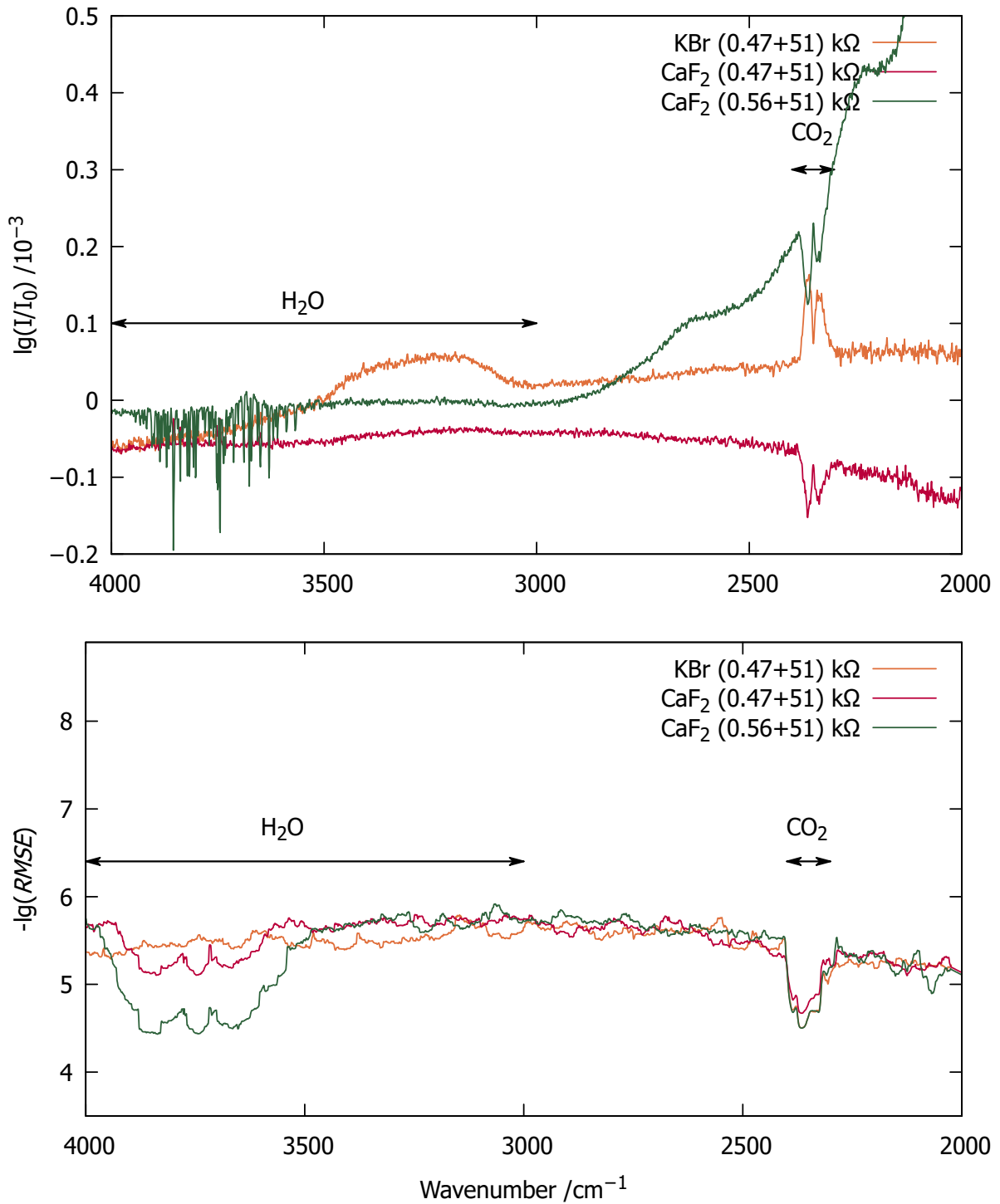


Fig. 2.9: Upper panel shows an average of 3 recorded *NOTCH* spectra of the InSb region in single detection mode using the same OPUS detector settings (Automatic, Ref) and the 150 W tungsten filament light source, but different beam splitters (KBr orange, CaF₂ red and green) and different resistors at the detector for the CaF₂ beam splitter. The lower panel shows the corresponding $-\lg(\text{RMSE})$ values.

Tab. 2.3: Internal OPUS detector setting options.

	amplification of	pre-amplification
“Probe” (sample)	Automatic, X1, X2	Ref, A, B, C
“Referenz” (reference)	Automatic, X1, X2	Ref, A, B, C

2.2.5 Higher Resolution

This work was performed together with Margarethe Bödecker during her bachelor thesis. A chapter with similar figures can be found in [29]. The BRUKER VERTEX 70V has the option available to measure at a higher resolution (1 cm^{-1}). As the length of the scan t_{scan} is longer as for the resolution used as standard (2 cm^{-1}), the gas pulse needed to be adapted. An oscilloscope was used to determine the time of the mirror movement (t_{TTL}) of the spectrometer and its scans time (t_{TKDA}). The time between the start of the scan and the end of the mirror movement is called t_{scan} . When setting the length of the gas pulse, the time of the magnetic valves opening (t_{on}) should be set a bit earlier than t_{scan} for the supersonic expansion to form before the spectrometer starts recording. As a last step the time between the start of the mirror movement (t_{TTL}), which is used as a trigger for the gas pulsing process, and t_{on} (t_{delay}) has to be determined. A $t_{\text{delay}} = 247 \text{ ms}$ and $t_{\text{on}} = 233 \text{ ms}$ was found to be the best suited option for the measurement. As a next step the waiting time between the gas pulses needed to be adjusted as the gas pulse needed to be longer than for a measurement with a resolution of 2 cm^{-1} ($t_{\text{on}} = 133 \text{ ms}$). A waiting time of 3+5 s in OPUS was best suited for a measurement with neon with a stagnation pressure of 400 mbar. For cyclooctanone + water, which was a system investigated for the HyDRA blind challenge, this option was tested because the signal assignment was more challenging. As the signal assignment is discussed in chapter 5.2.5, the focus lies on the spectral quality. The spectra are shown in Figure 2.10. In the upper panel the water monomer signals are labeled w, the hetero dimer signals OH_x and the signals of the eight-membered ring as CH. For the blue spectrum a resolution of 2 cm^{-1} is used and 500 scans were recorded. If the resolution is switched to 1 cm^{-1} (red spectrum) the noise level gets worse as depicted in the lower panel which shows the corresponding $-\log(\text{RMSE})$ value. To obtain a $-\log(\text{RMSE})$ as for the lower resolution, approximately 2400 scans are needed.

As the higher resolution requires a longer gas pulse and therefore a longer waiting time between the gas pulses to empty the buffer and almost five times as many scans as for a measurement with a resolution of 2 cm^{-1} , the use of higher resolution is not recommended for a standard measurement.

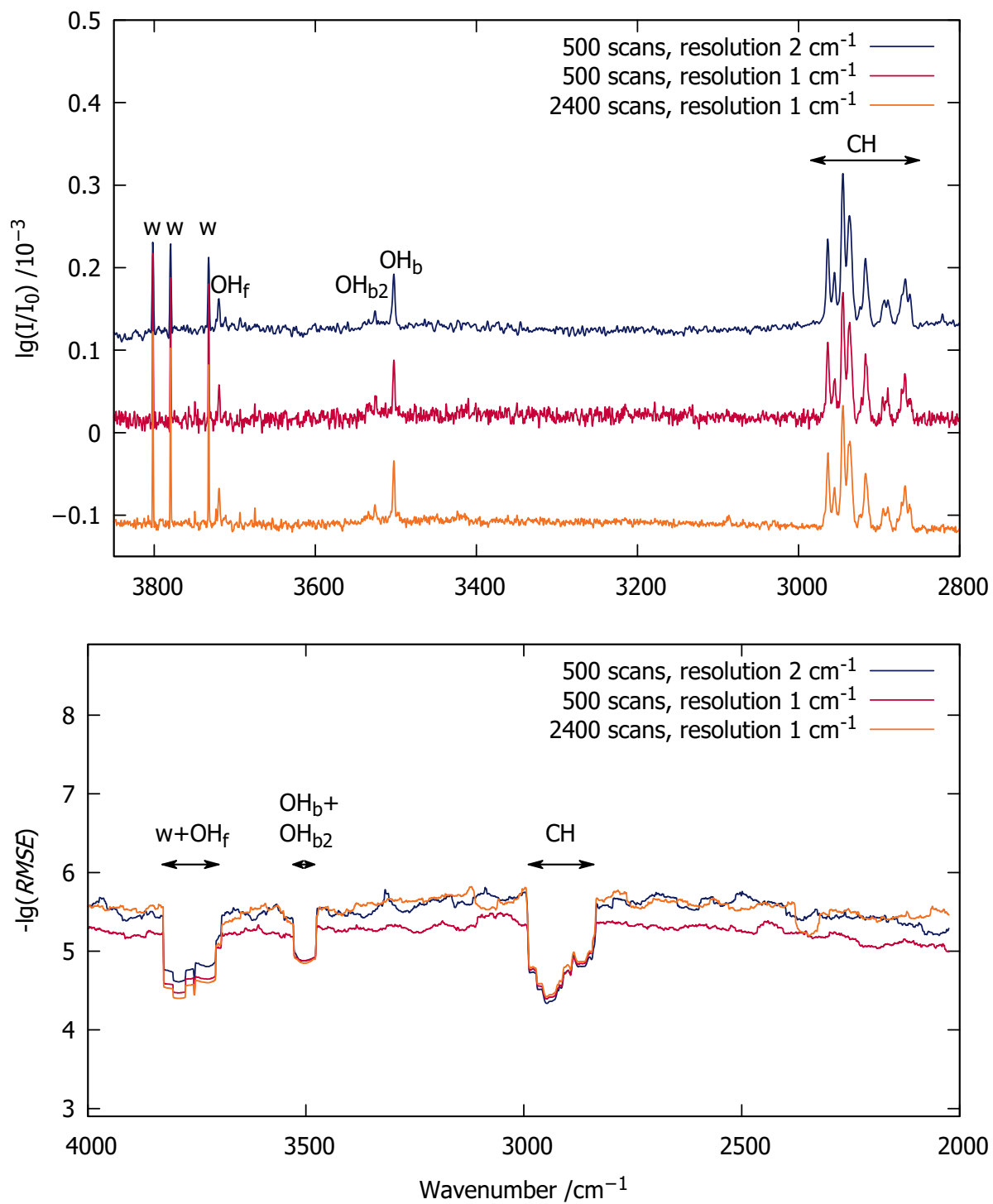


Fig. 2.10: Upper panel shows the FTIR spectrum of cyclooctanone and water expanded in 400 mbar neon using different resolutions and number of scans. The lower panel shows the corresponding $-\lg(\text{RMSE})$ value.

2.2.6 Future Work

When the *gratin* jet spectroscopy setup was planned even more applications were envisioned which have not been tested yet due to time issues. For example the nozzle is heatable, which would allow to measure less volatile compounds and to investigate conformers higher in energy. In order to avoid condensation all cold spots at the jet have to be found first.

Another option which has not yet been tested in detail is the usage of the gas cycling without some of the pumps and/or with lower stagnation pressures allowing to investigate warmer expansions.

One could also test if the stagnation pressure available (up to 1 bar) is high enough to obtain nano matrices when using a suitable carrier gas (Ne, Ar, N₂). One signal of N,N-dimethylformamide with water might be due to a complex with Ne.

To further improve the experimental setup it would be an idea to link the pressure in the buffer volume to the signal of starting the next gas pulse. First attempts by Hannes C. Gottschalk and me have not been successful.

The probably largest improvement possible is to lower the amount of water in the experimental setup or getting completely rid of the water traces. It would make measurements with more than one substance easier as the gas mixture would not have to be changed every n scans and would enable the investigation of more reactive substances which are sensitive to water. A first attempt using an ACP 40 CP, which can be evacuated, instead of the BUSCH COBRA NS 0070. First test are planned in 2023.

3 A Rather Universal Resonance

This chapter is largely based on the corresponding publication [14]. The results and especially my own contributions are shown and extended by new, yet unpublished data. In [14] an unknown resonance in water ketone complexes is investigated and characterized using FTIR spectroscopy and isotope substitution on the experimental side and a harmonic approach on B3LYP-D3(BJ)/def2-TZVP level on the theoretical side. It is found to be a resonance between the OH_b stretching vibration of the water and a combination of the bending overtone (b2) of water and the libration motion (lib) of the H atom involved in the hydrogen bond between water and the ketone.

3.1 Theory - Energy Flow and Resonances

Generally spoken energy can flow within a molecule or a molecular network. This also holds true for aqueous solutions in which the energy transfer is interesting due to a manifold of different mechanisms.[30–33] Here the energy flows between two solvent molecules is considered slow compared to energy transfer within one molecule. [34] One can differentiate between two types of coupling in aqueous solutions. Type I involves vibrations of water and intermolecular modes generated by the solute interaction. Vibrationally excited water molecules can transfer energy to their environment. The large number of different modes makes it unlikely that only one energy dissipation pattern exists and so far no universal pattern is known. (Here we report one way of type I energy dissipation.) Type II would include solvent and solute vibrations at the same time and have not yet been reported clearly, but it may contribute to fast energy flow in strong hydrogen bonds.[35–37] When it comes to energy flow between two nearly degenerate energy states within one molecule Fermi and Darling-Dennison resonances play an important role.[38, 39] The resonating states can be tuned by varying the chemical environment.[34, 40] For example the OH stretching vibration of water ($\tilde{\nu}(\text{OH}_b)$ in Figure 3.1) can couple with another state close in energy ($\tilde{\nu}(\text{b2lib})$ in Figure 3.1). This way a dark state ($\tilde{\nu}(\text{b2lib})$ in Figure 3.1) can gain intensity from a bright state by coupling. The two new resulting

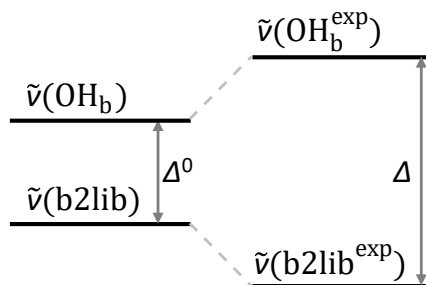


Fig. 3.1: Schematic sketch of coupling energy levels.

states ($\tilde{\nu}(\text{OH}_b^{\text{exp}})$ and $\tilde{\nu}(\text{b2lib}^{\text{exp}})$) are both visible in the spectrum and are shifted compared to the original energy levels. The intensity ratio of the resulting states depends on the energy difference between them (Δ^0) and the effective coupling element W_{ij} .

One can differentiate between different types of resonances depending on the number and the type of involved vibrations. The most famous ones in vibrational spectroscopy are Fermi resonances which occur between a fundamental and an accidentally degenerate overtone of another fundamental.[41, 42]

3.1.1 Theory Data Evaluation

In this study a higher order resonance including the bending overtone of water (b2) and the libration motion (lib) of the bound hydrogen atom in water ketone complexes, which is coupling to the OH stretching fundamental of water, is characterized.

As the latter spectra show, the combination band b2lib is gaining intensity from the OH_b fundamental. In order to calculate the original signal position of both bands, some formula and assumptions are needed. The intensity I of a signal in the spectrum depends on the concentration of a compound A (c_A) and the corresponding absorption cross-section σ_A (Equation 3.1).

$$I_A = c_A \cdot \sigma_A \quad (3.1)$$

It is assumed that b2lib has no own intensity and all intensity comes from OH_b^0 (Equation 3.2).

$$I_{\text{OH}_b^0} = I_{\text{OH}_b} + I_{\text{b2lib}} \quad (3.2)$$

Considering a two state model with W_{ij} as coupling matrix element the unperturbed signal positions of OH_b and b2lib can be determined using the Equations 3.3 and 3.4.

$$\tilde{\nu}(\text{OH}_b^0) = \frac{I_{\text{OH}_b} \cdot \tilde{\nu}(\text{OH}_b^{\text{exp}}) + I_{\text{b2lib}} \cdot \tilde{\nu}(\text{b2lib}^{\text{exp}})}{I_{\text{OH}_b} + I_{\text{b2lib}}} \quad (3.3)$$

$$\tilde{\nu}(\text{b2lib}^0) = \frac{I_{\text{b2lib}} \cdot \tilde{\nu}(\text{OH}_b^{\text{exp}}) + I_{\text{OH}_b} \cdot \tilde{\nu}(\text{b2lib}^{\text{exp}})}{I_{\text{OH}_b} + I_{\text{b2lib}}} \quad (3.4)$$

According to [43] W_{ij} can be calculated using Equation 3.5, where $\Delta\tilde{\nu}_{ij}$ is the wavenumber difference between the two resonating states ($\tilde{\nu}(\text{OH}_b^{\text{exp}})$, $\tilde{\nu}(\text{b2lib}^{\text{exp}})$) and r is the intensity ratio between the two.

$$W_{ij} = \Delta\tilde{\nu}_{ij} \sqrt{\frac{r}{(r+1)^2}} \quad (3.5)$$

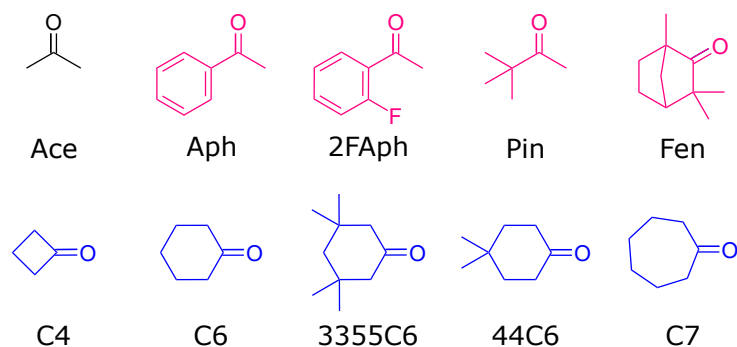


Fig. 3.2: Lewis structures of all studied ketones with the code used in this work. The purity, vendor and CAS number can be found in Table 3.1.

3.2 Experimental Results

The spectral FTIR data of ten ketone water complexes were obtained using the *gratin* jet spectroscopy setup (see 2.1 for more details) using helium as carrier gas, an average of # gas pulses with a stagnation pressure of 750 mbar, 28 s waiting time between the gas pulses, an InSb/HgCdTe sandwich detector and optical filters (F20: $< 4000\text{ cm}^{-1}$, F13: $2500\text{--}4100\text{ cm}^{-1}$), CaF_2 optics, a 150 W tungsten filament as light source with an Bruker VERTEX 70v FTIR spectrometer at 140 kHz scanning speed in double sided mode.

All ketones whose hydrates have been studied in this publication [14] are shown in Figure 3.2. The color indicates if the ketone ($\text{R}^1\text{-(C=O)-R}^2$) is symmetric ($\text{R}^1=\text{R}^2$ blue) or asymmetric ($\text{R}^1 \neq \text{R}^2$ pink). Acetone is shown in black, as it is the smallest investigated compound and serves as model system for isotope substitution experiments. The purity, vendors and abbreviations for the compounds used can be found in Table 3.1. Further details on the number of scans used for the spectra, the date the spectra were recorded and the used filter can be found in Table 8.2.

In the study we observed an energy flow of type I from the excited OH stretching vibration to a combination band of the water bending overtone (b2) and the libration motion of the bound hydrogen atom (lib). The atomic sequence of the water binding to the ketone $\text{H-O-H}\cdots\text{O}$ gives a good idea that the excitation of the middle O-H bond, the energy can dissipate to both sides giving a reasonable Darling-Dennison 1–3 coupling scenario.[44, 45] The contribution of lower frequency modes is credible as well as they play an important role when it comes to coupling in for instance water dimer.[46]

Here we reported the occurrence of a stable resonance over 10 keto hydrates and propose it to be applicable for other functional groups as well,[47] as discussed at the end of the

Tab. 3.1: List of substances, their abbreviations, CAS number, the supplier and purity.[14]

Name	Code	CAS No	Supplier	Purity
Acetone	Ace	67-64-1	Merck	99%
Acetone-2- ¹³ C	13CAce	3881-06-9	Sigma-Aldrich	99%, 99% atom ¹³ C
Acetone-D ₆	D6Ace	666-52-4	Sigma-Aldrich	99.9%, 99.9% atom D
Acetophenone	Aph	98-86-2	Sigma-Aldrich	99%
Cyclobutanone	C4	1191-95-3	Fluorochem	98% + 0.1% BHT as stabilizer
Cycloheptanone	C7	502-42-1	Sigma-Aldrich	99%
Cyclohexanone	C6	108-94-1	Sigma-Aldrich	99.8%
4,4-Dimethylcyclohexanone	44C6	4255-62-3	BLDpharm	98%
(-)-Fenchone	Fen	7787-20-4	Alfa Aesar	98%
2-Fluoroacetophenone	2FAph	445-27-2	Sigma-Aldrich	97%
Helium	He	7440-59-7	Linde	99.996%
Pinacolone	Pin	75-97-8	Alfa Aesar	97%
3,3,5,5-Tetramethylcyclohexanone	3355C6	14376-79-5	Sigma-Aldrich	98%
Water- ¹⁸ O	18OHH	14314-42-2	Sigma-Aldrich	97%, 97% atom ¹⁸ O

chapter. Experimental data on not yet published compounds that might show a b2lib resonance can be found in the Supplement 8.3.

The coupling matrix element W_{ij} was determined using Equation 3.5 and amounts approximately 10 cm^{-1} which indicates a slower energy dissipation than in neat water but a faster one compared to other 1–3 Darling-Dennison resonances.

The symmetric stretching vibration of water monomer is not visible in our IR spectra, but lies at 3657 cm^{-1} . [11] Whenever it is shifted towards 3500 cm^{-1} it can couple with the b2lib dark state generating two signals slightly shifted compared to the original band positions of the OH stretching band and the dark state (bending overtone: 3200 cm^{-1} , libration: 300 cm^{-1}) as schematically depicted in Figure 3.3.

Figure 3.4 shows the hydrate FTIR spectra of the ten investigated ketones respectively, 2-fluoroacetophenone, acetophenone, acetone, pinacolone, cyclohexanone, fenchone, 4,4-dimethylcyclohexanone, 3,3,5,5-tetramethylcyclohexanone and cycloheptanone, sorted by their OH_b shifts. Water monomer signals are labeled w and are marked with a gray line, the hetero dimer signals are labeled OH_f and OH_b as introduced in Section 1.1.1. Some asymmetric ketones show an additional signal for the side of the ketone not involved in a resonance that is labeled OH'_b (further information on carbonyl scales: [48]). In these

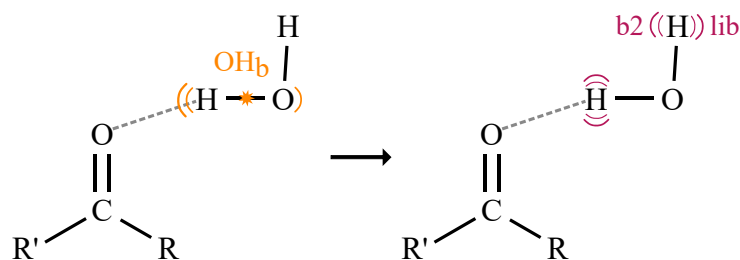


Fig. 3.3: Energy flow of the excited OH_b stretching vibration to the bending overtone of water (b2) and the libration motion of the hydrogen atom forming the H-bond (lib). Reprinted with permission from Fischer 2021[14]. Copyright 2021 American Chemical Society.

cases the resonating side is marked with a star in the Lewis structure. Close to 3500 cm^{-1} , the b2lib resonance appears as additional signal. To have a more uniform depiction some spectra are scaled by the factor of 2 (marked on right). The estimated amount of water is given as percentage in the expansion on the left. Using Equations 3.3 and 3.4, the original signal positions were calculated using the experimental signal positions and intensities. The experimental wavenumbers ($\tilde{\nu}(\text{OH}_f^{\text{exp}})$, $\tilde{\nu}(\text{OH}'_b^{\text{exp}})$, $\tilde{\nu}(\text{OH}_b^{\text{exp}})$, $\tilde{\nu}(\text{b2lib}^{\text{exp}})$) and deperturbed values ($\tilde{\nu}(\text{OH}_b^0)$, $\tilde{\nu}(\text{b2lib}^0)$) can be found in table 3.2. The deperturbed signal positions are given as black arrows in Figure 3.4. Above the arrows the value for $2W_{ij}$ is given, which was calculated using Equation 3.5. The intensity ratio was determined using all four methods described in Section 1.1.3. The determined values are given in Table 3.3. To uniformly obtain a r value below one the value lower in intensity is always divided by the value with higher intensity. In the first column it is indicated if the signal with a higher (h) or lower (l) wavenumber is divided or used as numerator. In the end an average ratio \bar{r} is formed to calculate W_{ij} . The average ratio and the corresponding coupling constant can also be found in table 3.2.

The minimum separation between the two resonating states amounts $2W_{ij}$ and lies between 14 and 20 cm^{-1} in the spectra. The smallest separation is found for 3355C6 and the largest for Ace. C6 shows an almost 1:1 distribution between the OH_b and b2lib signal.

After showing the universality of the resonance in ketone complexes, the next goal was to determine the involved vibrations. For that acetone was taken as model system as it is small, symmetric and commercially available in different isotope variants. In Figure 3.5 the FTIR spectra of acetone with water, deuterated acetone with water, ^{13}C labeled acetone with water and acetone with ^{18}O water are depicted respectively using He as carrier gas. As for Figure 3.4 the water monomer signals are labeled w and the OH stretching vibrations of the hetero dimer OH_x . In addition the value for $2W_{ij}$ and the arrows showing the deperturbed signal positions are given. When comparing the FTIR spectra of regular acetone (dark green) and deuterated acetone (green) with water the

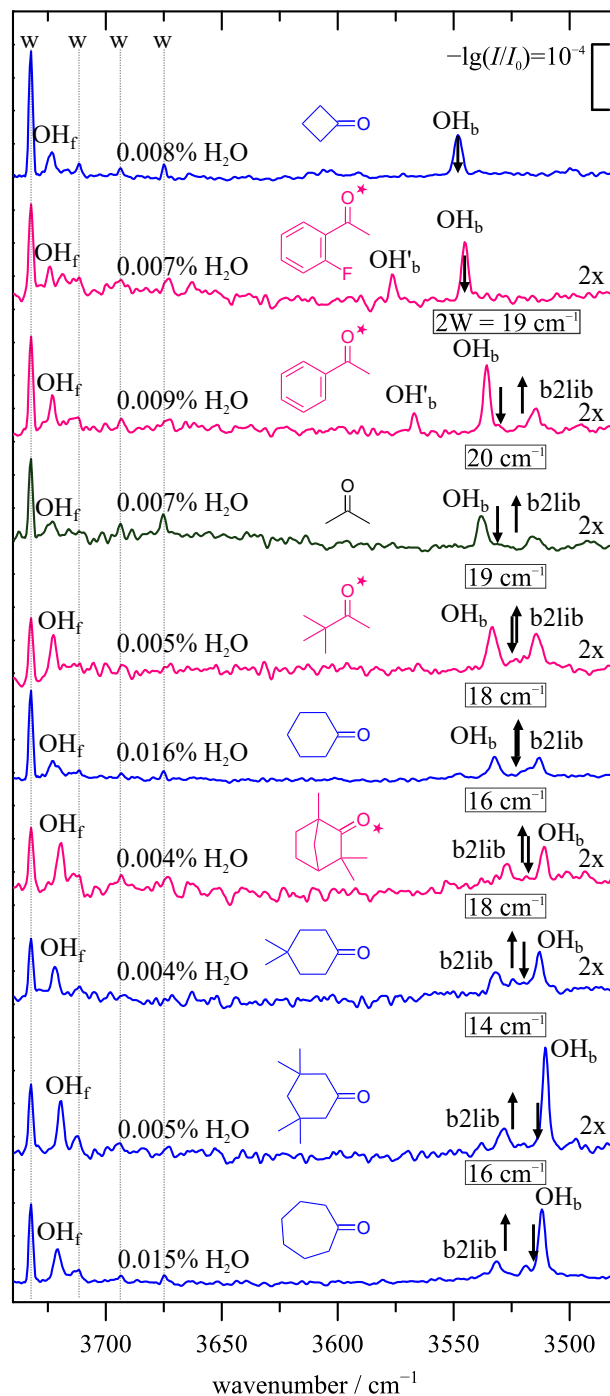


Fig. 3.4: FTIR spectra of all investigated compounds. The water monomer signals are labeled w, the hetero dimer signals OH_b/OH_f and the resonance b2lib. The deperturbed signal positions are given as black arrows and $2W_{ij}$ on top of them if a coupling is taking place. The estimated water concentration is given on the left side and the scaling factor for some spectra on the right. Reprinted with permission from Fischer 2021[14]. Copyright 2021 American Chemical Society.

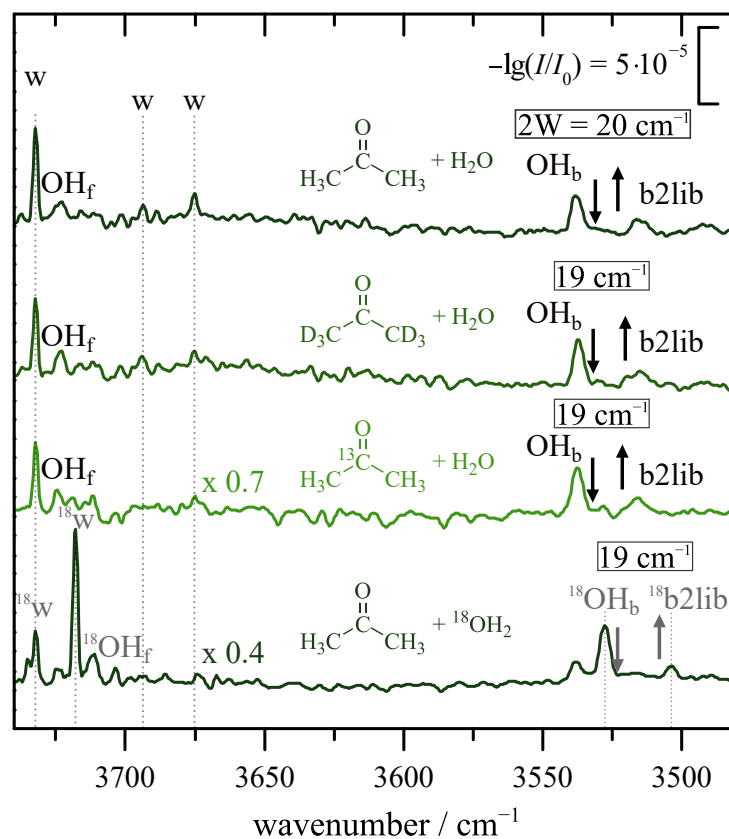


Fig. 3.5: FTIR spectrum of isotopically substituted acetone (D, ^{13}C) and acetone with water and ^{18}O . Again the water monomers are labeled w and the hetero dimer signals OH_x . The deperturbed signals are given as black arrows and the W_{ij} value above them. Reprinted with permission from Fischer 2021[14]. Copyright 2021 American Chemical Society.

Tab. 3.2: Experimental signal positions, the intensity ratios and calculated, unperturbed signal positions for Figures 3.4 and 3.5. All values except the intensity ratio r are given in cm^{-1} . [14]

Code	OH_f^{exp}	OH_b^{exp}	OH_b^{exp}	$\text{b2lib}^{\text{exp}}$	r	OH_b^0	b2lib^0	W_{ij}
C4	3724	-	3548	-	-	3548.00	-	-
2FAph	3734	3576	3545	-	-	3545.00	-	-
Aph	3723	3567	3536	3514	0.38	3529.79	3520.31	9.54
Ace	3723	-	3538	3516	0.47	3531.01	3522.99	10.24
Pin	3723	-	3533	3514	0.80	3524.92	3522.78	9.49
C6	3723	-	3532	3514	0.89	3523.07	3522.03	9.03
Fen	3720	-	3511	3527	0.72	3517.72	3520.28	7.90
44C6	3722	-	3513	3532	0.57	3519.79	3524.91	8.99
3355C6	3719	-	3510	3528	0.24	3513.72	3524.58	6.99
C7	3721	-	3512	3532	0.24	3515.56	3527.74	7.74
D6Ace	3723	-	3537	3515	0.31	3531.91	3520.19	9.37
13CAce	3725	-	3537	3516	0.34	3532.03	3521.37	9.28
Ace with 18OHH	3712	-	3528	3504	0.23	3523.05	3508.05	9.43

signal positions of OH_b and b2lib do not change, ruling out the CH vibrations to be involved in the resonance. This would have been rather surprising as the resonance occurs in many different ketones with a variety of structures, but with the new *gratin* jet setup the tests were affordable. When moving to acetone in which the central carbon atom is substituted with ^{13}C , again no changes in the signal positions were visible. This is interesting, because the C=O stretching vibration would be available in all ketones and the C=O stretching overtone would lie in the expected spectral range when coupling to the water bending mode. Also coupling between C=O and O-H stretching was reported in [36] for acetone and postulated for *N*-phenylformamide in [35]. As a next step ^{18}O water was used (bottom spectrum) and both signals OH_b and b2lib shift by approximately 10 cm^{-1} . So the criteria for the vibrations involved in the resonance were:

- must be water vibrations
- oxygen weight increase shifts resonance by 10 cm^{-1}
- universal over all molecular systems

As a next step a search for water vibrations with the named criteria began and the local minimum structures for all molecular systems were obtained by Till Wagner using CREST [49, 50] at the GFN2-xTB level of theory [51, 52]. The structures were later optimized with ri-B97-3c/def2-mTZVP level of theory [53] and finally optimized using marij-B3LYP-D3(BJ)/def2-TZVP level of theory [54–58] in TURBOMOLE 7.4.[59, 60] More details on

Tab. 3.3: Experimental intensity ratios r for the resonance doublets of ketone-water complexes (h/l or l/h, depending on whether the higher (h) or lower (l) OH wavenumber peak is on average weaker, respectively) for four integration methods A-D, the average result \bar{r} and the corresponding standard deviation s . [14]

Code		A	B		C	D		\bar{r}	s
		r	r	Δr	r	r	Δr		
C4	(-/h)	-	-	-	-	-	-	-	-
2FAph	(-/h)	-	-	-	-	-	-	-	-
Aph	(l/h)	0.30	0.31	0.05	0.51	0.41	0.22	0.38	0.10
Ace	(l/h)	0.32	0.33	0.09	0.67	0.54	0.33	0.47	0.17
Pin	(l/h)	0.83	0.81	0.15	0.80	0.75	0.39	0.80	0.03
C6	(l/h)	0.88	0.86	0.22	0.99	0.83	0.40	0.89	0.07
Fen	(h/l)	0.49	0.57	0.18	0.69	1.14	0.98	0.72	0.29
44C6	(h/l)	0.43	0.53	0.16	0.52	0.80	0.68	0.57	0.16
3355C6	(h/l)	0.18	0.21	0.04	0.29	0.27	0.14	0.24	0.05
C7	(h/l)	0.23	0.26	0.04	0.19	0.26	0.10	0.24	0.03
D6Ace	(l/h)	0.27	0.28	0.07	0.27	0.41	0.34	0.31	0.07
13CAce	(l/h)	0.32	0.33	0.10	0.31	0.38	0.17	0.34	0.03
Ace with 18OHH	(l/h)	0.24	0.27	0.07	0.21	0.21	0.11	0.23	0.03

the theory predictions can be found in the electronic supplement of [14]. The vibrations that were found to be the most likely are the water bending overtone (b2) and the libration modes (lib). The sum of the in-plane and out-of-plane libration is used and multiplied by 0.3, as the two modes cannot be separated easily, because of the water not coordinate to the ketone ideally and the two modes are expected to couple.

The theory model is then used to simulate the experimental spectrum using the harmonic frequencies and scaling factors. The scaling factors were obtained comparing theory predictions to experimentally obtained values of water dimer. As literature values gas phase data for water monomer[61] and dimer[62] and those in weakly bound matrices (Ne, He nanodroplets) are used.[63, 64] The values can be found in Table 3.4 together with unscaled values from theory predictions. In liquid water too many overlapping signals to see b2lib resonance but a strong mechanical coupling between bending and libration observed in liquid water[65] and clusters[66].

For the OH_b stretching vibration of water dimer a rounded scaling factor of 0.98 was determined. As the in plane (lib_{ip}) and out of plane (lib_{oop}) libration motion are hard to separate in the theory predictions, because they depend on the tilt angle of the water molecule, they were summed up and compared to the literature and a scaling factor of 0.30 was derived. For the water dimer bending overtone (b2) a scaling factor of 1.95 was determined. In order to calculate a theory prediction for b2lib^0 Equation 3.6 was used.

Tab. 3.4: Literature values for water dimer vibrations $\tilde{\nu}$ to determine a scaling factor for the harmonic frequency values on B3LYP-D3(BJ)/def2-TZVP level of theory.[14]

Experimental method	$\tilde{\nu}(\text{lib}_{\text{ip}})$ cm ⁻¹	$\tilde{\nu}(\text{lib}_{\text{oop}})$ cm ⁻¹	$\tilde{\nu}(\text{b})$ cm ⁻¹	$\tilde{\nu}(\text{b2})$ cm ⁻¹	$\tilde{\nu}(\text{OH}_\text{b})$ cm ⁻¹
Ne-matrix[67]	309.1	522.4	1616.4		3590.5
Ne-matrix[64]	310	522.6	1616.5	3193.7	3590.5
He-jet[24]					3602
He-droplet[63]			1614.8		
He-jet[68]			1621.2		
Theoretical method	$\omega(\text{lib}_{\text{ip}})$ cm ⁻¹	$\omega(\text{lib}_{\text{oop}})$ cm ⁻¹	$\omega(\text{b})$ cm ⁻¹	$\omega(\text{b2})$ cm ⁻¹	$\omega(\text{OH}_\text{b})$ cm ⁻¹
B3LYP-D3(BJ)/def2-TZVP	379.7	643.8	1639.4		3667.2

$$\tilde{\nu}(\text{b2lib}^0) = (\omega(\text{lib}_{\text{ip}}) + \omega(\text{lib}_{\text{oop}})) \cdot 0.30 + \omega(\text{b}) \cdot 1.95 \quad (3.6)$$

To give a prediction on the position of resonance and the OH_b values of the 10 investigated complexes, the theory predictions of the unscaled values for OH_b , b2, lib_{ip} , lib_{oop} and the resonance (b2+ lib_{ip}) are summarized in table 3.5 together with the scaled values of OH_b and b2lib.

Later the values from Table 3.5 were used to calculate the perturbed signal positions using Equation 3.7 and 3.8. For W_{ij} the average value from the experimentally determined W_{ij} of 9 cm⁻¹ was used (compare to values in Table 3.2). Further the expected ratio of the two resulting signals was determined using Equation 3.9.

$$\tilde{\nu}(\text{b2lib}) = 0.5 \cdot \left[\tilde{\nu}(\text{OH}_\text{b}^0) + \tilde{\nu}(\text{b2lib}^0) + \sqrt{\{\tilde{\nu}(\text{b2lib}^0) - \tilde{\nu}(\text{OH}_\text{b}^0)\}^2 + 4\{W_{ij}\}^2} \right] \quad (3.7)$$

$$\tilde{\nu}(\text{OH}_\text{b}) = 0.5 \cdot \left[\tilde{\nu}(\text{OH}_\text{b}^0) + \tilde{\nu}(\text{b2lib}^0) - \sqrt{\{\tilde{\nu}(\text{b2lib}^0) - \tilde{\nu}(\text{OH}_\text{b}^0)\}^2 + 4\{W_{ij}\}^2} \right] \quad (3.8)$$

$$r^{\text{calc}} = \frac{\{\Delta\tilde{\nu}_{ij}\}^2}{2\{W_{ij}\}^2} - 1 - \frac{\Delta\tilde{\nu}_{ij}}{W_{ij}} \sqrt{\frac{\{\Delta\tilde{\nu}_{ij}\}^2}{4\{W_{ij}\}^2} - 1} \quad (3.9)$$

The results are given in Table 3.6 and by creating a simulated spectrum by using the perturbed signal positions, Gaussian curves and the signal ratio (assuming the total intensity

to be 1), Figure 3.6 was created. As in Figure 3.4 the deperturbed signal positions from Table 3.5 are depicted as black arrows. The unscaled, deperturbed signal positions are also given as orange (OH_b) and magenta colored ($\text{b2+lib}_{\text{ip}}$) arrow (values in Table 3.5).

In Figure 3.6 the scaled (black) arrows come much closer to the experimental values in Figure 3.4 than the unscaled arrow (magenta and orange). Also the sequence of b2lib and OH_b matches the experimental values in eight of ten cases. By using the averaged experimental W_{ij} of 9 cm^{-1} to plot the perturbed signal positions using a Gaussian for broadening as simulated spectrum, the result is remarkably close to the experimental spectrum. A change from 0.98 to 0.985 would already detune most of the resonances and a change of ± 0.005 would give the exact experimental pattern. Regarding the usage of a harmonic model and scaling factors the results are surprisingly good.

To find evidence for the b2lib resonance anharmonic calculations by Dr. Arman Nejad were performed. He used formaldehyde water as a model system, a system which is later analysed in the evaluation of the HyDRA blind challenge in Chapter 5. As the calculations were performed before the blind challenge started, they can be compared to the experimental wavenumber like other theory submissions.

Tab. 3.5: Theoretical predictions for the OH_b , b2, lib_{ip} and lib_{oop} on B3LYP-def2/TZVP level and their corresponding perturbed OH_b and b2lib values.[14]

Code	ω^{calc}					$\tilde{\nu}^{\text{calc},0}(\text{arrows})$	
	OH_b /cm ⁻¹	b2 /cm ⁻¹	lib_{oop} /cm ⁻¹	lib_{ip} /cm ⁻¹	b2+ lib_{ip} /cm ⁻¹	OH_b /cm ⁻¹	b2lib /cm ⁻¹
C4	3635.34	3293.16	539.30	386.56	3679.72	3562.63	3488.59
2FAph	3624.92	3298.66	601.99	350.11	3648.77	3552.42	3501.82
Aph	3610.48	3297.36	624.02	364.97	3662.33	3538.27	3511.62
Ace	3612.54	3294.68	600.68	380.02	3674.70	3540.29	3506.52
Pin	3605.51	3298.74	612.48	382.51	3681.25	3533.40	3514.77
C6	3601.62	3297.02	588.56	393.52	3690.54	3529.59	3509.22
Fen	3591.67	3302.50	603.87	396.82	3699.32	3519.84	3520.14
44C6	3599.19	3299.24	591.35	387.55	3686.79	3527.21	3510.43
3355C6	3590.66	3302.38	603.66	404.45	3706.83	3518.85	3522.25
C7	3593.66	3299.24	596.21	404.30	3703.54	3521.79	3516.91

Tab. 3.6: Determined ratio r^{calc} and perturbed values for the spectral simulation (Figure 3.6).[14]

Code	r^{calc}	$\tilde{\nu}^{\text{calc}}(\text{curves})$	
		OH_b /cm ⁻¹	b2lib /cm ⁻¹
C4	0.014	3563.71	3487.51
2FAph	0.030	3553.96	3500.27
Aph	0.094	3541.03	3508.87
Ace	0.062	3542.54	3504.27
Pin	0.163	3537.04	3511.13
C6	0.143	3532.99	3505.81
Fen	0.966	3510.99	3528.99
44C6	0.189	3531.12	3506.51
3355C6	0.686	3511.39	3529.71
C7	0.586	3528.67	3510.03

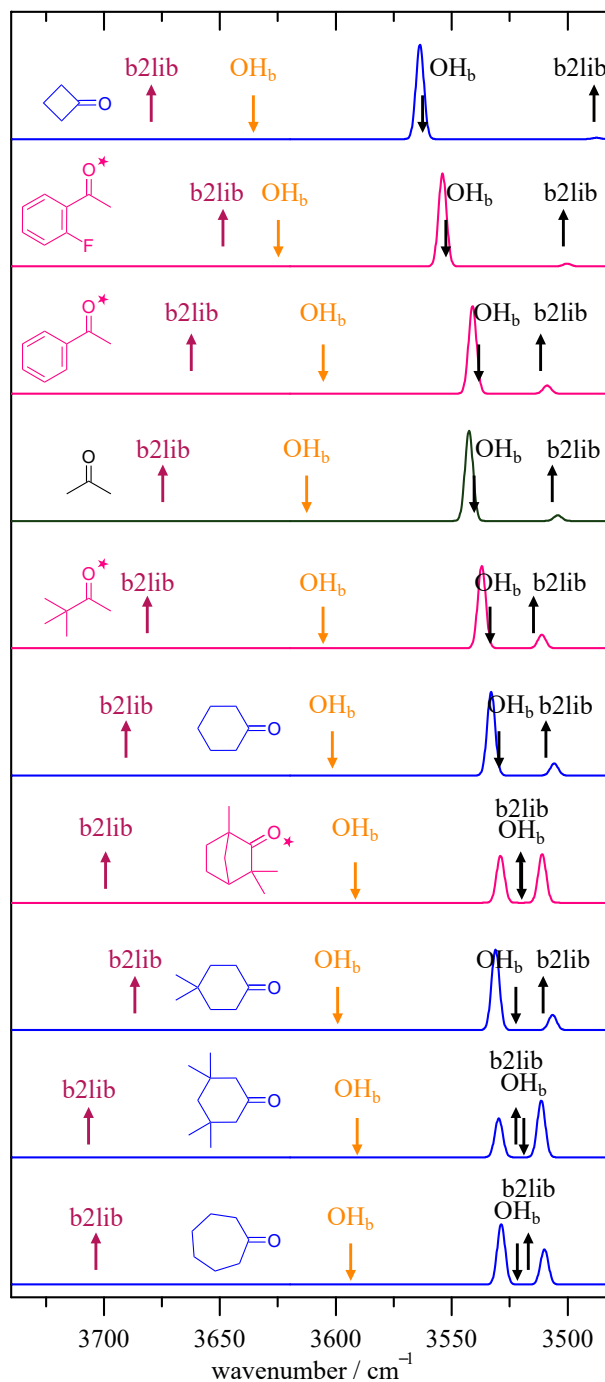


Fig. 3.6: Simulated spectra using the data from Table 3.5 and 3.6. The unscaled signal positions for OH_b and b2lib are given in orange and magenta respectively. The unperturbed, scaled signal positions for OH_b and b2lib are given as black arrows and the perturbed positions are depicted as Gaussian curves with a calculated ratio using an average W_{ij} value of 9 cm^{-1} . Reprinted with permission from Fischer 2021[14]. Copyright 2021 American Chemical Society.

3.2.1 Outlook

We propose that the resonance might also exist beyond ketones, so the search of the resonance in compounds with other functional groups became a side project. In his master thesis Till Wagner [69] investigated hydrate clusters of different amides as they are interesting for understanding the interaction of water with peptides. Unfortunately a resonance could not be reported, but when using neon as carrier gas for *N,N*-dimethylformamide, which was the most promising candidate for a b2lib resonance within the amides, a new signal was observed. It might belong to a complex of the hetero dimer with a neon atom. Further investigations are needed before a conclusive result can be presented.

The hydrates of a few alcohols were also investigated. For example for *tert*-butylalcohol+H₂O another signal is observed, but is more likely to belong to a higher cluster than to a resonance (see Chapter 8.3.5).

DABCO (1,4-diazabicyclo[2.2.2]octane) is the first amine compound that was investigated. More signals are visible than expected, making it an interesting candidate for b2lib. Unfortunately it offers two docking sites for the water to attach, making distinctions between hetero dimers and higher clusters challenging as the *gratin* jet spectroscopy setup cannot work size selectively. Here a collaboration with Anne Zehnacker-Rentien from France with their size selective UV/IR action spectroscopy setup could help to understand the spectral data. Another approach would be to investigate the related compound, 1,4-diazabicyclo[2.2.2]octane (ABCO), with only one binding site for water.

Some unpublished spectra can be found in the Supplement in Section 8.3.

The OH_b vibrations and the corresponding OH shift to the symmetric water stretching vibration (3657 cm⁻¹) can be used for benchmarking and can be found in Chapter 7 in Table 7.1.

4 Radicals

4.1 Investigation of Stable Radicals in the Gas Phase

4.1.1 Hydrates of TEMPO and TEMCO

This chapter is largely based on the corresponding publication [20]. The results and especially my own contributions are shown and extended by new, yet unpublished data. In [20] the hydrates of the stable radical TEMPO ((2,2,6,6-tetramethylpiperidin-1-yl)oxyl) $((\text{H}_2\text{O})_n, n=1,2)$ are investigated using FTIR spectroscopy, isotope substitution and computational methods. The hydrates show a variety of different conformers compared to the hydrates of its keto derivative TEMCO (2,2,6,6-tetramethylcyclohexanone) and the spectral complexity can be drastically reduced by using D_2O instead of H_2O . The spectral complexity might be due to the sb2lib resonance, as later discussed.

The microhydration of TEMPO has not been investigated previously even though TEMPO is essential in many fields of chemistry [70–77] and its behavior in aqueous solutions is of large interest [78]. As a persistent nitroxide radical TEMPO is stable enough to be investigated in the gas phase and survives multiple hundred scanning cycles in the novel *gratin* jet spectroscopy setup - even under humid conditions and additional water. It is also compared to the related ketone species TEMCO and the structural differences of the corresponding mono- and dihydrates are compared using quantum chemical methods and FTIR absorption spectroscopy.

In Figure 4.1 the results from quantum chemical calculations on (U)B3LYP-D3(BJ)/def2-QZVP level of theory are summarized. The minimum structures for the TEMPO and TEMCO monomer, the three monohydrate structures, and the dihydrates are depicted. A nomenclature depending on the orientation of the H bond formed between water and TEM(P/C)O relative to the methyl groups of TEM(P/C)O is introduced. If the water binds to the N-O/C=O group in the plane of the ring and between the methyl groups of one side of the ring, the conformation is called p (plane). Due to the conformation of the ring, the water can also approach the N-O/C=O group from two different sides, one with

the methyl groups in equatorial and one with the methyl groups in axial position. As the axial methyl groups are providing less space for the water to bind it is labeled t (tight). For the water binding from the side with equatorially positioned methyl groups, providing more space, the label o (open) is used. When moving from the monohydrate structures to the dihydrates, the second water attaches to the first water in the TEM(P/C)O o structure. Additionally the relative energies between the conformers of the monohydrates, the dissociation energies, the unscaled harmonic frequencies (hydrogen bond forming OH stretching vibration), and the IR intensities are given. The predicted wavenumber for the TEMCO t structure is imaginary and belongs rather to a transition state than minimum structure.

In Figure 4.2 the spectroscopic data for TEMPO and TEMCO with water is shown. The chemicals used in this study are listed in Table 4.1. For the spectra a stagnation pressure of 750 mbar was used. The spectra A, C, H, and J are labeled warm as pure helium was used as carrier gas, while for D and F a 1:1 mixture of helium and neon was used. As heavier carrier gasses can cool clusters in supersonic expansion more efficiently the corresponding spectra are labelled cold. Trace B, E, G, and I are showing the scaled harmonic predictions for the mixed species of TEMPO+H₂O and TEMCO+H₂O. The position is marked with a red triangle for p structures, a yellow diamond shape is marking t structures and a circle in green the o structures. A gray circle is marking the position of the dihydrates (oo). The harmonic frequencies are scaled by a scaling factor of 0.975 for the bound OH stretching vibration and with 0.959 for the free OH stretching vibrations. The scaling factors were derived by comparing the water dimer stretching vibrations of the same level of theory to experimental data (like in [14], see Table 3.4 first three rows).

Tab. 4.1: Table of investigated compounds, their abbreviation, their CAS number, the supplier and purity.[20]

Name	Abbreviation	CAS Number	Supplier	Purity
(2,2,6,6-Tetramethyl-piperidin-1-yl)oxyl	TEMPO	2564-83-2	Sigma Aldrich	98%
2,2,6,6-Tetramethyl-cyclohexanone	TEMCO	1195-93-3	Abcr	95%
Di- <i>t</i> -butyl nitroxide	DTBN	2406-25-9	Sigma Aldrich	90%
Deuterium oxide	D ₂ O	7789-20-0	Abcr	99.85%
Water- ¹⁸ O	H ₂ ¹⁸ O	14314-42-2	Sigma Aldrich	97%, 97% atom ¹⁸ O
Helium	He	7440-59-7	Linde	99.996%
Neon	Ne	7440-01-9	Linde	99.995%

The spectrum of TEMCO+H₂O in line A is rather simple compared to the one of

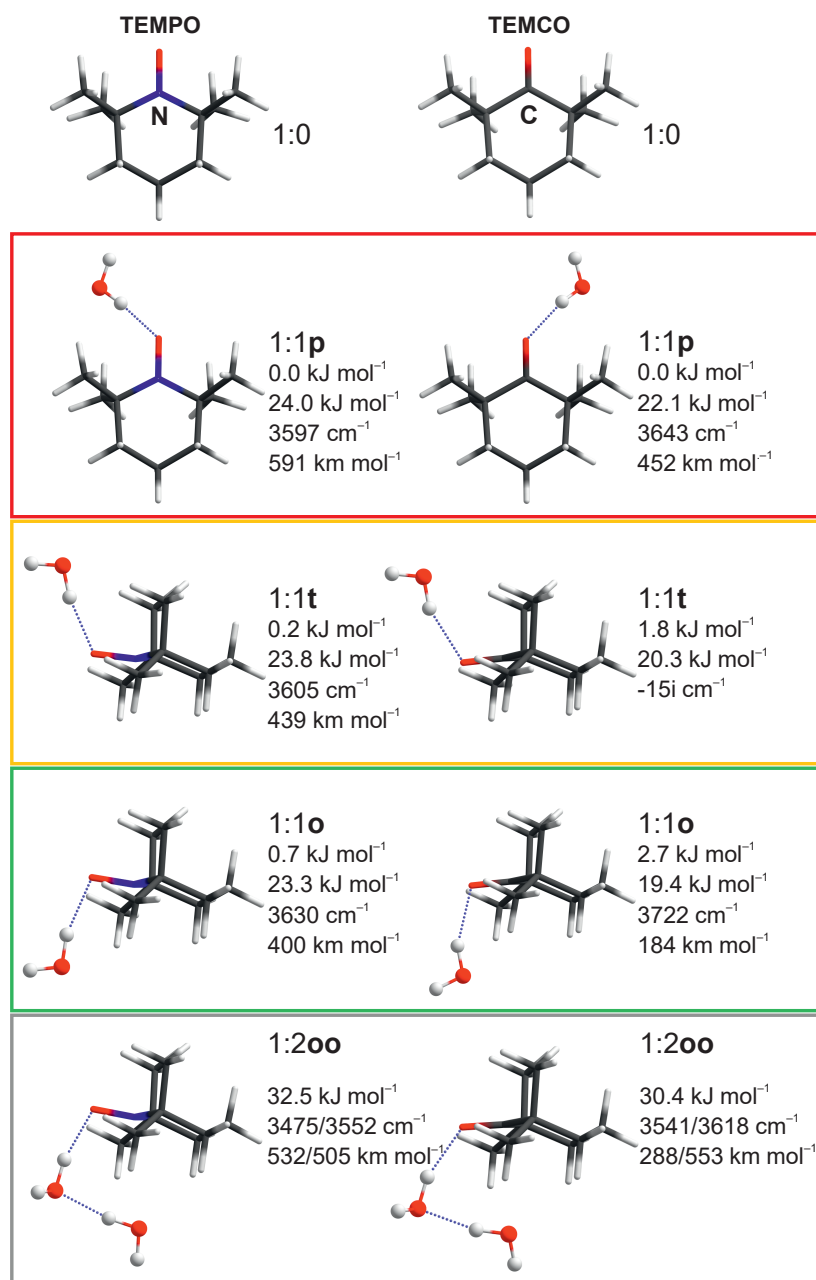


Fig. 4.1: Structures of the monomer, mono-, and dihydrate structures for TEMPO and TEMCO. The relative energies between the monohydrates and the dissociation energies, the unscaled harmonic wavenumber predictions and IR intensities are given for (U)B3LYP-D3(BJ)/def2-QZVP level of theory. The colored frames align with the spectral interpretation in Figure 4.2.[20]

TEMPO+H₂O. Due to the relatively high energy difference between the dimer conformers (see Figure 4.1 and Table 4.4), one main OH_b signal is expected. This matches with the observed spectrum in which the OH_b stretching vibration of the p conformer is labeled p···HOH and the corresponding OH_f signal ···HOH. The spectrum is showing another signal, which belongs to the monohydrate. It is labeled b2lib as it is most likely to belong to a b2lib resonance rather than to another conformer as the o conformer would be expected at higher wavenumbers and is 2.7 kJ mol⁻¹ higher in energy (compare to Figure 4.1). Like in chapter 3 the coupling constant W_{ij} was determined using method A and C (described in 1.1.3) to determine the intensity ratio. The signal ratios r , average signal ratio \bar{r} , coupling element W_{ij} and deperturbed signal positions are given in Table 4.2. In addition the dihydrate positions are also reported and labeled oo···HOH. To verify the dihydrate signal assignment concentration series were used, which are shown in Figure 4.3 (A). Here the spectrum is scaled to the height of the dominant signal of the p isomer for two different concentrations, showing that the oo···HOH scales differently.

The signal assignment for TEMPO+H₂O is more tricky as the three dihydrates are closer in energy and more than 3 signals are visible under the same conditions the spectrum for TEMCO+H₂O was recorded. In order to assign the signals different carrier gas mixture and water isotopes are used. When moving from spectrum C to D (Figure 4.2) the carrier gas was changed from pure helium (warm) to a 1:1 helium neon mixture (cold) and one signal disappears due to the colder expansion conditions. This hints towards the signal belonging to one of the less stable conformers (o or t) and the largest signal most probably belongs to the p conformer. Here it is interesting, that the intensity ratio of the three remaining signals remains the same. When H₂O is changed to ¹⁸O-water (spectrum F) and cold expansion conditions are applied, all three signals shifted by approximately the same wavenumber. A more drastic change happens when the water isotope is changed to D₂O (spectrum J and H). Here only one signal is visible for pure D₂O. The signal is assigned to the most stable p conformer (p···DOD). As water impurities remain in the jet and the H₂O and D₂O exchange H atoms over time, also the mixed HDO species become visible, and were assigned in the spectrum (p···DOH, p···HOD). As after cooling the spectrum more efficiently when moving from C to D, one signal disappeared and was assigned to one of the less stable conformers of the minimum structure. There are three signals remaining, whose intensity ration also remained under colder conditions and three minimum structures were found in total. The main signal in the spectrum and the most stable structure in the calculations has a OH_b close to 3500 cm⁻¹. As all three remaining signals are shifted when ¹⁸O water is used, we believe that one of the signals belongs to a b2lib resonance. The most probable candidate is the signal at 3505 cm⁻¹, as the distance matches with other examples from the resonance Chapter 3 and it gives a W_{ij} value of

9 cm^{-1} , which lies in the expected range. The dihydrate signals could also be assigned for TEMPO+H₂O and the signal position is also verified in Figure 4.3 using concentration series. All experimental wavenumbers and scaled harmonic frequencies for all assigned signals are listed in Table 4.3.

Tab. 4.2: Intensity ratios for the deperturbation analysis for the 1:1 monohydrates of TEMCO and TEMPO.[20]

System	r_A	r_B	\bar{r}	W_{ij} / cm^{-1}	$\tilde{\nu}(\text{OH}_b^0) / \text{cm}^{-1}$	$\tilde{\nu}(\text{b2lib}^0) / \text{cm}^{-1}$
TEMCO	0.076	0.058	0.067	11	3547	3508
TEMPO	0.446	0.405	0.426	9	3503	3511

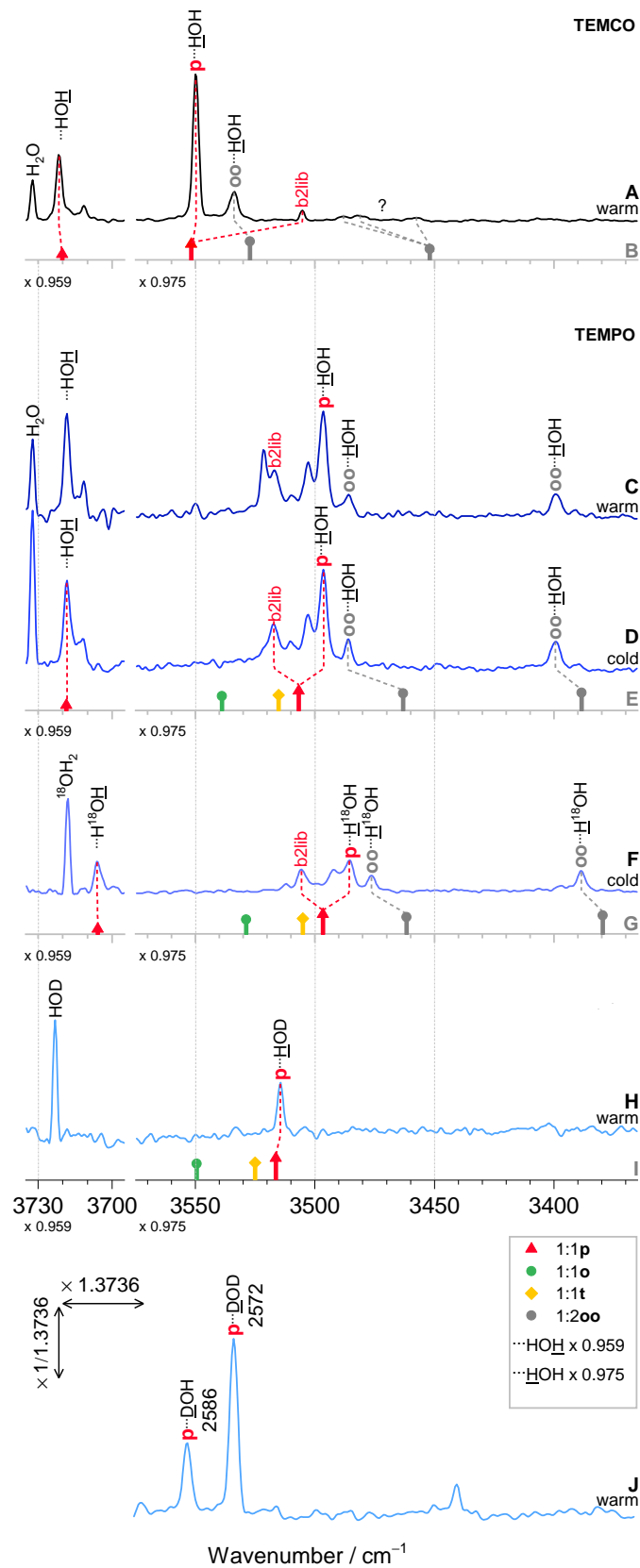


Fig. 4.2: FTIR spectra of jet cooled TEM(P/C)O water clusters and the corresponding scaled predictions on (U)B3LYP-D3(BJ)/def2-QZVP level of theory in B, E, G, and I. In A, C, H, and J solely He was used as carrier gas, while in D and F a 1:1 He:Ne mixture was used.[20]

Tab. 4.3: Experimental IR wavenumbers of TEMCO and TEMPO hydrates $\tilde{\nu}$ (in cm^{-1}) along with the unscaled computed wavenumbers ω (in cm^{-1}) and IR intensities σ (in km mol^{-1}) at closed- and unrestricted open-shell B3LYP-D3(BJ)/def2-QZVP level. For the dihydrates two wavenumbers are given as two water molecules are acting as donor molecules and have an OH_b vibration.[20]

Structure TEMCO	Experiment	Computed	
	$\tilde{\nu}$ cm^{-1}	ω cm^{-1}	σ km mol^{-1}
p \cdots <u>H</u> OH	3550	3643	452
o \cdots <u>H</u> OH	-	3722	184
b2lib	3505		
oo \cdots <u>H</u> OH	3534 / 3488? / 3482? / 3457?	3618 / 3541	553 / 288
p \cdots HO <u>H</u>	3722	3879	91
TEMPO			
p \cdots <u>H</u> OH	3497	3597	591
t \cdots <u>H</u> OH	-	3605	439
o \cdots <u>H</u> OH	3521? (He)	3630	400
b2lib	3517		
oo \cdots <u>H</u> OH	3486 / 3399	3552 / 3475	505 / 532
p \cdots HO <u>H</u>	3718	3878	85
p \cdots <u>H</u> ¹⁸ OH	3486	3586	592
t \cdots <u>H</u> ¹⁸ OH	-	3595	441
o \cdots <u>H</u> ¹⁸ OH	3512? (He)	3619	402
b2lib	3506		
oo \cdots <u>H</u> ¹⁸ OH	3476 / 3389	3550 / 3466	490 / 547
p \cdots H ¹⁸ <u>O</u> H	3706	3864	77
p \cdots <u>H</u> OD	3514	3607	659
t \cdots <u>H</u> OD	-	3616	505
o \cdots <u>H</u> OD	-	3641	469
p \cdots HO <u>D</u>	-	2819	10
p \cdots <u>D</u> OD	2572	2615	291
t \cdots <u>D</u> OD	-	2621	213
o \cdots <u>D</u> OD	-	2638	191
p \cdots DO <u>D</u>	2751	2836	79
p \cdots <u>D</u> OH	2586	2629	337
t \cdots <u>D</u> OH	-	2635	256
o \cdots <u>D</u> OH	-	2653	237
p \cdots DO <u>H</u>	-	3871	40

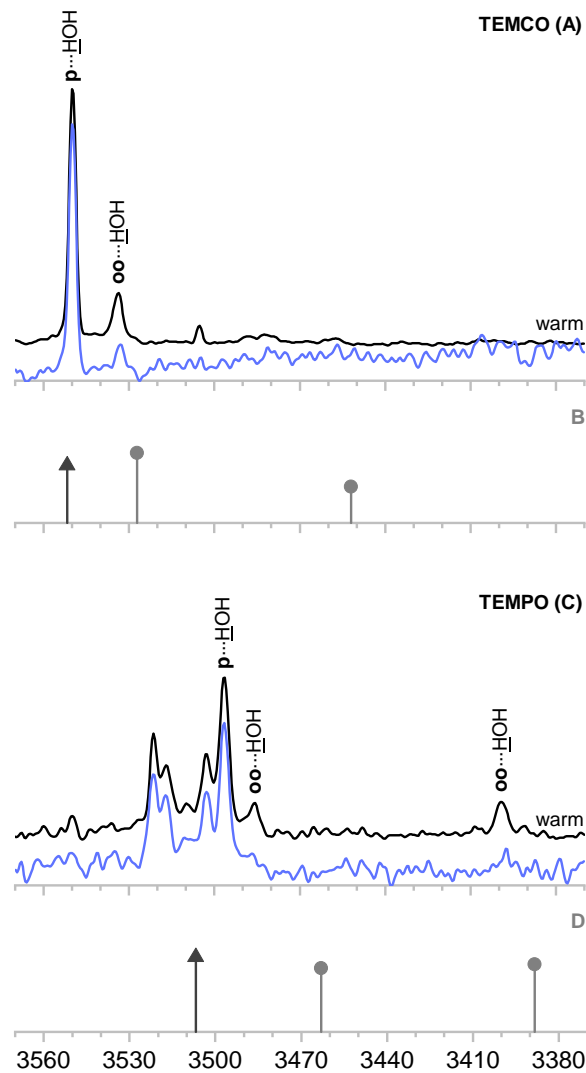


Fig. 4.3: TEM(P/C)O+H₂O spectra recorded with warm expansion conditions but with different concentrations. The spectra are scaled to the dominant $p\cdot\cdot\text{HOH}$ signal. The spectra depicted in black are also shown in Figure 4.2.[20]

To further verify the energetic order of the monohydrates and the signal assignment, further calculations were carried out on unrestricted open-shell DLPNO-CCSD(T)/aug-cc-pVQZ and DLPNO-CCSD(T)/aug-cc-pVTZ level of theory. The results are summarized in Table 4.4. While for TEMCO+H₂O the energetic order remained the same, the TEMPO+H₂O t and o structures switch places when moving from B3LYP to DLPNO-CCSD(T). As the predicted energy differences between the monohydrate structures are rather small ($< 1 \text{ kJ mol}^{-1}$), the result is not surprising but also does not allow further signal assignment.

Tab. 4.4: Predicted relative energies within one group of donor molecules (TEM(C/P)O) with different water isotopes (H₂O, HDO, D₂O). The energy difference is given without ZPVE correction on closed- and unrestricted open-shell B3LYP-D3(BJ)/def2-QZVP level of theory ($E_{\text{el}}^{\text{B3LYP}}$) and with ZPVE correction on DLPNO-CCSD(T)/aug-cc-pVQZ//B3LYP-D3(BJ)/def2-QZVP and DLPNO-CCSD(T)/aug-cc-pVTZ//B3LYP-D3(BJ)/def2-QZVP level of theory ($\Delta E_0^{\text{DLPNO}}$, $\Delta E_0^{\text{DLPNO}}$). Imaginary frequencies (i freq) at saddle points are not included into the zero point energy.[20]

	$E_{\text{el}}^{\text{B3LYP}}$ def2-QZVP (kJ mol ⁻¹)	$\Delta E_0^{\text{DLPNO}}$ aug-cc-pVQZ (kJ mol ⁻¹)	$\Delta E_0^{\text{DLPNO}}$ aug-cc-pVTZ (kJ mol ⁻¹)
TEMCO			
p··HOH	0.0	0.0	0.0
t··HOH(i freq)	1.8	1.8	1.9
o··HOH	2.7	2.5	2.4
TEMPO			
p··HOH	0.0	0.0	0.0
t··HOH	0.2	0.7	0.8
o··HOH	0.7	0.2	0.1
p··HOD	0.9	0.9	
t··HOD	1.1	1.6	
o··HOD	1.6	1.1	
p··DOH	0.0	0.0	
t··DOH	0.3	0.8	
o··DOH	0.8	0.3	
p··DOD	0.0	0.0	
t··DOD	0.3	0.8	
o··DOD	0.9	0.4	

To further explore the different behavior of TEMPO and TEMCO when it comes to binding a water molecule, a relaxed scan of the torsional angle of the C-(N/C)-O···O on (U)B3LYP level of theory was performed. The resulting curves are shown in Figure 4.4.

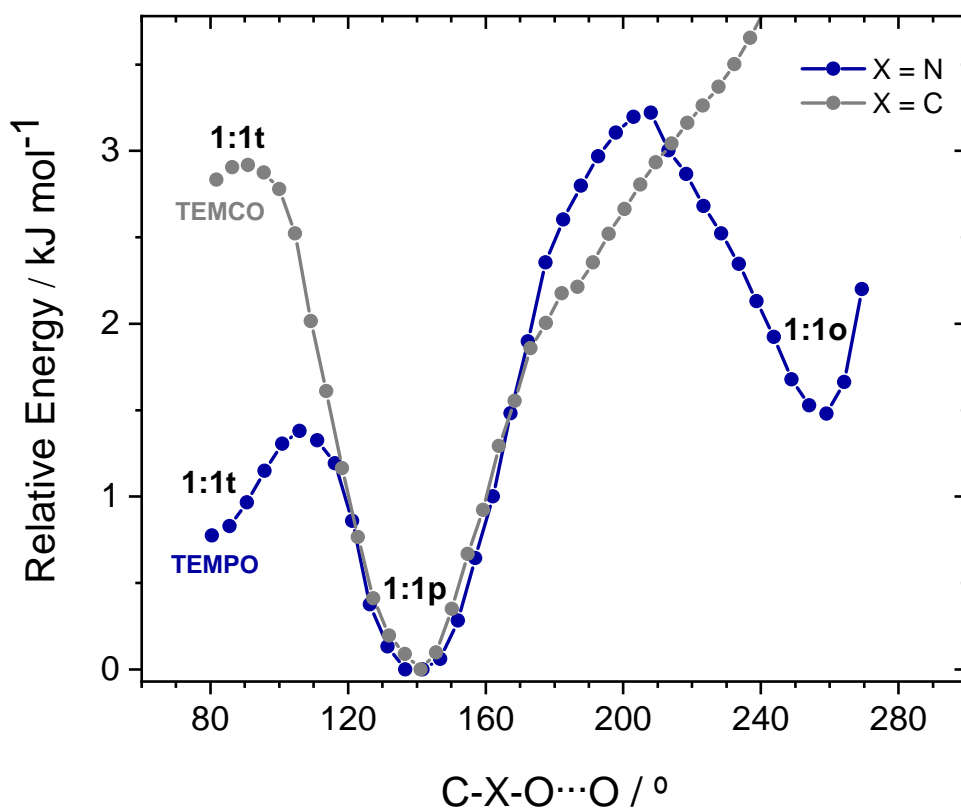


Fig. 4.4: B3LYP and (U)B3LYP relaxed torsional scans of a single water molecule (O) around the N-O / C=O bond for TEMPO (blue) and TEMCO (grey), showing that the oxygen end of the C=O bond has a stronger hydrogen bond accepting anisotropy and preference for p-coordination than the oxygen end of the N-O bond. The barriers for TEMPO, which may be further lowered by zero-point energy of the relaxed modes, are low enough to allow for relaxation into the 1:1p global minimum, at least in colder neon expansions.[20]

The relative energy to the minimum of each structure is plotted against the torsional angle. The blue TEMPO-curve shows 3 minima, while the gray TEMCO-curve only shows one. This is in good agreement with the experimental data and also agrees with the chemical intuition. While for a keto group two binding sites at the oxygen lone pairs of the keto group are expected, for a nitroxy radical a more diffuse binding behavior is expected, as the lone electron is not located. For a less sterically hindered radical, also binding to the N of the nitroxy group might be observed.

In addition Elisa Brás also performed a local energy decomposition (LED) analysis for the TEMP/CO which can be found in the supplemental information of [20].

4.1.2 Hydrates of DTBN and HMA

In the supplement of [20] the open ring analogue of TEMPO (di-*tert*-butyl nitroxide radical, short DTBN) was also investigated. Unfortunately it is less stable and does not survive for a long time in the recycling jet setup. The decay over time is shown in Figure 4.5. The upper green traces show the DTBN+H₂O mixture expanded in He, while the lower blue traces show the expansion in a He:Ne 1:1 mixture. Within one group (green or blue) the time evolution is depicted starting at the top and moving further down with time. Interestingly, the decay is faster for the He:Ne mixture than for pure He. The spectrum shows one dominant signal at 3484 cm⁻¹ and several other signals. After the TEM(P/C)O paper was published the related ketone, HMA (hexamethylacetone) was investigated as well.

The minimum structures, derived from (U)B3LYP-D3(BJ)/def2-TZVP level of theory, for both species, DTBN+H₂O and HMA+H₂O are given in Figure 4.6. The structures look comparable between the nitroxide radical and ketone. The most dominant difference is, that the C-(N-O)-C angle is tilted while the arrangement in HMA is planar. Another difference to the TEM(P/C)O hydrates is, that the methyl groups of the DTBN/HMA are in staggered relative position. For both species only one distinguishable minimum structure was found.

Tab. 4.5: Table of investigated compounds, their codes in this supplement, their CAS number, the supplier and purity.

Name	Abbreviation	CAS Number	Supplier	Purity
Di- <i>t</i> -butyl nitroxide	DTBN	2406-25-9	Sigma Aldrich	90%
Hexamethylacetone	HMA	815-24-7	Alfa Aesar	98%
Helium	He	7440-59-7	Linde	99.996%
Neon	Ne	7440-01-9	Linde	99.995%

The FTIR spectra of HMA+H₂O (blue) and DTBN+H₂O (magenta), the averaged spectrum of the green traces from Figure 4.5, are shown in Figure 4.7. One gets the impression, that both spectra are showing two main signals. In Table 4.6 the wavenumbers and scaled and unscaled wavenumber predictions are given.

The theoretically derived minimum structures fit the minor signal labeled OH_{b2} better than the main signal in both cases. Probably the computational method is missing the real minimum structure for both cases or a b2lib resonance is visible. This is more probable for DTBN, as the main signal is closer to 3500 cm⁻¹ and we believe to observe it in TEMPO. As for HMA further concentration ratios of water and HMA were recorded, but the

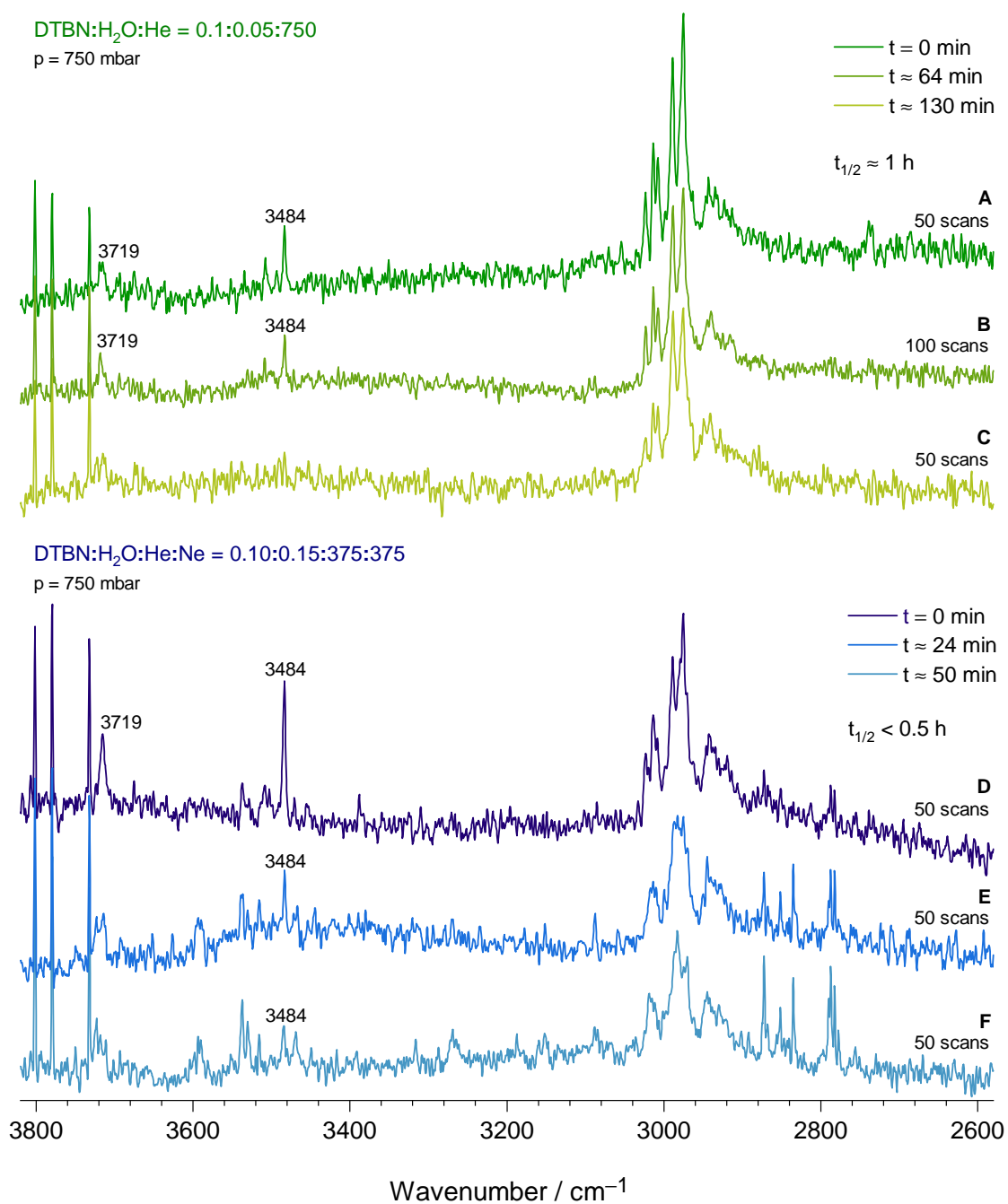


Fig. 4.5: Two sets of FTIR spectra of DTBN with water. The green set of spectra was recorded with pure helium as carrier gas, while the blue set was recorded with a 1:1 He:Ne mixture. Within a set the time evolution of the spectra is shown from top to bottom. Interestingly the DTBN decays faster in the He-Ne mixture.[20]

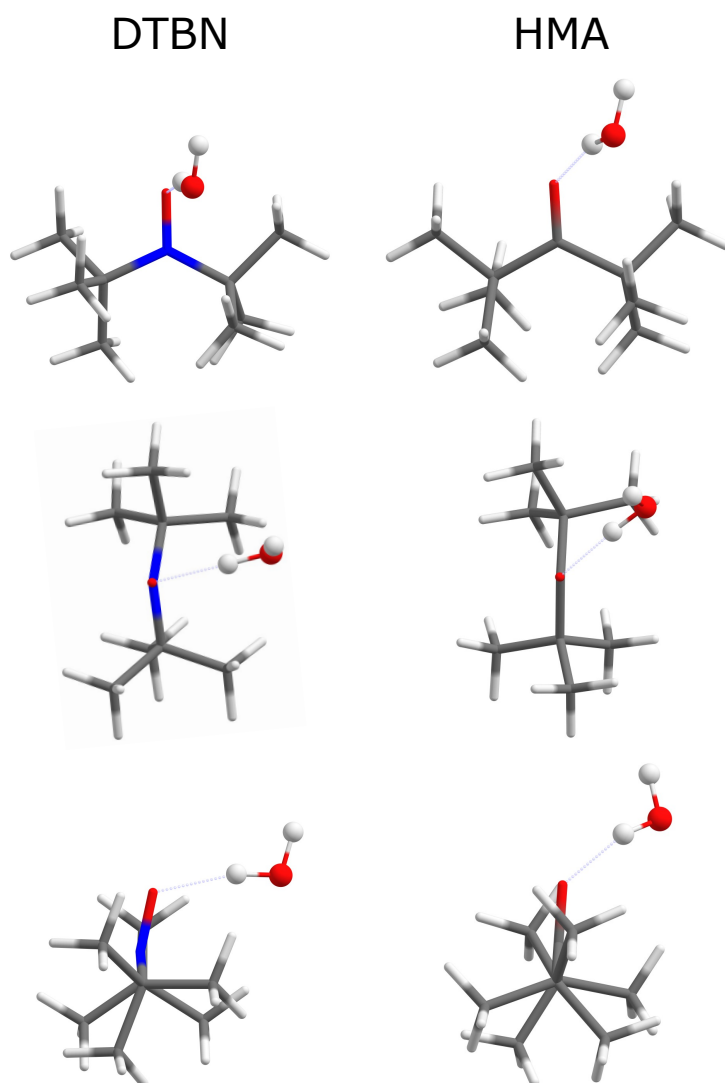


Fig. 4.6: The predicted minimum structure for DTBN and HMA monohydrate on (U)B3LYP-D3(BJ)/def2-TZVP level of theory.

Tab. 4.6: Experimental wavenumbers and the comparison to theory predictions. The wavenumbers derived from (U)B3LYP-D3(BJ)/def2-TZVP level of theory and scaled by a factor of 0.975. In addition the predicted IR intensity σ is given.

Name	Vibration	$\tilde{\nu}^{\text{exp}}$ cm^{-1}	ω^{theo} cm^{-1}	σ km mol^{-1}	scaled ω^{theo} cm^{-1}
HMA	OH _b	3534	3658	340	3567
	OH _{b2}	3564			
	OH _f	3723			
DTBN	OH _b	3484	3592	420	3502
	OH _{b2}	3509			

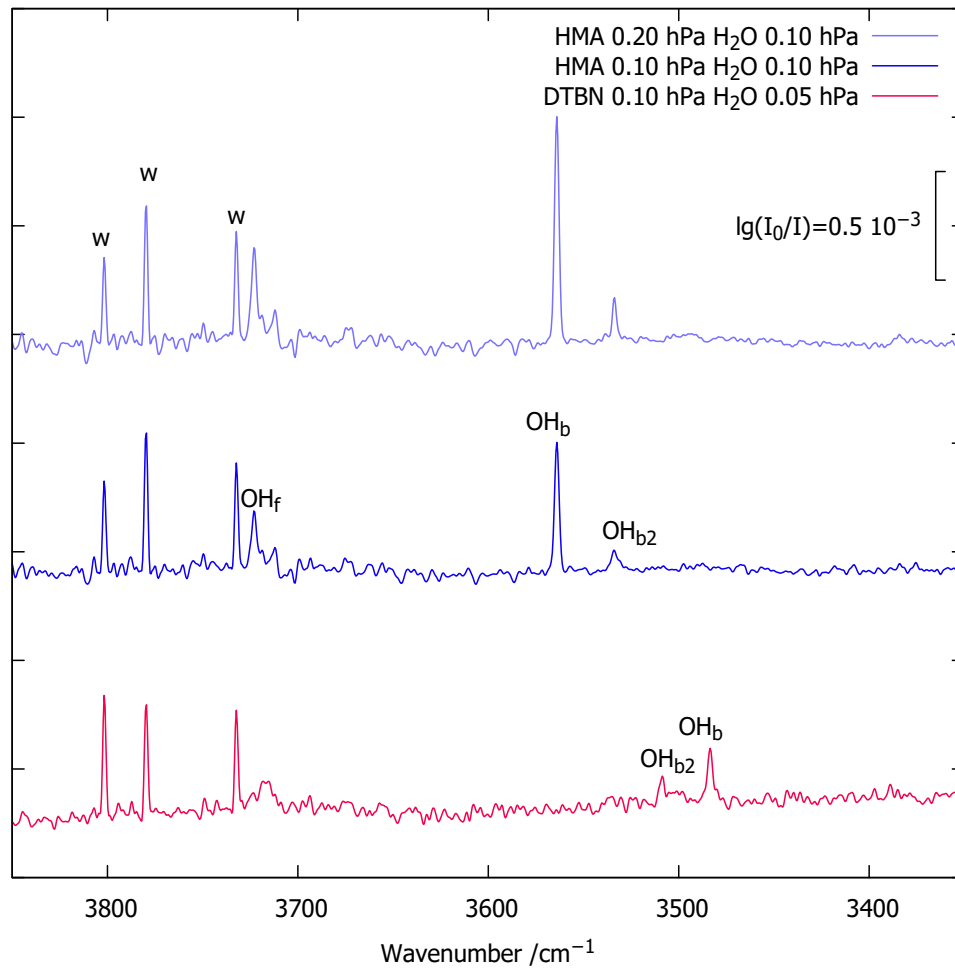


Fig. 4.7: FTIR spectra of DTBN+H₂O and HMA+H₂O in 750 mbar He. Water monomer is labelled w and hetero dimer signal OH_{b/f}.

signal ratio remained the same, hinting towards both signals belonging to hetero dimers close in energy or the second signal is due to a resonance. An experiment with a He:Ne expansion might help to distinguish between a b2lib resonance and two different hetero dimer conformations. For DTBN more experiments were performed by Elisa Bràs, using a variety of different donor molecules (alcohols). Her work and measurements at a non-recycling setup and might give new insights on the binding behavior of the compound. Further work on the computational side is also needed as one minimum conformation might be missing.

4.1.3 TEMPO-H + TEMPO Hydrogen Transfer

This subsection briefly describes the main results of [79] as it was published recently and no new data has been collected yet. In the work the hydrogen sharing between TEMPO-H (TH) and TEMPO (T) is investigated and information on the TEMPO-H dimer and TEMPO-H monohydrate are collected. The investigation is carried out using FTIR spectroscopy of the jet cooled molecules and harmonic predictions on B3LYP-D3(BJ)/def2-TZVP level of theory. For most theoretical values in this work ORCA 4.2.1 was used. In this work however, ORCA 5.0.2 was also used to determine the barrier heights for hydrogen transfer and is later compared to ORCA 4.2.1. The TEMPO-H for this study was synthesized by Martijn Tepaske.

Figure 4.8 shows the minimum structures of the TEMPO-H \cdots TEMPO hetero dimer (THT) and the TEMPO-H homo dimer (THTH) obtained by B3LYP-D3(BJ)/def2-TZVP level of theory. In the nomenclature, which works similar to the one introduced in the first subsection, the orientation of the OH bond is regarded relative to the position of the methyl groups. o is used for the side of the ring with equatorial methyl groups, t describes the side of the ring with axial methyl groups. p describes a bond parallel to the ring plane, between the two methyl groups attached to one carbon atom. In the following the small letters (o,t,p) are used after the abbreviation for the substance (TH,T) in a way such as [donor][o,p,t]-[acceptor][o,p,t] where the first part gives the OH bond orientation of the donor molecule and the second part how the conformation of the OH bond would be after hydrogen transfer. In Figure 4.8 it is interesting to point out, that while on the upper THT complex the H atom is donated to the O of the nitroxy radical, in the lower THTH complex the H atom is donated to the N of the nitroxy group. This is particularly interesting as studies have shown, that in TEMPO-H crystals three (anhydrous) or six (trient, 0.33-hydrate) TH are connecting trough the o side and bind preferentially to the oxygen atom of the nitroxy radical or water.[80, 81]

Before investigating the proton sharing of TEMPO-H \cdots TEMPO, the binding behavior of TEMPO-H was explored. The chemicals used for the FTIR studies are listed in Table 4.7 and the experimental details can be found in Table 8.4 in the Supplement. An NMR spectrum, proving the purity of the TEMPO-H synthesized by Martijn Tepaske, can be found in the supporting information of [79].

In Figure 4.9 the spectra of TH with and without additional water are shown. Helium was used as a carrier gas and a stagnation pressure of 750 mbar was applied. Again, the water monomer is labeled w. The main signal at 3631 cm^{-1} is assigned to the TEMPO-H monomer OH stretching vibration and is labeled TH. When moving from the top to the

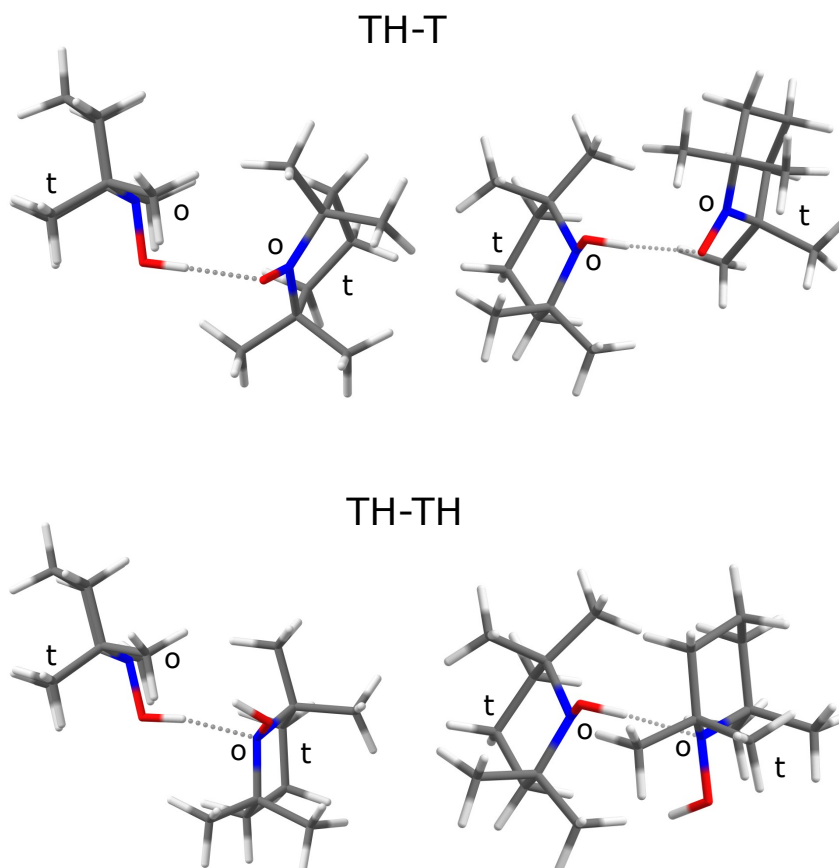


Fig. 4.8: Minimum structures of the THT and THTH dimers using B3LYP-D3(BJ)/def2-TZVP level of theory on ORCA 4.2.1.[79]

middle spectrum the TH amount is increased and new peaks appear in the spectrum at 3609 cm^{-1} and approximately 3230 cm^{-1} , which are assigned to the TH-TH dimer. When additional water is added (lowest spectrum), another peak becomes visible, which is assigned to the water-TH dimer.

Tab. 4.7: Table of investigated compounds, their codes in this supplement, their CAS number, the supplier and purity.[79]

Name	Code	CAS Number	Supplier	Purity	Lot#
TEMPO	T	2564-83-2	Sigma-Aldrich	98%	Lot#BCCF8320
TEMPO-H	TH	7031-93-8	synthesized by M. A. Tepaske		
Helium	-	7440-59-7	Nippon	99.996%	

When TEMPO (T) is added to the TEMPO-H (TH) expansion the H-atom-sharing of the two TEMPO moieties can be investigated. The spectral data is shown in Figure 4.10 and the experimental details are listed in Table 8.4 in the Supplement. Mainly two new

signals become visible in the spectra, which scale with the T and TH concentration. As water cannot be removed from the spectrum also the wT and wTH species become visible and are labeled accordingly. To figure out which THT conformers are formed during the expansion, the results are compared to scaled harmonic frequency calculations. In order to obtain a suitable scaling factor for nitroxide radicals, the results of theory predictions on B3LYP-D3(BJ)/def2-TZVP level of theory are compared to the literature known nitroxide vibrations of hydroxylamine [82] and water monomer [11]. The theory predictions and literature values, as well as the resulting scaling factor can be found in Table 4.9. With the scaling factor first the TH monomers regarded, as it can form 2–3 conformations when it comes to the orientation of the OH bond relative to the methyl groups. The results are given in table 4.8 and the THt structure is predicted to be 10.8 kJ/mol higher in energy than the THo structure, which is why the TH monomer peak is assigned to the THo structure. The THp structure always relaxes to the THt or THo structure and is therefore neglected. When moving to the THT dimers the most stable conformer for the donor TH is in THo orientation, which also holds true for the predicted acceptor. But when the wavenumbers of the experimental signals are compared to the dimer scaled harmonic frequencies, the most dominant signal is in better agreement with the conformation of the acceptor T moiety is the Tt structure. To further investigate this case, the energy differences with and without zero point vibrational energy correction and the energies with a bigger basis set (QZVP) were regarded (all values in Table 4.8). All predictions for the minimum structure determine the THoTo structure to be more stable than the THoTp structure, but the spectrum seems to show the opposite. The energetic order of the THT dimers is also visualized in Figure 4.11. The peak positions, with their respected experimental signal assignment are listed in Table 4.10 and 4.11.

In order to understand the binding behavior and the energy landscape of the hydrogen transfer of the two dimer structures THo-Tt and THo-To is explored. For that a NEB (nudged elastic band) scan was performed to get an idea of the transition state (TS), then a TS search was conducted using ORCA 5.0.2 instead of ORCA 4.2.1 as it is known to be faster. Later the start, end, and TS structure were optimized using B3LYP-D3(BJ)/def2-TZVP level of theory using ORCA 4.2.1 and ORCA 5.0.2 in order to compare the two. The results are summarized in Figure 4.12. The relative energy differences between the two ORCA versions are rather small and amount 0.1 kJ/mol for the electronic energies and 0.5 kJ/mol for the zero point corrected energies. The energy needed for the hydrogen transfer in the THo-Tt conformer amounts 55.0 kJ/mol (in ORCA 4.2.1) and is higher than the energy of the OH stretching vibration and is visualized as orange arrow, which might be the reason why a tunneling splitting is not observed. The barrier for the THo-To is a bit lower with 45.5 kJ/mol, but lies again above the OH stretching vibration.

Tab. 4.8: Theoretical predictions for different conformers of TH monomer and TH-T dimer on B3LYP-D3(BJ)/def2-TZVP level. Relative electronic energies (ΔE^e) and zero point corrected energies (ΔE^0) are given within the monomer and dimer group each. The predicted wavenumber (ω) of the TEMPO-H vibration (unscaled and scaled by multiplying with 0.96) and its infrared intensity σ is given. Additionally the energy differences for B3LYP-D3(BJ)/def2-QZVP single point calculations are given for TH-T dimer structures.[79]

Structure	ΔE_{TZVP}^e /kJ mol ⁻¹	ΔE_{TZVP}^0 /kJ mol ⁻¹	ω_{TZVP} /cm ⁻¹	$\omega_{\text{TZVP}}^{\text{scaled}}$ /cm ⁻¹	σ_{TZVP} / km mol ⁻¹	$\Delta E_{\text{QZVP}}^{e, \text{sp}}$ /kJ mol ⁻¹
TH monomer						
THo	0.0	0.0	3794	3642	41	
THt	12.0	10.8	3631	3486	2	
TH-T dimer						
THo-To	0.0	0.0	3554	3412	560	0.0
THo-Tp	1.8	1.9	3588	3444	850	1.8
THo-Tt	0.9	0.5	3572	3429	610	0.7

As a result it can be reported, that the proton transfer takes longer than 15 ps / 1500 OH vibrational periods and the tunneling process cannot be observed, even though the excitation of the OH stretching vibration comes close to the barrier height (compare barrier height and orange arrow in Figure 4.11). In the future it would be interesting to investigate a system in which the tunneling can be observed.

The wavenumbers of hydrate complexes from this Chapter will be added to the data base for benchmarking.

Tab. 4.9: Experimental wavenumbers $\tilde{\nu}$ of hydroxylamine [82], water monomer [11] and TH (this work), their assignments and corresponding harmonic values ω on B3LYP-D3(BJ)/def2-TZVP level. f is the resulting scaling factor required to match the experimental value.[79]

Assignment	$\tilde{\nu}/\text{cm}^{-1}$	ω/cm^{-1}	f
H ₂ NOH			
OH (stretch)	3649.89	3789.03	0.963
NH (stretch)	3358.76	3506.4	0.958
NH (stretch)	3294.25	3427.9	0.961
w			
OH _{asym}	3756	3887.57	0.966
OH _{sym}	3657	3782.40	0.967
TH			
OH (stretch)	3631	3794.21	0.957

Tab. 4.10: Experimentally observed OH stretching wavenumbers $\tilde{\nu}$ compared to harmonic B3LYP-D3(BJ)/def2-TZVP predictions ω uniformly scaled by 0.96 for TH and binary donor-acceptor complexes observed for the first time in this work.[79]

Species	$\tilde{\nu}/\text{cm}^{-1}$	$0.96 \omega/\text{cm}^{-1}$
TH	3631	3642
TH-TH	3609	3624
w-TH	3534	3510
TH-T	3449	3429
TH-T	3418	3412
TH-TH	≈ 3230	3237

Tab. 4.11: Experimentally observed OH stretching wavenumbers $\tilde{\nu}$ compared to harmonic B3LYP-D3(BJ)/def2-TZVP predictions ω unscaled and scaled by 0.96 for all species including TH in figure 2 and 3 in the main document. The value in parentheses refers to an unlikely alternative assignment of the strong transition to the predicted third-most stable THo-Tp isomer, see Table 4.8.

Species	$\tilde{\nu}/\text{cm}^{-1}$	ω/cm^{-1}	$0.96 \omega/\text{cm}^{-1}$
THo	3631	3794	3642
THo-THo (accep.)	3609	3775	3624
w-TH	3534	3656	3510
THo-Tt (THo-Tp)	3449	3572 (3588)	3429 (3444)
THo-To	3418	3554	3412
THo-THo (don.)	≈ 3230	3372	3237

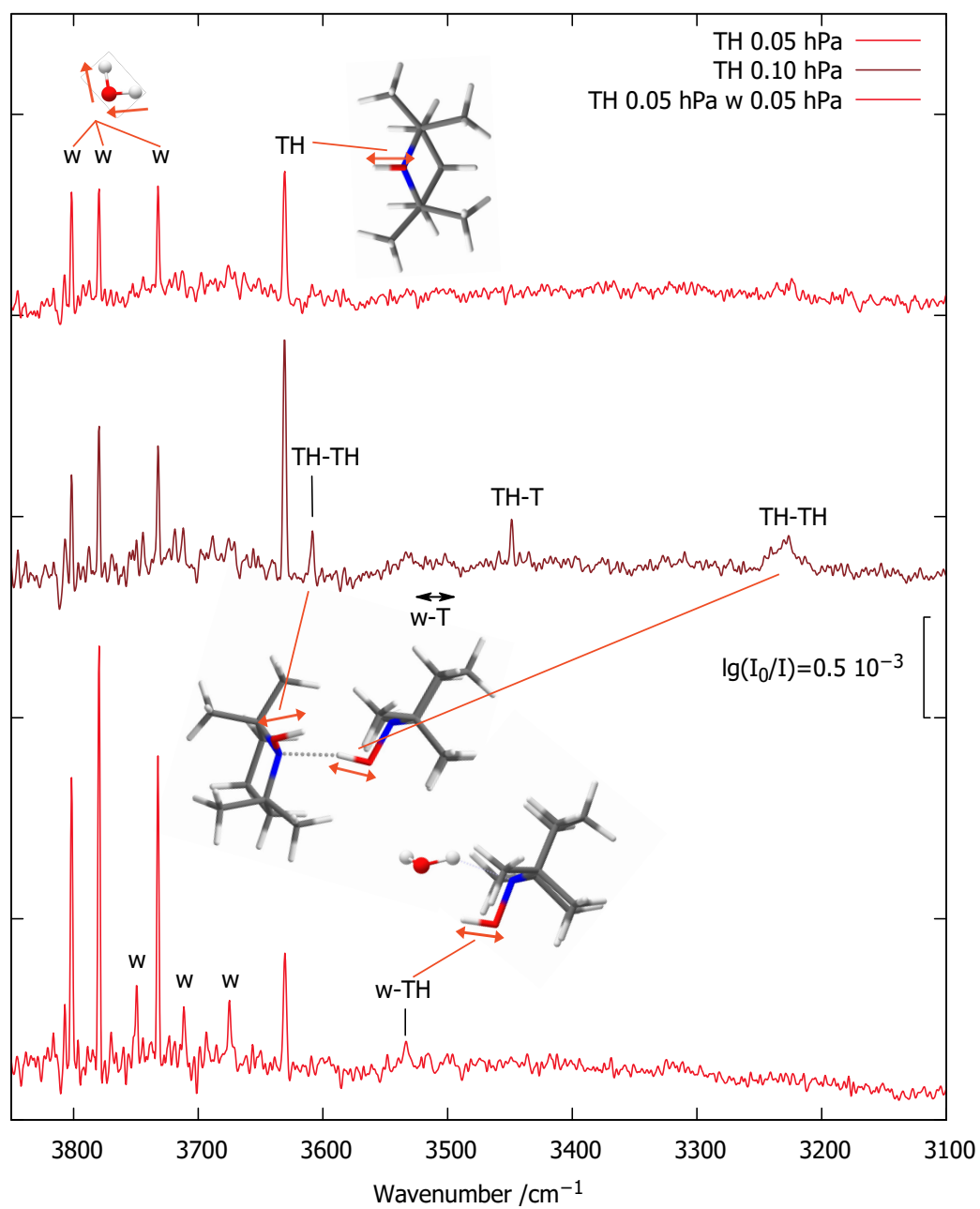


Fig. 4.9: FTIR spectra of TH in He with and without additional water.[79]

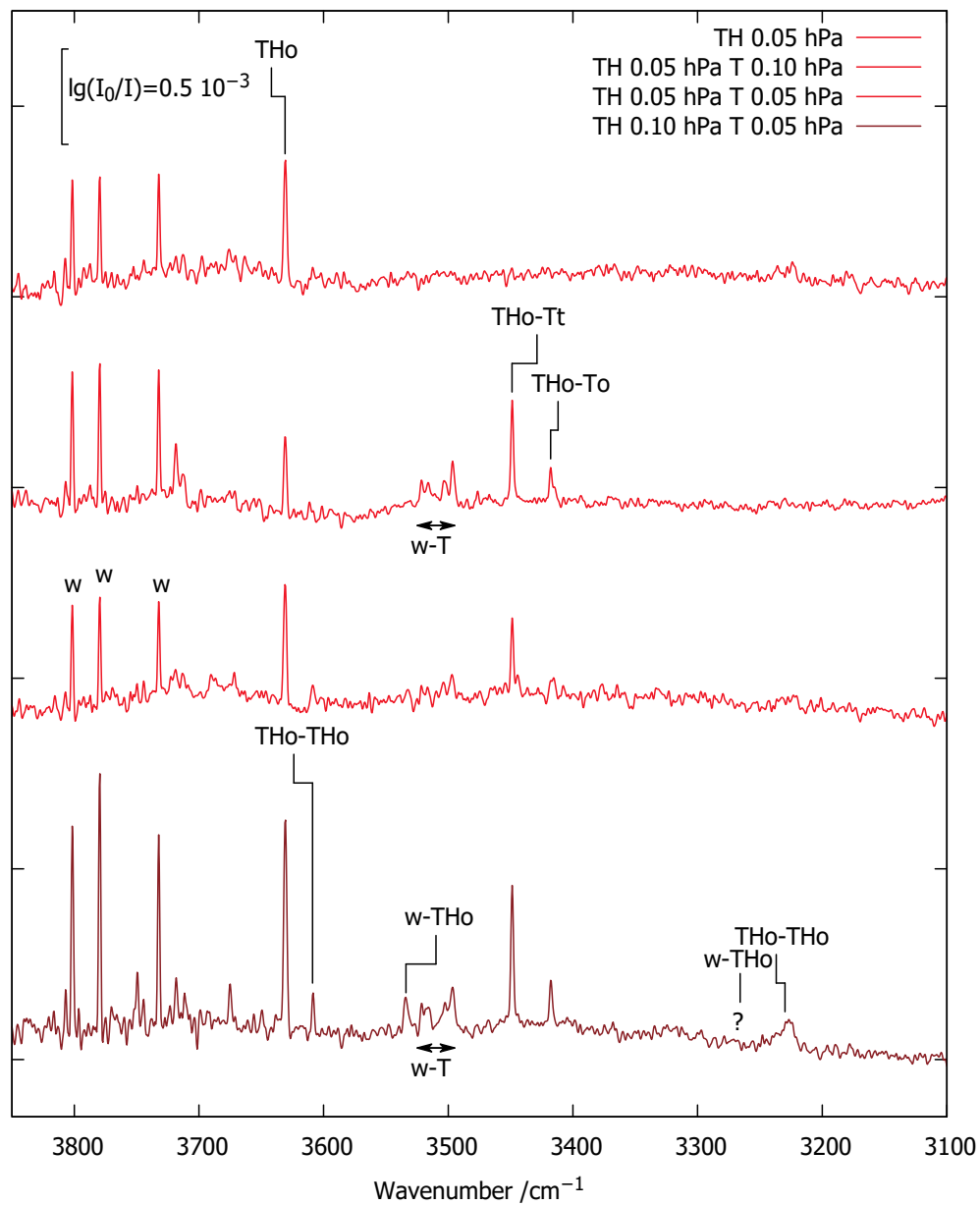


Fig. 4.10: FTIR spectra of TH and T in different concentrations expanded in 750 mbar He. [79]

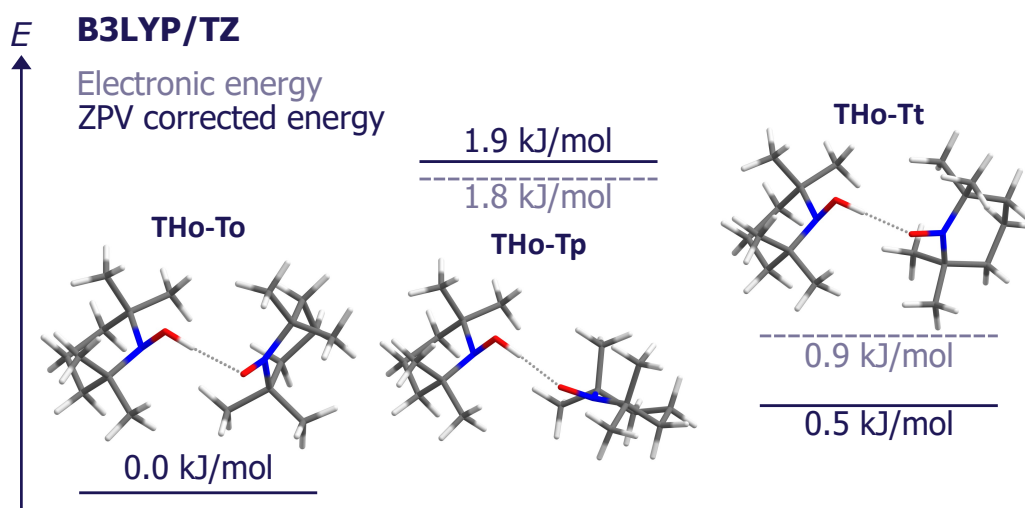


Fig. 4.11: THo-Tx (x=o,p,t) minimum structures one B3LYP-D3(BJ)/def2-TZVP level of theory. Lines are showing the energy with (dark blue solid line) and without ZPVE correction (light blue dotted line) relative to each other.[79]

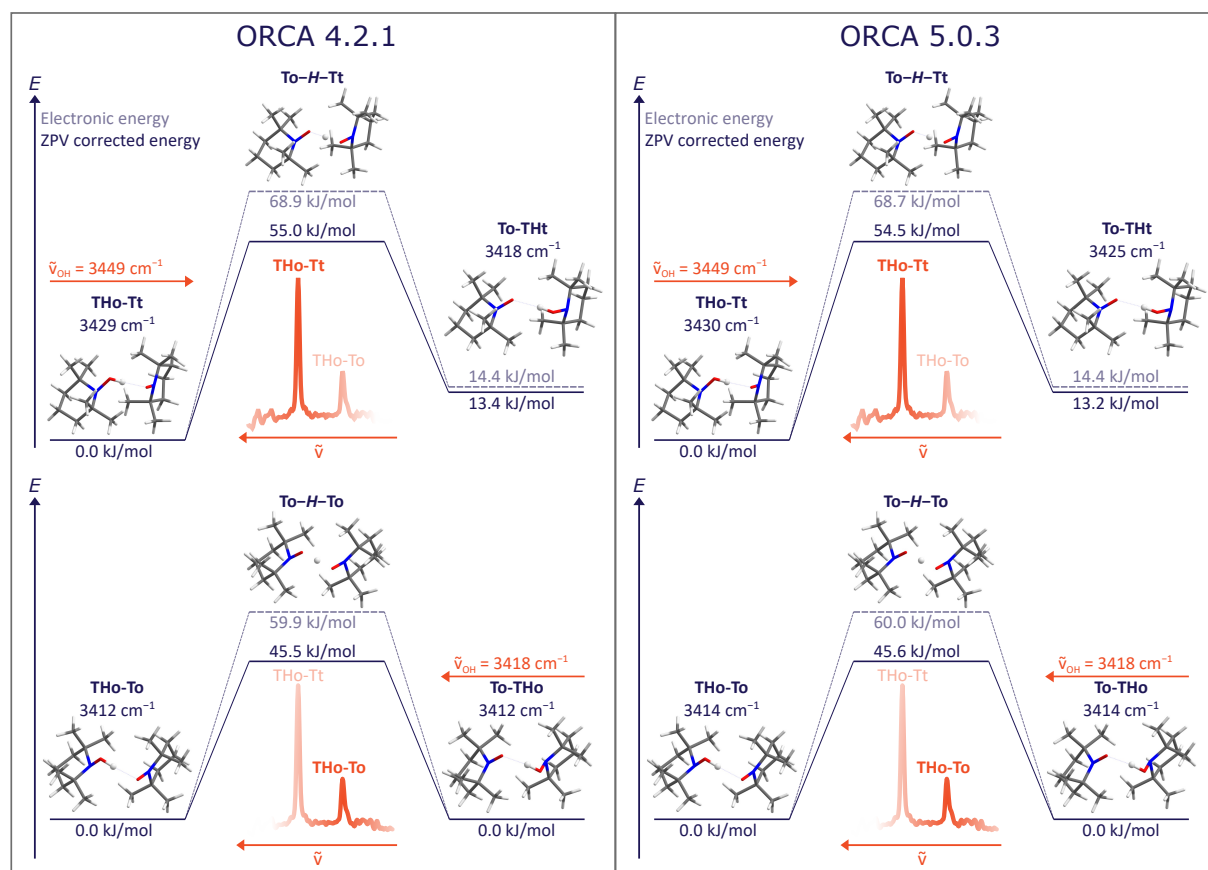


Fig. 4.12: Results of the optimization after a NEB scan followed by a TS search on B3LYP-D3(BJ)/def2-TZVP level of theory performed for the THo-Tt and the THo-To complexes in ORCA 4.2.1 and ORCA 5.0.2.[79]

5 The HyDRA Blind Challenge

5.1 Implementation of the Blind Challenge

As already discussed in the introduction benchmarking quantum numerical methods using experiments is important but challenging for both sides. The most difficult part is to find matching conditions for simulations and experiment and a property which can be derived by both sides. In order to provide an unbiased benchmarking opportunity for theory groups a blind challenge was organized. The goal was to predict the shift of the symmetric water OH stretching vibration (3657 cm^{-1} [11]) when binding to an organic molecule ($\text{OH}_{\text{sym}} - \text{OH}_{\text{b}}$). If the OH shift would match the spectral range of the b2lib resonance, information on the potential b2lib resonance could be added to the corresponding submission. The groups could also voluntarily submit data on water isotopes (D_2O , H_2^{18}O).

The procedure that was followed for the so-called HyDRA blind challenge is described in [29, 83]. The key aspects will be described here as well as the experimental results (available as electronic supplement in [84] and [85]), while the analysis of the performance of the participating groups can be found in the corresponding publication [84]. The analysis and evaluation of the theory submissions was mostly conducted by Prof. Dr. Ricardo Mata and Dr. Benjamin Schröder.

As a first step and in order to provide a training set for the theory groups we asked vibrational spectroscopy groups for their already published data on monohydrates of organic molecules. Then the data was curated by a team of two professors (Anne Zehnacker-Rentien and Martin Suhm), a bachelor student (Margarethe Bödecker), and me. The criteria the data had to match was:

- coverage of a moderate OH shift wavenumber range to prevent further resonances
- chemical diversity (size, functional groups, and elements)
- different experimental techniques

- water as donor molecule
- signal assignment unambiguous
- examples for b2lib resonance should be included
- unique 1:1 conformer
- global minimum
- isotope data available
- less than 100 e⁻ (not too large)
- lowest monomer vibration > 30 cm⁻¹ (limited monomer flexibility)

All submissions from vibrational spectroscopy groups can be found on the qmbench.net website [86]. The selected molecules for the training set are shown in Figure 5.1 and the Table 5.1 is giving the full name of the training set candidates, the corresponding abbreviation, and CAS registry number, the experimental OH_b stretching vibration, and the OH shift (Δ_b). The values in parenthesis are an error estimate and the values in square brackets the deperturbed values if a b2lib resonance is observed. More details of the selection process can be found in [83].

For the test set similar selection criteria as for the training set were applied, except that the hydrates should not be vibrationally characterized yet. Also the limitations from the experimental FTIR setup had to be taken into account (volatile compounds). Because of the criteria of a small number of conformers and the water acting as donor in the minimum structure, it is desirable to pick substances which are characterized by rotational spectroscopy as it can provide conformational information as well as relative energies.[94–97]. Therefore rotational spectroscopy groups were asked for their suggestions of acceptor molecules to study with vibrational spectroscopy. After some first experimental tests and a structural search with CREST and an optimization on B3LYP-D3(BJ)/def2-TZVP level of theory the decision on the final test set was made by the same committee as for the training set. The test set is shown in Figure 5.2 and the chemicals with their abbreviation, BC (blind challenge) codes, CAS registry number and number of expected OH stretching vibrations are listed in Table 5.2. All the data about which candidates are discussed and all experimental tests had to be kept secret to make the blind challenge a fair competition between theoretical methods, which is why the molecule candidates got code names and not even my colleagues knew what measurements were conducted.

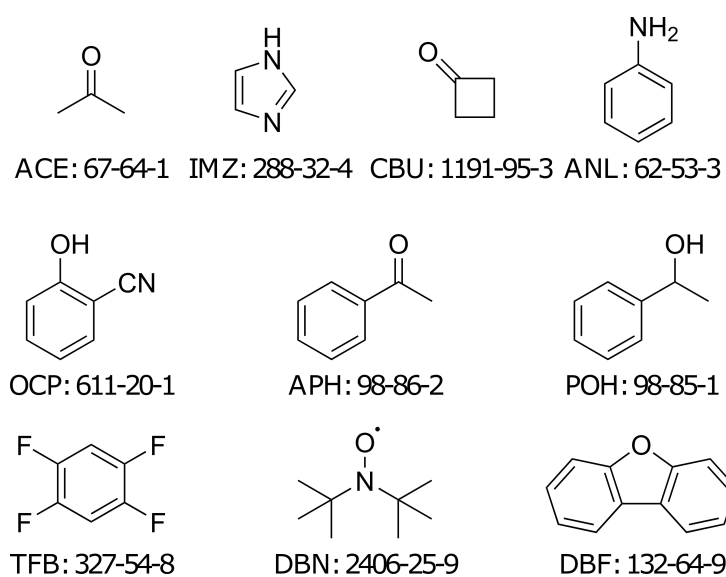


Fig. 5.1: Training set for the HyDRA blind challenge showing the structure, abbreviation, and CAS number.[83]

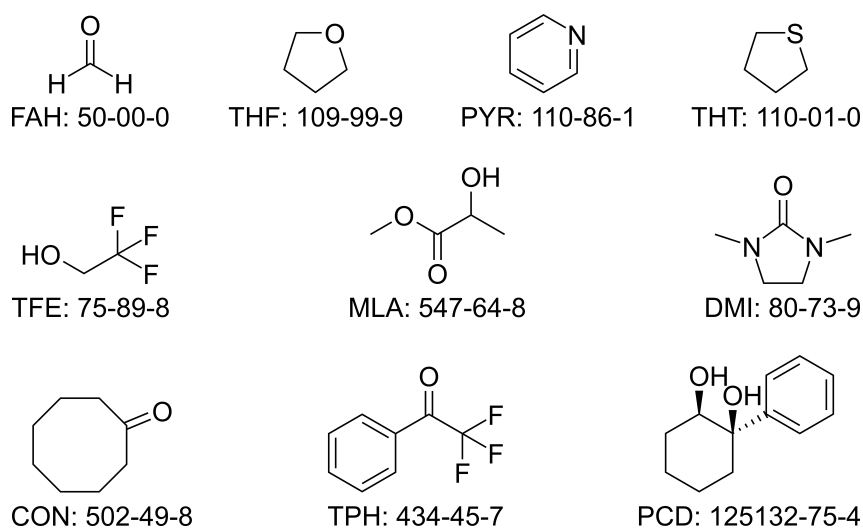


Fig. 5.2: Test set for the HyDRA blind challenge showing the structure, abbreviation, and CAS number.[83]

Tab. 5.1: The molecules abbreviations (abbr.), CAS registry numbers (CAS RN) and published experimental OH_b -wavenumbers $\tilde{\nu}_{\text{exp}}(\text{OH}_b)$ (with estimated uncertainty in parentheses) of the acceptor molecules in the monohydrates selected for the training set. In square brackets, estimated deperturbed OH_b wavenumbers after removal of a three-quantum resonance (see text) are provided. These wavenumbers in brackets should be targeted by vibrational models which do not include such an anharmonic resonance. Where the resonance remains hypothetical, the deperturbed wavenumber uncertainty (in parentheses) spans the experimentally observed main transition wavenumber. Also provided are downshifts $\Delta_{\text{OH}}/\text{cm}^{-1}$ (positive, if the complex has a lower wavenumber) from the water monomer fundamental at 3657 cm^{-1} . [83]

acceptor molecule	abbr.	CAS RN	$\tilde{\nu}_{\text{exp}}(\text{OH}_b)$ cm^{-1}	Δ_{OH} cm^{-1}
Acetone[87]	ACE	67-64-1	3538(1) [3531(2)]	119(1) [126(2)]
Acetophenone[87]	APH	98-86-2	3536(1) [3530(2)]	121(1) [127(2)]
Aniline[88]	ANL	62-53-3	3524(1) [3526(3)]	133(1) [131(3)]
Cyclobutanone[87]	CBU	1191-95-3	3548(1)	109(1)
Dibenzofuran[89]	DBF	132-64-9	3623(1)	34(1)
Di- <i>tert</i> -butyl nitroxide[20]	DBN	2406-25-9	3484(2) [3487(4)]	173(2) [170(4)]
Imidazole[90]	IMZ	288-32-4	3458(2)	199(2)
<i>o</i> -Cyanophenol[91]	OCP	611-20-1	3595(2)	62(2)
1-Phenylethanol[92]	POH	98-85-1	3620(2)	37(2)
1,2,4,5-Tetrafluorobenzene[93]	TFB	327-54-8	3647(1)	10(1)

After the decision on the final test set was published on the qmbench.net website and the measurement of the data was intensified. A list of all substances discussed and additional spectroscopic data that was recorded can be found in the Supplement 8.3 and 8.4.

Tab. 5.2: Test set of 10 acceptor molecules, their abbreviations, CAS registry numbers (CAS RN) and expected minimum number of OH stretching signals in the most stable monohydrate $n(\text{OH})$, among which the hydrogen-bonded water OH_b wavenumber $\tilde{\nu}_{\text{exp}}(\text{OH}_b)$ (or its downshift $\Delta_{\text{OH}} \text{ cm}^{-1}$ from the water monomer fundamental at 3657 cm^{-1}) should be predicted.[83]

acceptor molecule	abbreviation	CAS RN	$n(\text{OH})$
Cyclooctanone [98, 99]	CON	502-49-8	2
1,3-Dimethyl-2-imidazolidinone [100, 101]	DMI	80-73-9	2
Formaldehyde [102, 103]	FAH	50-00-0	2
Methyl lactate [104, 105]	MLA	547-64-8	3
1-Phenylcyclohexane-cis-1,2-diol [106]	PCD	125132-75-4	4
Pyridine [107, 108]	PYR	110-86-1	2
Tetrahydrofuran [109, 110]	THF	109-99-9	2
Tetrahydrothiophene [111]	THT	110-01-0	2
2,2,2-Trifluoroacetophenone [112]	TPH	434-45-7	2
2,2,2-Trifluoroethan-1-ol [104, 113]	TFE	75-89-8	3

5.2 Experimental Results

In the end all OH shifts for the test set could be obtained. Three different experimental setups were used, most substances were measured using the *gratin* jet spectroscopy setup [2], for two substances the Raman setup (so-called *curry* jet) was used [114] and for one measurement the UV/IR setup of the Zehnacker-Rentien group from France was used [115]. In the following the spectral data for all substances is presented and shortly discussed.

All chemicals used in the study are listed in Table 5.3.

Tab. 5.3: List of substances giving their abbreviations, CAS number, the supplier and purity.

Name	Code	BC Code	Supplier	Purity
(Para-)Formaldehyde	FAH	BC02	Alfa Aesar	97%
Pyridine	PYR	BC16	Sigma Aldrich	>99.9%
2,2,2-Trifluoroacetophenone	TPH	BC18	Sigma Aldrich	>99%
Tetrahydrofuran	THF	BC20	Sigma Aldrich	>99.9
Cyclooctanone	CON	BC22	Sigma Aldrich	98%
1,3-Dimethyl-2-imidazolidinone	DMI	BC27	Sigma Aldrich	reagent grade
Tetrahydrothiophene	THT	BC29	Sigma Aldrich	99%
Methyl lactate	MLA	BC30	Sigma Aldrich	98%
1-Phenylcyclohexane-cis-1,2-diol	PCD	BC36	Santa Cruz Biotechnology	99%
2,2,2-Trifluoroethan-1-ol	TFE	BC38	abcr	99%
D ₂ O			abcr	99.85%
Water- ¹⁸ O			Sigma-Aldrich	97%, 97% atom ¹⁸ O

5.2.1 Formaldehyde - BC02

We were surprised that there was no vibrational gas phase data on formaldehyde water available already as it is one of the smallest organic hydrates one could think of. This makes it a good candidate for the blind challenge as it is accessible to high level theory methods. To fill in the substance into the jet, the vessel with paraformaldehyde was carefully heated with a heat gun until the desired partial pressure in the reservoir was reached. Attempts to use a commercially available formaldehyde in aqueous solution failed as the vapor pressure of water was much higher and only water was observed in the spectrum. The spectra shown in Figure 5.3 were recorded using the *gratin* jet spectroscopy setup using the concentrations/partial pressures listed in Table 5.4 and the chemicals in Table 5.3.

In the upper panel of Figure 5.3 the upper two spectra are showing formaldehyde (BC02) water spectra in different concentrations. As in previous spectra the water monomer is labeled w. One signal at 3591 cm^{-1} scaling with the concentration of BC02 can be assigned to the heterodimer and is labeled OH_b . In addition a spectrum of pure water is shown in gray, to prove that the signal does not belong to the water dimer signal which is labeled with a triangle. When the signal position of the jet spectrum is compared to OH_b vibrations derived from matrix isolation experiments, in which the signal position is shifted towards lower wavenumbers and is split due to environmental effects, the values in Ne are 3580 and 3685 cm^{-1} and 3573 and 3578 cm^{-1} in N_2 and lie at an expected position relative to the gas phase signal.[102, 116]

As a further step the jet spectrum of BC02 with D_2O was measured. It is depicted in the lower panel together with a pure D_2O spectrum, as again the water dimer lies close to the mixed dimer. The BC02+ D_2O signal lies at 2629 cm^{-1} .

The structure search with CREST and later optimization on B3LYP-D3(BJ)/def2-TZVP only predict one stable 1:1 conformer, which is in good agreement with previous theoretical studies [117–119] and data from rotational spectroscopy [103].

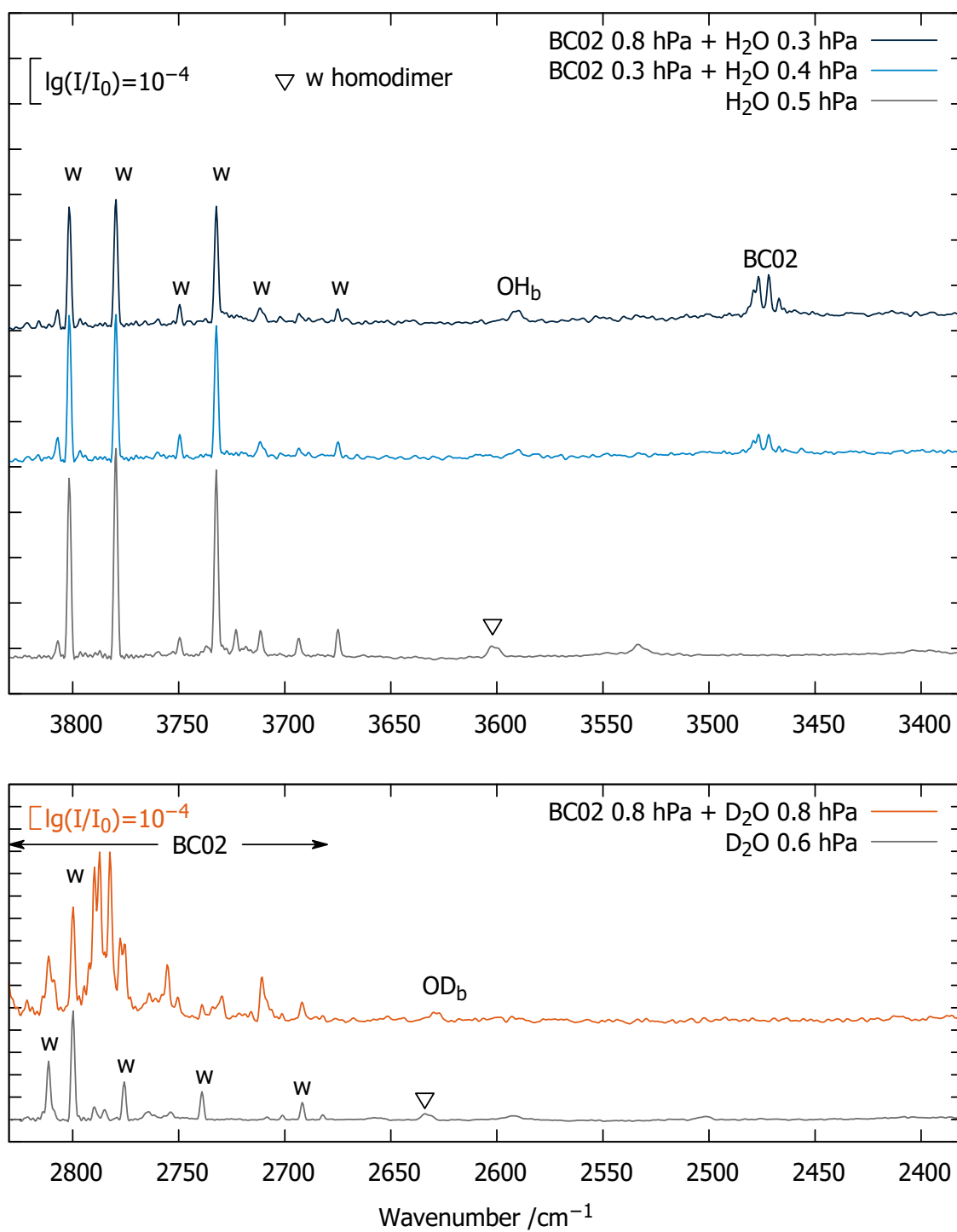


Fig. 5.3: FTIR spectrum of formaldehyde with water using 750 mbar He as carrier gas using H₂O in the upper panel (blue) and D₂O in the lower panel (orange). Pure water isotope spectra are shown in gray.[84]

Tab. 5.4: Experimental details on the spectroscopic data on formaldehyde (BC02) water giving the spectral identifiers ([yyyymmdd]-[averaged spectra]), the partial pressures, stagnation pressure and color in the spectrum.[84] The water spectra are taken from [2].

identifier	# pulses	$\frac{p(\text{BC02})}{\text{hPa}}$	$\frac{p(\text{H}_2\text{O})}{\text{hPa}}$	$\frac{p(\text{He})}{\text{hPa}}$	note
20211126-abcd	800	0.7	0.4	750	see figure 5.3, upper panel, black
20211125-abcd	800	0.3	0.4	750	see figure 5.3, upper panel, blue
[2] (Ne)	2200	0.0	0.5	750 Ne	see figure 5.3, upper panel, grey
20220119-ad+0120-abde	400	0.7	0.8D	750	see figure 5.3, lower panel, orange
[2] (Ne)	1950	0.0	0.6D	750 Ne	see figure 5.3, lower panel, grey

5.2.2 Pyridine - BC16

As for BC02 the theoretical predictions only expected one dominant 1:1 hetero dimer signal. The water is binding to the nitrogen atom in the ring and not to the π system. The FTIR spectra shown in Figure 5.4 were recorded using the *gratin* jet spectroscopy setup using the concentrations/partial pressures listed in Table 5.5 and the chemicals in Table 5.3. In the upper panel the water concentration was varied while the BC16 concentration was kept constant. The signal labeled OH_b was identified as hetero dimer signal and lies at 3454 cm^{-1} . Another measurement with D_2O was performed and the OD_b peak was assigned at 2541 cm^{-1} . As side effect of the isotope exchange between H_2O and D_2O , the signals for the OH_b and OD_b signal for the mixed DOH species could also be assigned at 3464 and 2549 cm^{-1} (not shown in spectrum).

The signal positions agree with a warm gas phase spectrum in which the signal lies at higher wavenumbers [120] and a recent study of the system does not show the spectral range of interest [107]. For the related imidazole water complex the helium nanodroplet wavenumber lies at slightly lower wavenumbers [121] compared to the jet cooled wavenumber [90] due to environmental effects. The literature value for the molecular system in an Ar matrix was found to be at 3400 cm^{-1} [122] and an IR-UV study could not identify the relevant signal because a tagging agent was needed, but not stable [123]. One can point out, that the non-size selective method is simple, but can securely give the wavenumber without environmental effects.

Tab. 5.5: Experimental details on the spectroscopic data on pyridine (BC16) water giving the spectral identifiers ([yyyymmdd]-[averaged spectra]), the partial pressures, stagnation pressure and color in the spectrum.[84]

identifier	# pulses	$p(\text{BC16})$ hPa	$p(\text{H}_2\text{O})$ hPa	$p(\text{He})$ hPa	note
20210503-abcdefg	700	0.2	0.1	750	see figure 5.4, dark blue
20211013-abcde	800	0.2	0.3	750	see figure 5.4, light blue
20210511-abcdefg	800	0.3	0.3	750	not shown, similar to light blue
20210512-abgh+0510-ef	300	0.3	0.3D	750	see figure 5.4, orange

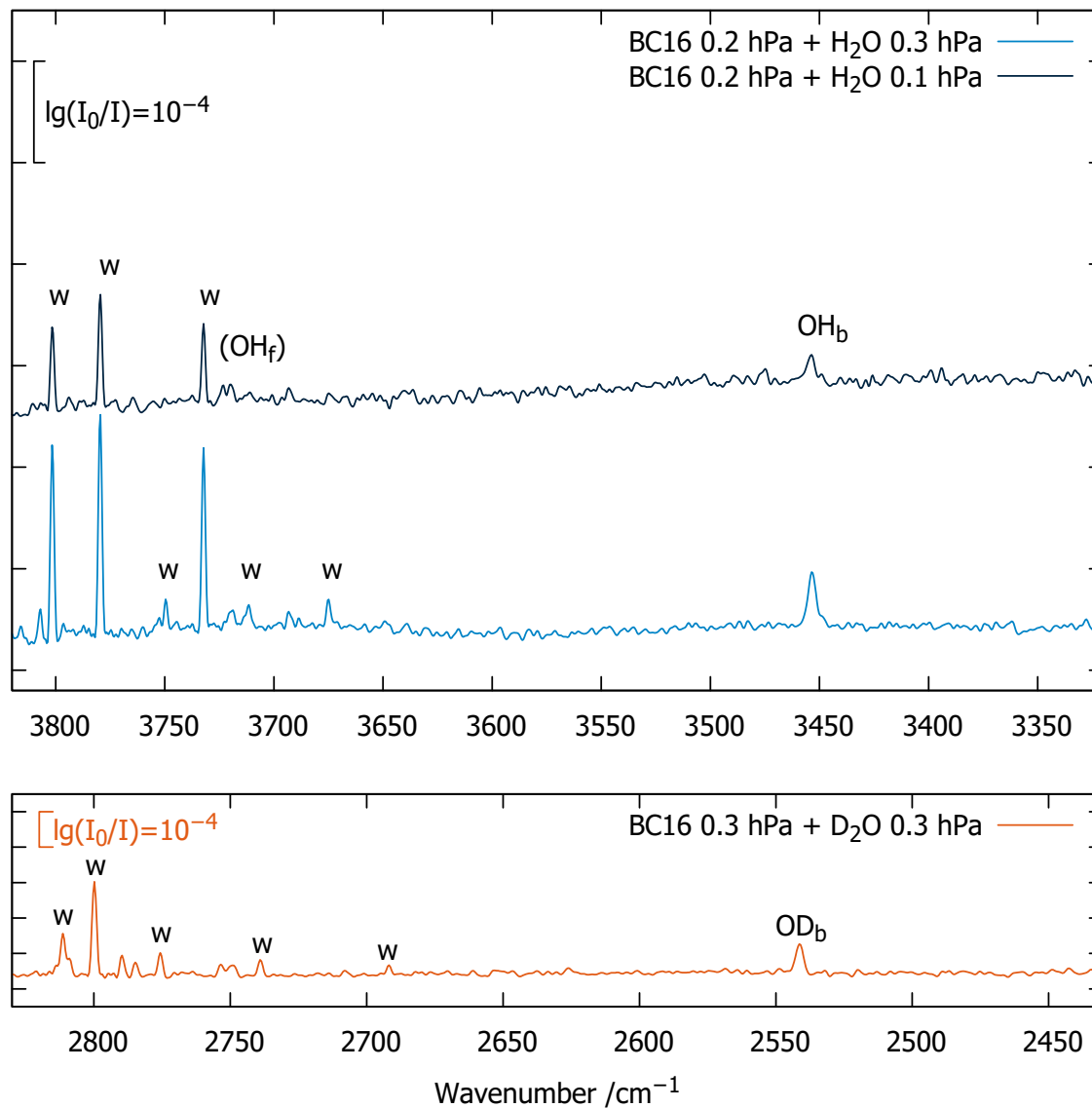


Fig. 5.4: FTIR spectrum of pyridine with water using 750 mbar He as carrier gas using H₂O in the upper panel (blue) and D₂O in the lower panel (orange).[84]

5.2.3 2,2,2-Trifluoroacetophenone - BC18

For the 2,2,2-trifluoroacetophenone (BC18) one can think of two different hetero dimer structures, as the water could potentially bind to both of the sides of the asymmetric ketone. Theory predictions on B3LYP-D3(BJ)/def2-TZVP level and a rotational spectroscopic investigation [112] suggest only one stable conformer. The experiments were conducted using the *gratin* jet spectroscopy setup and the experimental details can be found in Table 5.6. The spectra in Figure 5.5 only show one dominant hetero dimer signal, which scales with the water concentration and is therefore labeled OH_b. This is in good agreement with the theory predictions and [112]. The OH_b peak lies at 3611 cm⁻¹. At lower wavenumbers (at approximately 3450 cm⁻¹) the overtone of the C=O stretching vibration is visible.

Tab. 5.6: Experimental details on the spectroscopic data on 2,2,2-trifluoroacetophenone (BC18) water giving the spectral identifiers ([yyyymmdd]-[averaged spectra]), the partial pressures, stagnation pressure and color in the spectrum.[84]

identifier	# pulses	$p(\text{BC18})$ hPa	$p(\text{H}_2\text{O})$ hPa	$p(\text{He})$ hPa	note
20210602-abcdefg	800	0.2	0.1	750	see figure 5.5, blue
20210603-abcdef	700	0.2	0.2	750	see figure 5.5, dark blue

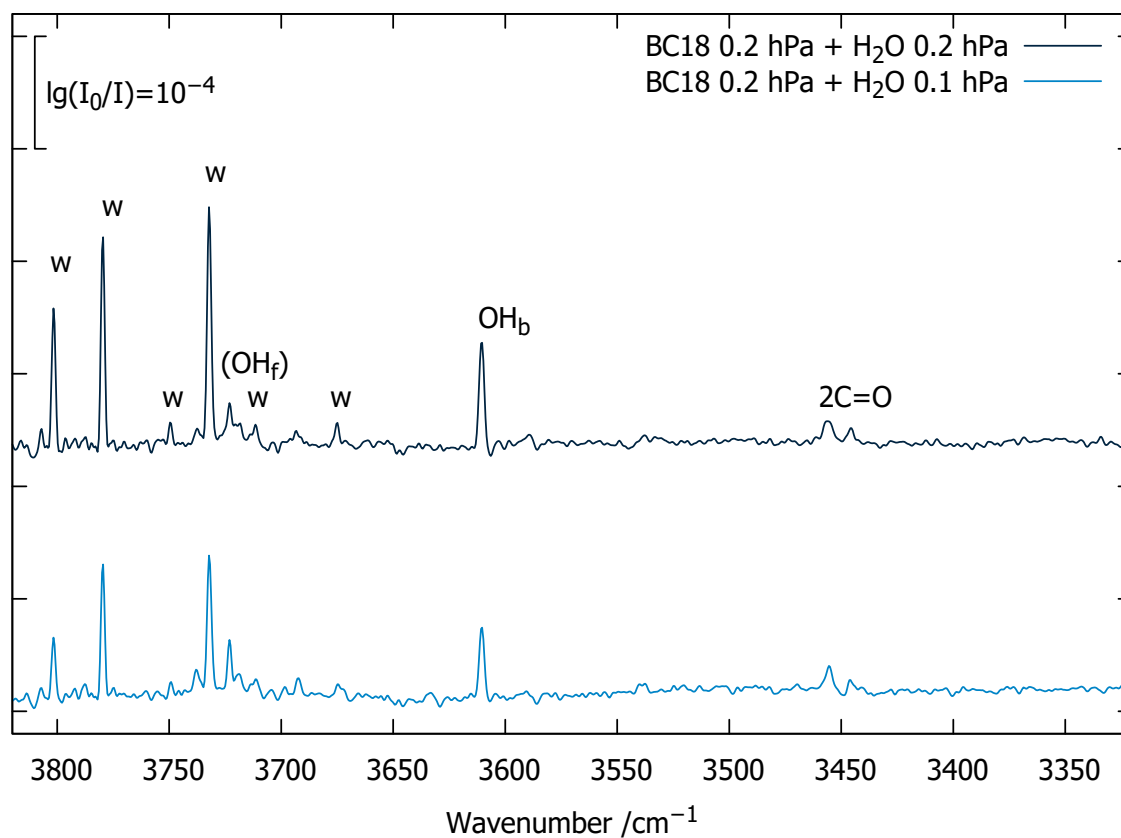


Fig. 5.5: FTIR spectrum of 2,2,2-trifluoroacetophenone with water using 750 mbar He as carrier gas.[84]

5.2.4 Tetrahydrofuran - BC20

For tetrahydrofuran (BC20) our theoretical structure search with CREST and later optimization on B3LYP-D3(BJ)/def2- level of theory and previous theoretical studies [110] predict one stable hetero dimer structure. When looking into the spectra in Figure 5.6 one can identify one stable hetero dimer conformer as well, which lies at 3491 cm^{-1} for water (upper panel in Figure 5.6) and at 2568 cm^{-1} for D_2O (lower panel in Figure 5.6). The spectrum is not complicated by pseudo rotation, that was observed in [109, 124]. The *gratin* jet spectroscopy setup was used to record the spectra and more data on the shown spectra can be found in Table 5.7.

Tab. 5.7: Experimental details on the spectroscopic data on tetrahydrofuran (BC20) water giving the spectral identifiers ([yyyymmdd]-[averaged spectra]), the partial pressures, stagnation pressure and color in the spectrum.[84]

identifier	# pulses	$\frac{p(\text{BC20})}{\text{hPa}}$	$\frac{p(\text{H}_2\text{O})}{\text{hPa}}$	$\frac{p(\text{He})}{\text{hPa}}$	note
20211012-abcde2	800	0.2	0.2	750	see figure 5.6, dark blue
20210831-abcdf	900	0.1	0.1	750	see figure 5.6, blue
20210901-abcde	800	0.1	0.25	750	see figure 5.6, light blue
20210526-abgh+0527-abgh	400	0.2	0.2D	750	see figure 5.6, orange

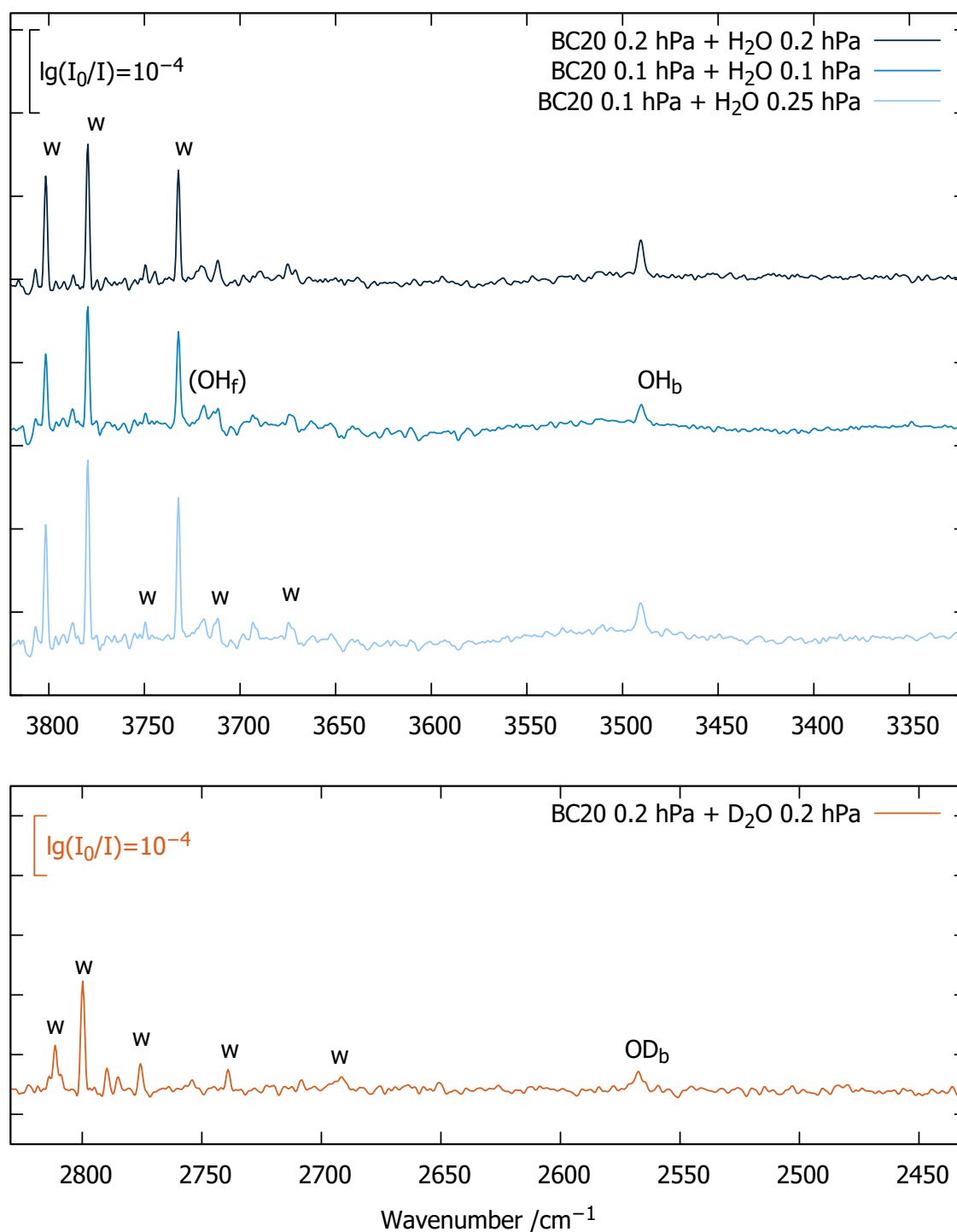


Fig. 5.6: FTIR spectrum of tetrahydrofuran with water using 750 mbar He as carrier gas using H₂O in the upper panel (blue) and D₂O in the lower panel (orange).[84]

5.2.5 Cyclooctanone - BC22

Cyclooctanone (BC22) was one of the more tricky candidates even though the spectrum in Figure 5.7 shows two potential hetero dimer conformers with H₂O and D₂O as expected from theory predictions. But the main signal at 3503 cm⁻¹ is in a range where a b2lib resonance would be expected, and other familiar compounds like cyclohexanone and cycloheptanone (see Chapter 3) are showing a b2lib resonance. In order to find out if the two signals are two conformers different carrier gas mixtures were tried in order to relax one signal. Unfortunately the minor signal at 3525 cm⁻¹ is much smaller and it is hard to evaluate whether the relative intensity ratio is changing. Higher BC22 concentrations could not be used, as larger clusters start to be present in the spectrum. A measurement with D₂O showing two signals as well is a strong indicator that the second signal belongs to another conformer and not a b2lib resonance, which is why the signals are labeled OH_b and OH_{b2} (, and OD_{b1} + OD_{b2} respectively). The main signal in the BC22+D₂O spectrum lies at 2587 cm⁻¹ and the minor peak at 2599 cm⁻¹. All spectroscopic data was recorded using the *gratin* jet spectroscopy setup and additional details on the shown spectra can be found in Table 5.8.

A controversial finding comes from microwave spectroscopy, where evidence for a reaction of cyclooctanone and water to a geminal diol was reported [99].

Tab. 5.8: Experimental details on the spectroscopic data on cyclooctanone (BC20) water giving the spectral identifiers ([yyyymmdd]-[averaged spectra]), the partial pressures, stagnation pressure and color in the spectrum.[84]

identifier	# pulses	$p(\text{BC22})$ hPa	$p(\text{H}_2\text{O})$ hPa	$p(\text{He})$ hPa	note
20211015-abcd	700	0.1	0.2	750	see figure 5.7, dark blue
20211014-abcde	800	0.1	0.1	750	see figure 5.7, blue
20210430-abcde	500	0.1	0.1	375 Ne	see figure 5.7, light blue
20210426-a+0427-ag	150	0.2	0.2D	750	see figure 5.7, orange

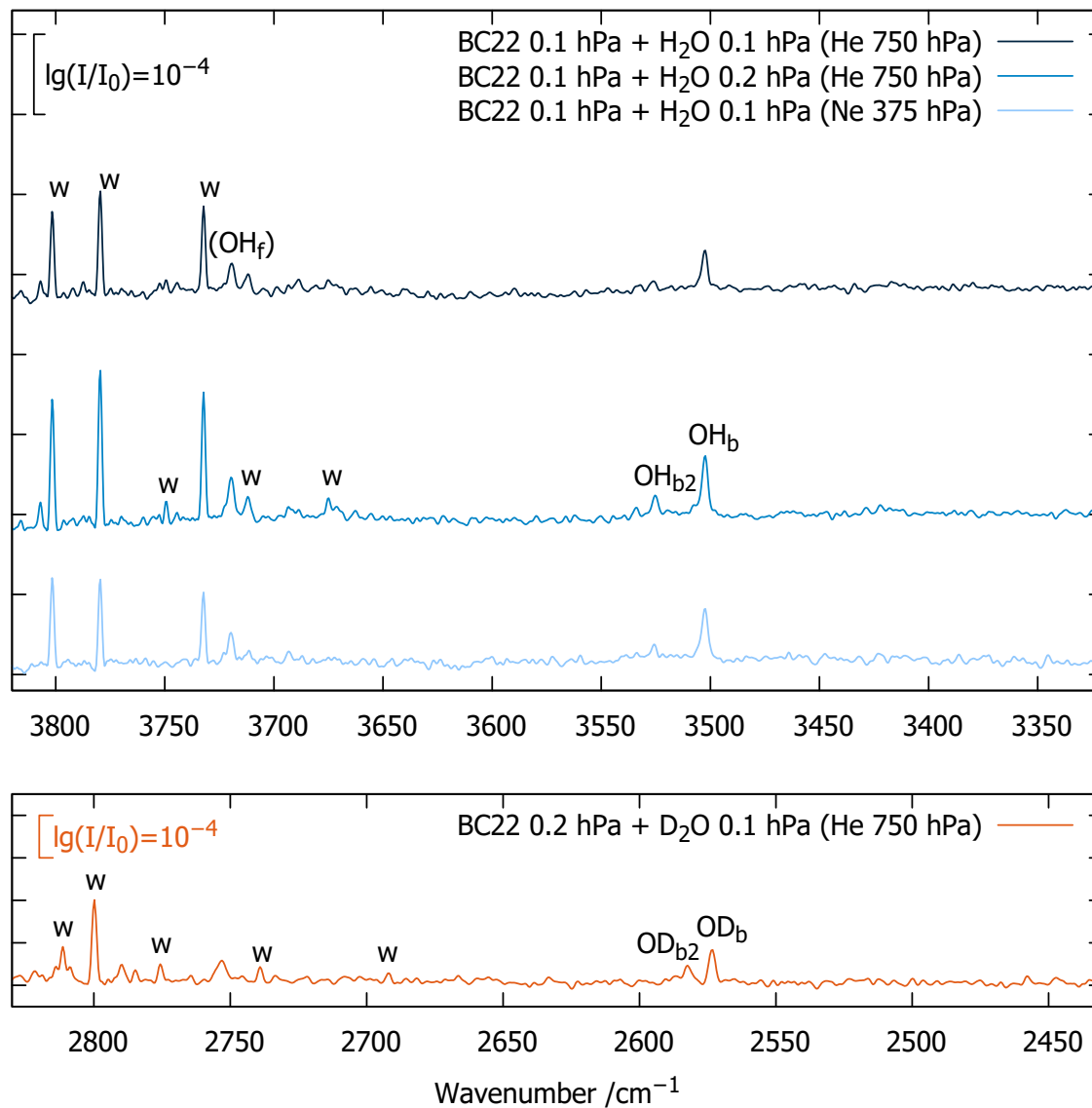


Fig. 5.7: FTIR spectrum of cyclooctanone with water using 750 mbar He or 375 mbar Ne as carrier gas using H₂O in the upper panel (blue) and D₂O in the lower panel (orange).[84]

5.2.6 1,3-Dimethyl-2-imidazolidinone - BC27

The 1,3-dimethyl-2-imidazolidinone (BC27) was picked to widen the range of functional groups and the related species tetramethylurea which was investigated in Till Wagners thesis only showed one stable conformation of the hetero dimer [69]. It is also interesting for microwave spectroscopy as it is a relatively rigid molecule. The theory predicts only one stable conformer and the spectra in Figure 5.8 do only show one signal scaling with the water and BC27 concentration at 3492 cm^{-1} . This makes the signal assignment clear. The *gratin* jet spectroscopy setup was used to record the spectra and more details on the shown spectra can be found in Table 5.9. A study of the 1:1 complex in CCl_4 gives a wavenumber of 3490 cm^{-1} and 3431 cm^{-1} in 1,2-dichloroethane.[100] Both values are close to the recorded jet cooled gas phase value.

Tab. 5.9: Experimental details on the spectroscopic data on 1,3-dimethyl-2-imidazolidinone (BC27) water giving the spectral identifiers ([yyyymmdd]-[averaged spectra]), the partial pressures, stagnation pressure and color in the spectrum.[84]

identifier	# pulses	$\frac{p(\text{BC27})}{\text{hPa}}$	$\frac{p(\text{H}_2\text{O})}{\text{hPa}}$	$\frac{p(\text{He})}{\text{hPa}}$	note
20210625-edef	500	0.15	0.03	750	see figure 5.8, dark blue
20210812-abcdefg	800	0.1	0.1	750	see figure 5.8, blue

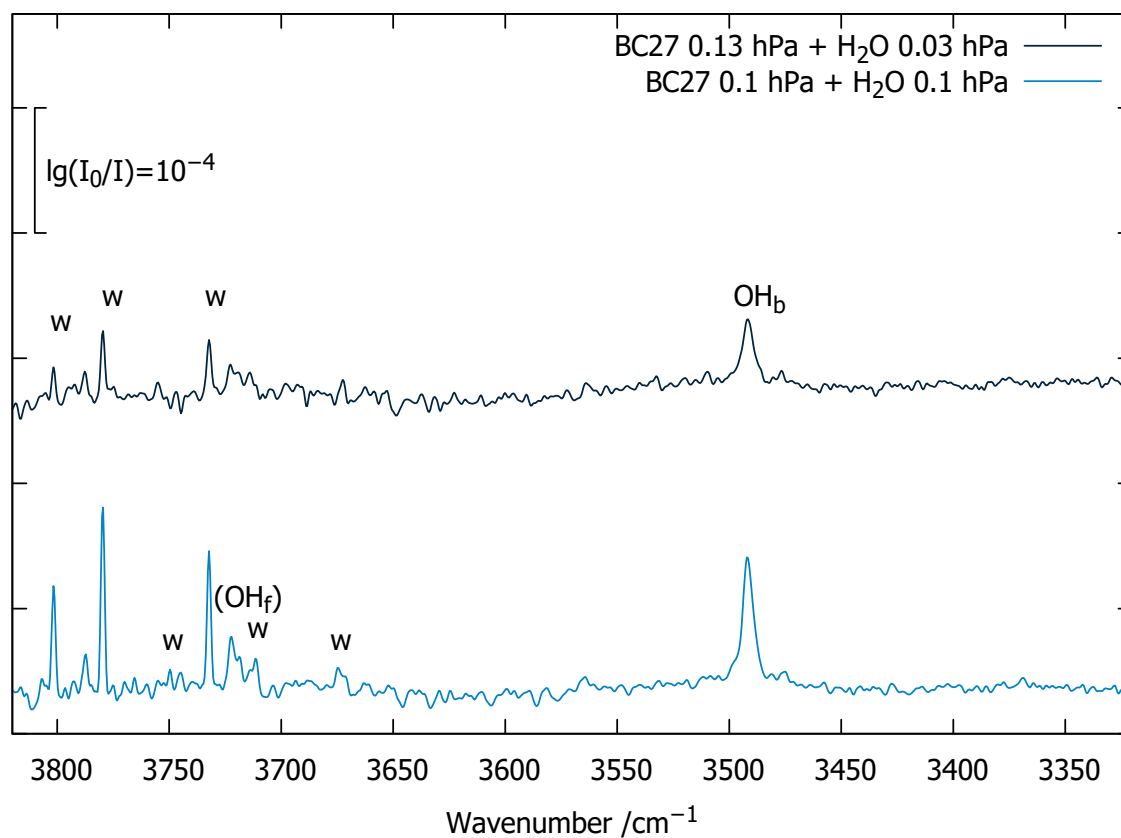


Fig. 5.8: FTIR spectrum of 1,3-dimethyl-2-imidazolidinone with water using 750 mbar He as carrier gas.[84]

5.2.7 Tetrahydrothiophene - BC29

To include heavier atoms in the blind challenge the sulfur compound tetrahydrothiophene was examined. Again, theory only predicts one signal. This agrees with the spectral data, that is showing one signal scaling with the water and BC29 concentration and corresponds to the hetero dimer (see OH_b in Figure 5.9) at 3507 cm^{-1} . The data was collected using the *gratin* jet spectroscopy setup and more information on the depicted spectra can be found in 5.10. The signal assignment is clear and the number of observed conformers aligns with structural assignment from rotational spectroscopy [111].

Tab. 5.10: Experimental details on the spectroscopic data on tetrahydrothiophene (BC29) water giving the spectral identifiers ([yyyymmdd]-[averaged spectra]), the partial pressures, stagnation pressure and color in the spectrum.[84]

identifier	# pulses	$\frac{p(\text{BC29})}{\text{hPa}}$	$\frac{p(\text{H}_2\text{O})}{\text{hPa}}$	$\frac{p(\text{He})}{\text{hPa}}$	note
20210721-abcde	800	0.2	0.2	750	see figure 5.9, dark blue
20210722-abcde	700	0.2	0.25	750	see figure 5.9, blue

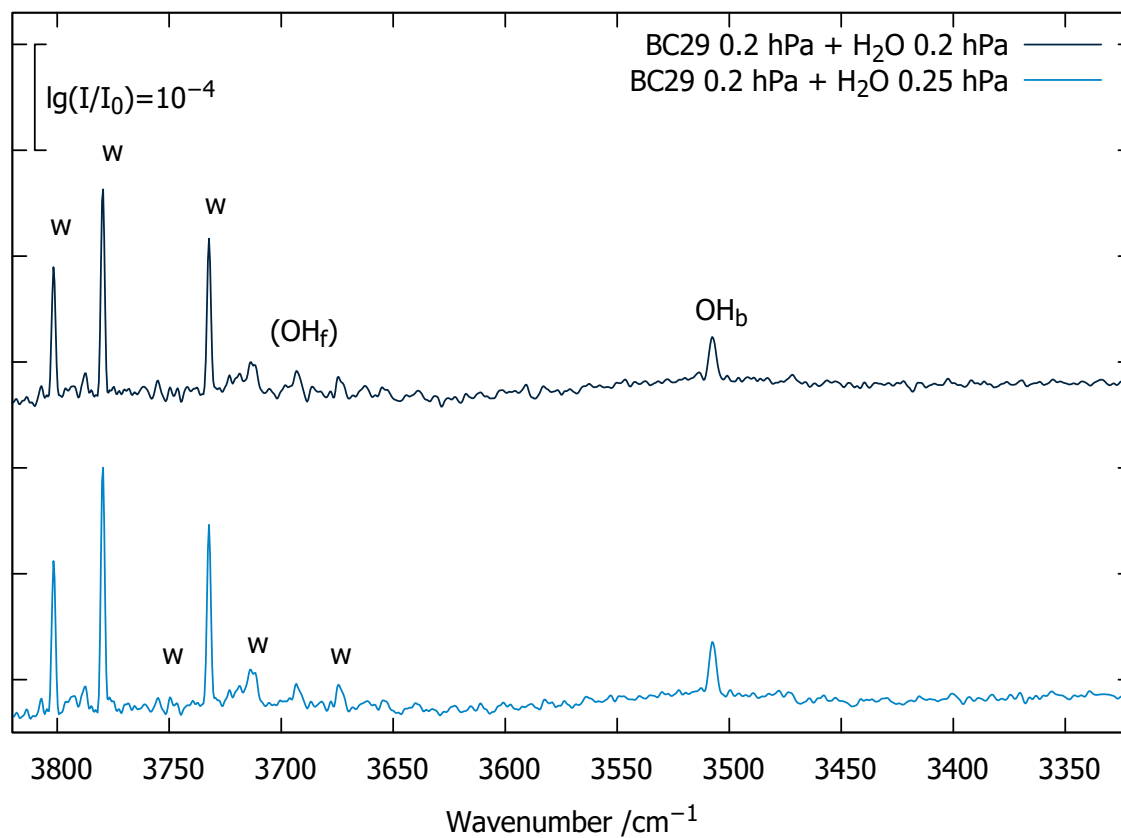


Fig. 5.9: FTIR spectrum of tetrahydrothiophene with water using 750 mbar He as carrier gas.[84]

5.2.8 Methyl lactate - BC30

Methyl lactate (BC30) was one of the most challenging compounds for the theory and the experimental side as it contains an OH group, has multiple docking sites for water and readily forms higher clusters with itself. To investigate the hydrates of BC30 IR (*gratin* jet spectroscopy setup) and Raman (*curry* jet setup) spectroscopy were used as complementary techniques, as well as ^{18}O water to ensure that the vibration belongs to water and not to the methyl lactate itself. In Figure 5.10 the Raman spectra are shown at the top (lighter tones) and the FTIR spectra at the bottom (darker tones). Spectra with ^{16}O -water are shown in blue, and spectra with ^{18}O -water in green. The experimental details are given in Table 5.11 and 5.12. The alcohols stretching vibration of BC30 is labeled BC30 and higher clusters of the pure compound are labeled with a triangle. Two signals with complementary intensity strength in IR and Raman can be identified as water signals as they are changing when ^{18}O -water is used. The signal at 3524 cm^{-1} is labeled OH_{b1} as it shifts by 8 cm^{-1} , while the peak at 3474 cm^{-1} only shifts by 5 cm^{-1} and is labeled OH_{b2} . As the water couples to the alcohol of the lactate, the strength of the shift is indicating how much water character the corresponding vibration has. The theory predictions on B3LYP-D3(BJ)/def2-TZVP level anticipate one most stable structure. The water seems to insert into the intramolecular OH bond between the alcohol and ketone group.[104] This action might be kinetically hindered, giving the conformations higher in energy a chance to form.[125] The spectral range of the OH_{b1} would fit the range for a b2lib resonance. Unfortunately BC30 is forming too many clusters with itself to securely identify a potential resonance.[126, 127] More experimental data is needed to evaluate the occurrence of a resonance. A spectrum of the hydrate of the related methyl 2-hydroxyacetate for comparison was recorded and is shown in the Supplement 8.3.4, but further work is needed before the work can be published.

Tab. 5.11: Experimental details on the Raman spectroscopic data on methyl lactate (BC30) + water giving the spectral identifiers ([yyyymmdd]-[averaged spectra]), the total detection duration t_{tot} of added recording, the a rough estimate of the partial pressures assuming saturated vapor at the mass flow controllers, the stagnation pressure and color in the spectrum.[84]

identifier	t_{tot} s	$p(\text{BC30})$ hPa	$p(\text{H}_2\text{O})$ hPa	$p(\text{He})$ hPa	note
Raman					
20211027-a	6000	0.5	1	700	^{16}O , see figure 5.10, blue
20211215-a	6000	0.5	1	700	^{18}O , see figure 5.10, green

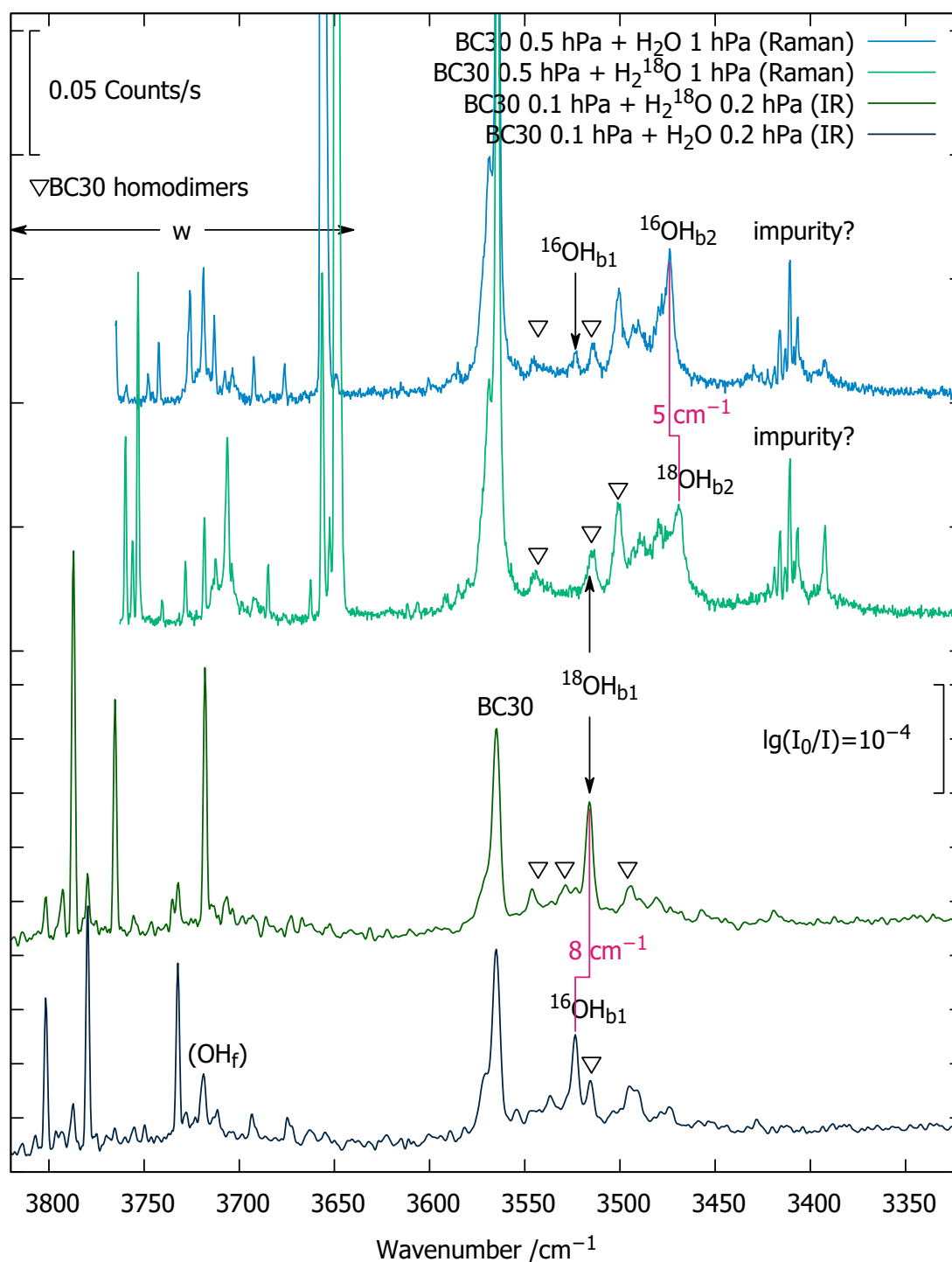


Fig. 5.10: Raman (lighter shades) and IR spectra (darker shades) of methyl lactate with ¹⁶O-water (blue tones) and ¹⁸O-water (green tones). Helium is used as carrier gas in both experiments and additional information on the spectra can be found in the Tables ??.[84]

Tab. 5.12: Experimental details on the IR spectroscopic data on methyl lactate (BC30) with water giving the spectral identifiers ([yyyymmdd]-[averaged spectra]), the partial pressures, stagnation pressure and color in the spectrum.[84]

identifier	# pulses	$\frac{p(\text{BC30})}{\text{hPa}}$	$\frac{p(\text{H}_2\text{O})}{\text{hPa}}$	$\frac{p(\text{He})}{\text{hPa}}$	note
IR 20210811-abcdef+0809-abcdef	600	0.1	0.2	750	¹⁸ O, see figure 5.10, dark green
20210810-abcdefg	800	0.1	0.2	750	¹⁶ O, see figure 5.10, dark blue

5.2.9 1-Phenylcyclohexane-cis-1,2-diol - BC36

The 1-phenylcyclohexane-cis-1,2-diol (BC36) was measured by the group of Prof. Anne Zehnacker-Rentien from France as it was not suited for our experimental setups. Their setup is allowing a size selective investigation of the complex using an IR-UV double resonance method [128, 129]. More information can be found in the Supplement of [84].

In Figure 5.11 depletion spectra are shown, with ^{16}O water in the upper spectrum and ^{18}O -water in the lower one. Jet cooled molecular clusters are ionized using an UV (ultra-violet) laser and the mass to charge ratio (m/z) is detected at a time of flight mass (TOF) detector. When the UV absorption maximum of the species of interest (here hydrate) is found, the UV wavelength is kept constant and the m/z ratio of the species is monitored over time while an additional IR laser comes into play. Whenever the IR excitation matches a vibrational frequency, the later UV excitation does no longer match the ionization energy and the signal in the TOF decreases. This is observed for four peaks in the OH stretching region. When comparing the spectra with the two different water isotopes one can observe, that two of them are not changing position (3542 and 3480 cm^{-1}) and they can be assigned to the OH groups of the diol. The other two signals change position, the one at higher wavenumber changes from 3722 to 3707 cm^{-1} when changing from ^{16}O - to ^{18}O -water and belongs to the OH_f vibration. The other signal shifting from 3597 to 3589 cm^{-1} is labeled OH_b . The experimental data in the figure is smoothed by 5-point smoothing.

The signal assignment is further supported by a study in which BC36 monomer was measured in CCl_4 solution, revealing signals close to the alcohols stretching vibrations in this spectrum at 3549 and 3586 cm^{-1} [106].

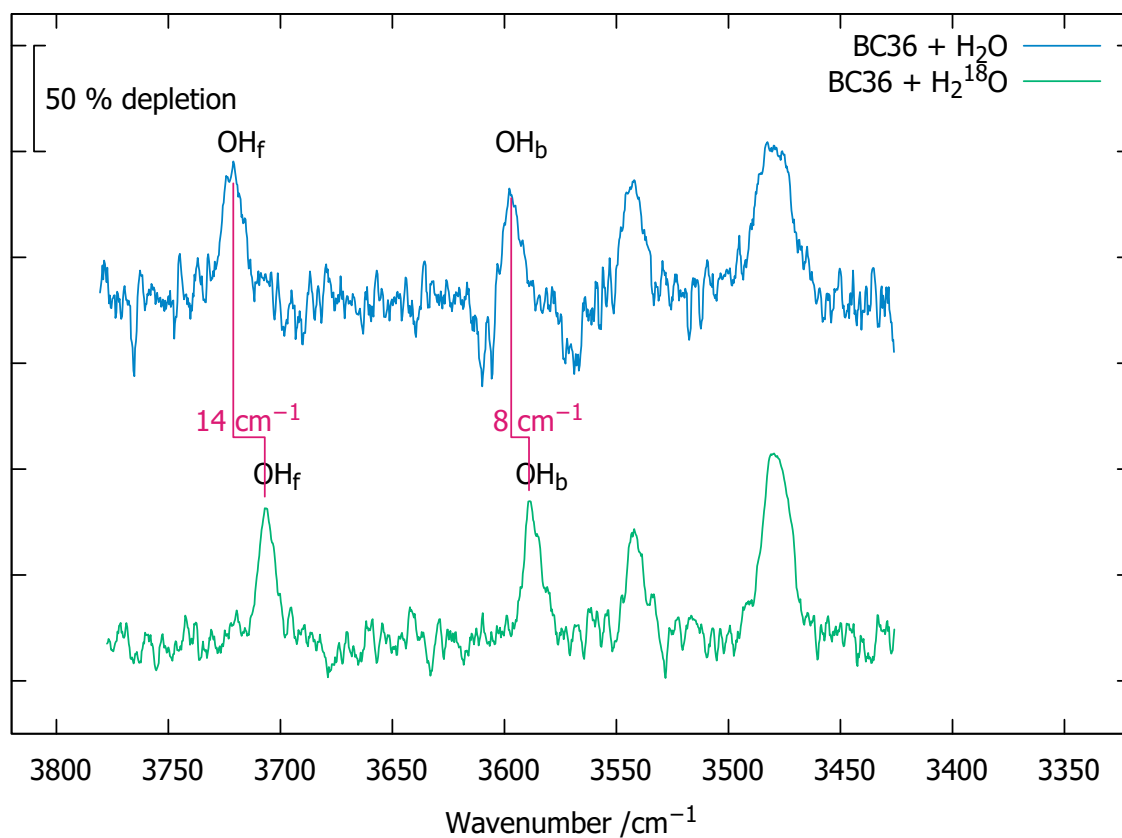


Fig. 5.11: IR depletion spectrum of BC36+water using ¹⁶O- and ¹⁸O-water to securely assign the OH stretching vibrations of water.[84]

5.2.10 2,2,2-Trifluoroethan-1-ol - BC38

2,2,2-Trifluoroethan-1-ol (BC38) is the only compound that was only studied using Raman spectroscopy at the *curry* jet setup as only a weak shift is expected, because water acts as an acceptor for the alcohol functional group in the predicted minimum structure, but is also donating to the fluorine of BC39. Theory predictions give one dominant hetero dimer, which goes along with observations from rotational spectroscopy [104]. The spectra of BC39+H₂O are shown in the upper two traces and H₂O alone is shown in the lowest trace in Figure 5.12. The experimental details are given in Table 5.13. In the two mixed spectra the prominent shoulder next to the symmetric OH stretching vibration of water and BC39 monomer (both at 3657 cm⁻¹) is well visible and belongs to the OH_b stretching vibration, and lies at 3649 cm⁻¹. The OH_f vibration is very weak and can be found at 3719 cm⁻¹. The shifted OH stretching vibration of the alcohol is labeled OH_{b2}. The OH_b signal can also be spotted in [113].

Tab. 5.13: Experimental details on the spectroscopic data on 2,2,2-trifluoroethan-1-ol (BC38) + water giving the spectral identifiers ([yyyymmdd]-[averaged spectra]), the total detection duration t_{tot} of added recording, the a rough estimate of the partial pressures assuming saturated vapor at the mass flow controllers, the stagnation pressure and color in the spectrum.[84]

identifier	t_{tot} s	$p(\text{BC38})$ hPa	$p(\text{H}_2\text{O})$ hPa	$p(\text{He})$ hPa	note
Raman					
20210907_a	4800	1	1	700	see figure 5.12, light blue
20210908_a	5760	1	2	700	see figure 5.12, dark blue
20210907_c	4800	0	2	700	see figure 5.12, gray

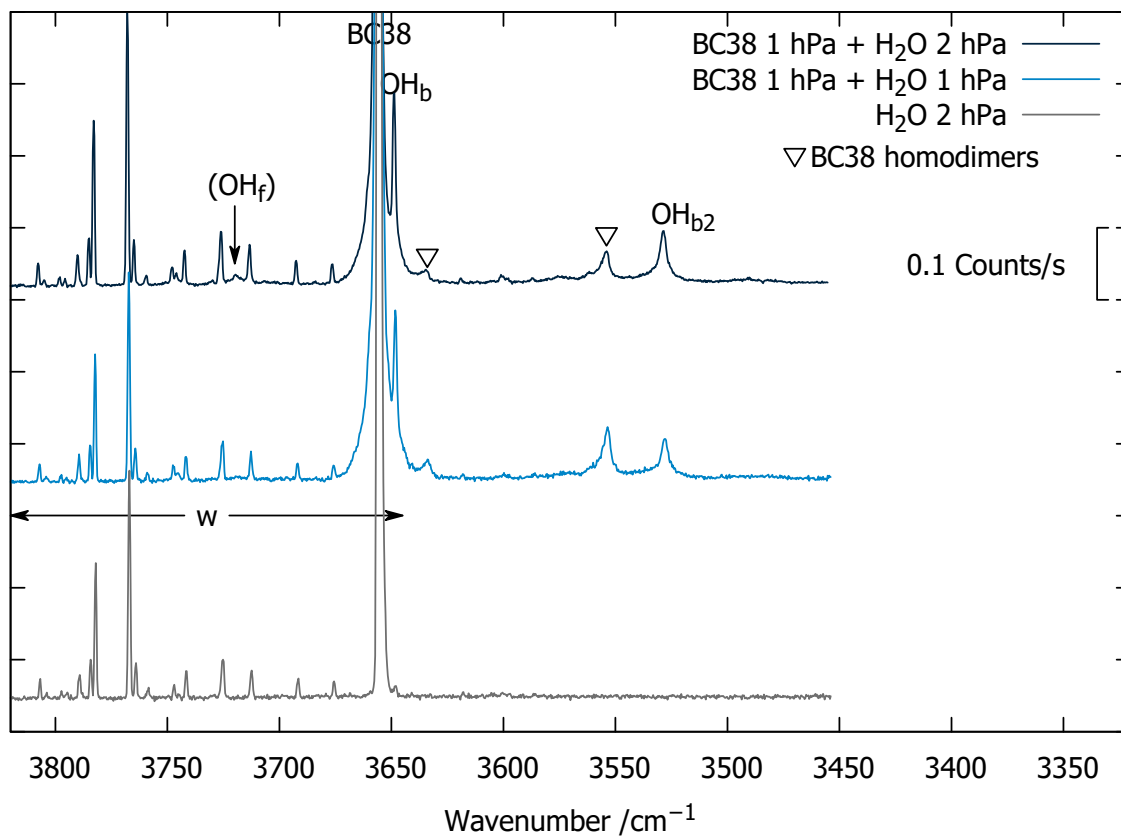


Fig. 5.12: Raman spectrum of 2,2,2-trifluoroethan-1-ol with water (blue tones) and a spectrum with pure water in black. Helium was used as carrier gas.[84]

5.2.11 Statistics

A lot of people were involved in the HyDRA blind challenge, 7 people from two groups from two different countries were involved in collecting all the experimental data, deciding on the training and test set and curating the data. On the theoretical side 28 people from 11 groups from 8 different countries and 3 continents were involved and submitted 20 sets of data.

The theory submissions were mainly evaluated by Prof. Ricardo A. Mata and Dr. Benjamin Schröder and can be found in [84]. As the evaluation took a long time and the paper was submitted to Phys. Chem. Chem. Phys. in March 2023, there was no time to include the results in this thesis.

In Table 5.14 it is listed how many of the theory submissions featured a molecule from the training and test set using the three letter codes which were introduced in Chapter 5.1.

Tab. 5.14: Statistics on the submissions featuring specific molecules from the training and test set and the average.[84]

training set										
molecule	ACE	IMZ	CBU	ANL	OCP	APH	POH	TFB	DBN	DBF
Submitted by	65	50	45	50	50	45	45	50	40	40
/%										
test set										
molecule	FAH	THF	PYR	THT	TFE	MLA	DMI	CON	TPH	PCD
Submitted by	100	100	95	100	90	60	60	70	70	50
/%										

From the training set half of the molecules were included in the submissions on average. Acetone was submitted most often and the large dibenzofuran and the nitroxy radical DBN the least often. For the test set a molecule was submitted in 80% of the data sets on average. Here 3 molecules were included in all 20 submissions (formaldehyde, tetrahydrofuran, and tetrahydrothiophene) and pyridine and 2,2,2-trifluoroethan-1-ol were included in most of the submissions (in $\geq 90\%$). PCD was submitted the least often. In general larger molecules and molecules with more OH groups seemed to be less favored by theory.

5.2.12 Summary and Outlook

With this project we could successfully characterize the ten systems from the test set using different spectroscopy techniques and adding isotope data for 6 of the investigated systems. A b2lib resonance could not be observed in the monohydrates of the test set, which is not too bad as none of the theory submissions featured additional information on it. Neither did any of the theory submissions contain information on the deuterated or ^{18}O -water. One way of a potential next round of HyDRA would be to focus on the effects isotopes have on the energy landscape of a molecular system with different conformers. In this work multiple examples for drastic changes in the conformer stability are shown. For TEMPO+H₂O for example the spectrum changes from at least 4 signals to only one signal when changing from water to deuterated water (further information see Chapter 4.1.1 and [20]). But also the intensity ratio of the cyclooctanone+H₂O spectrum changes when deuterated water is used (see Chapter 5.2.5). The most challenging part of planning such a challenge would probably be to find suitable candidates for the experiments.

The OH shifts covered in this blind challenge are listed in Table 5.15 in which the wavenumber of OH_b vibration and OH shifts ($\Delta\tilde{\nu}_{\text{OH}}$) for the training and test set are listed. For the training set a range of 10–199 cm⁻¹, and for the test set a wavenumber range of 8–203 cm⁻¹ is covered, which is close to the training set. One possible extension to HyDRA would be to aim for stronger OH shifts.

Tab. 5.15: Wavenumbers of the OH_b vibration and the corresponding OH shifts ($\Delta\tilde{\nu}_{\text{OH}}$) for the training and test set molecules giving the 3 letter code.[84]

Training Set			Test Set		
Code	OH _b cm ⁻¹	$\Delta\tilde{\nu}_{\text{OH}}$ cm ⁻¹	Code	OH _b cm ⁻¹	$\Delta\tilde{\nu}_{\text{OH}}$ cm ⁻¹
ACE	3538	119	FAH	3591	66
IMZ	3458	199	THF	3491	166
CBU	3548	109	PYR	3454	203
ANL	3524	133	THT	3507	150
OCP	3595	62	TFE	3649	8
APH	3536	121	MLA	3524	133
POH	3620	37	DMI	3492	165
TFB	3647	10	CON	3503	154
DBN	3484	173	TPH	3611	46
DBF	3623	34	PCD	3597	60

The data collected for HyDRA and other data presented in this work will be made available on qmbench.net as an experimental data set for benchmarking. We hope to be able to

extend this set in the future by more substances with more chemical diversity and even stronger shifts, dihydrates or even charged particles. Another round for HyDRA might also be launched in the future.

6 Benzaldehyde Hydrates - an IR Study

6.1 Motivation

After benzaldehyde and 4-fluorobenzaldehyde were considered as candidates for the HYDRA blind challenge, but first tests during the bachelor thesis of Margarethe Bödecker [29] were not conclusive, we reached out to microwave spectroscopists. Luckily Jun.-Prof. Daniel Obenchain and his PhD student Robin Dohmen were working with benzaldehydes as well as Weixing Li, who was about to publish a paper of benzaldehyde-water complexes.[130] He was measuring the data at the DESY in Hamburg and successfully assigned benzaldehyde+(H₂O)_n with n=1–6. On one hand he was kind enough to give us the number of monohydrates and enabled the IR study to proceed, on the other hand he asked Robin and Daniel to look for a splitting of the benzaldehyde (H₂O)_{5,6} complex, which gave me a topic for my lab rotation in the Obenchain group. In return, Robin joint me for the IR investigation of the benzaldehyde monohydrates at the *gratin* jet spectroscopy setup. Benzaldehyde monohydrates can be regarded as carbonyl scales, which I investigated during my master thesis [131] and have been used in the Suhm group as model to investigate dispersion interactions since 2017.[18, 48, 131–133] These so-called carbonyl scales are particularly useful for the investigation and benchmarking dispersive forces, because the keto group of an asymmetric carbonyl offers the donor molecule two docking sites at the oxygen lone pairs with comparable ZPVEs.[48] In earlier studies the more complicated comparison between an eg. oxygen lone pair and the π -system of an aromatic ring has been an issue.[9] In this work the binding preference of the water is determined.

Due to technical problems with the instrument of the Obenchain group, further steps to investigate the potential splitting of the benzaldehyde (H₂O)_{5,6} complex are not planned.

Tab. 6.1: All benzaldehyde derivatives, their abbreviation, vendor, purity and spectral identifier ([yyyyymmdd]-[averaged spectra]).

Chemical	Code	Purity	Vendor	Identifier
Benzaldehyde	BA	> 99%	Sigma Aldrich	20221007-abc
2-Fluorobenzaldehyde	2FBA	97%	Sigma Aldrich	20221011-abcd
3-Fluorobenzaldehyde	3FBA	97%	Sigma Aldrich	20221125-abcd
4-Fluorobenzaldehyde	4FBA	98%	Sigma Aldrich	20220510-abc
3,5-Difluorobenzaldehyde	35DFBA	99.86%	BLD PHARMA-TECH	20220615-ab

6.2 IR Investigation

For the IR study the monohydrates of five different benzaldehydes were investigated, benzaldehyde (BA), 2-fluorobenzaldehyde (2FBA), 3-fluorobenzaldehyde (3FBA), 4-fluorobenzaldehyde (4FBA) and 3,5-difluorobenzaldehyde (35DFBA). The expected conformers from a theoretical structure search with CREST and a follow up optimization on B3LYP-D3(BJ)/def2-TZVP are depicted in figure 6.1 and 6.2. For each benzaldehyde species the relative energy differences between the different monohydrate conformers are given. For BA, 2FBA, 4FBA and 35DFBA monomer only one stable conformer was found, while for 3FBA the fluorine atom can point in *cis* or *trans* direction relative to the carbonyl group. For 2FBA the same applies, but the *cis* conformer is predicted to be 9 kJ mol⁻¹ higher in energy and the spectrum does not show any evidence for more than two conformers. Each monomer conformation offers water at least two binding sites at the carbonyl group and for all BAs the water binding from the side of the phenyl ring is predicted to be more stable. A more detailed analysis of the theoretical predictions is given in Table 6.2 where the relative energies ΔE^0 , the predicted OH_b stretching vibration ω (predicted value and scaled value, scaling factor 0.98 (compare to scaling factor derived in Chapter 3)), the IR intensity and the difference of the predicted, scaled wavenumbers $\Delta\omega^{\text{scaled}}$ between the conformers are given.

The chemicals, their vendor, purities, abbreviations and spectral identifiers used in this study are given in table 6.1.

Figure 6.3 shows the infrared spectra of the different benzaldehyde species with water expanded in 750 mbar He in the novel *gratin* jet spectroscopy setup. Water monomer signals are labeled w and the mixed dimer signals OH_{Ph} and OH_H. In order to assign the signals to the different conformers, a comparison to theory values was performed. For the assignment, the scaled wavenumbers from the theory predictions and the relative

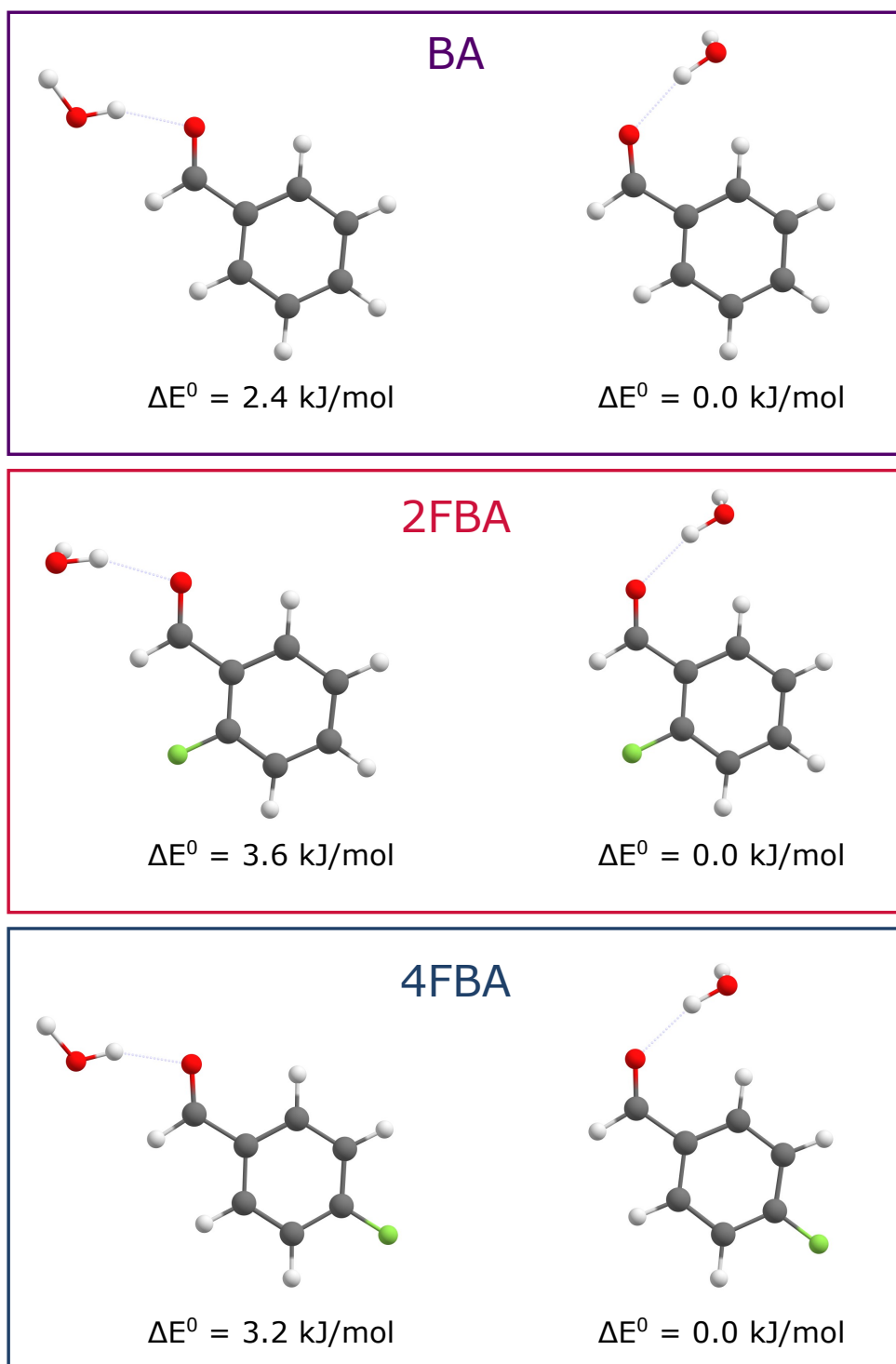


Fig. 6.1: Minimum structures of investigated benzaldehyde water complexes and the energy difference compared to the most stable conformer within one group. The minimum structures were determined using CREST and later optimized on B3LYP-D3(BJ)/def2-TZVP level on ORCA 4.2.1. Benzaldehyde is shortened as BA, 2-fluorobenzaldehyde as 2FBA and 4-fluorobenzaldehyde as 4FBA.

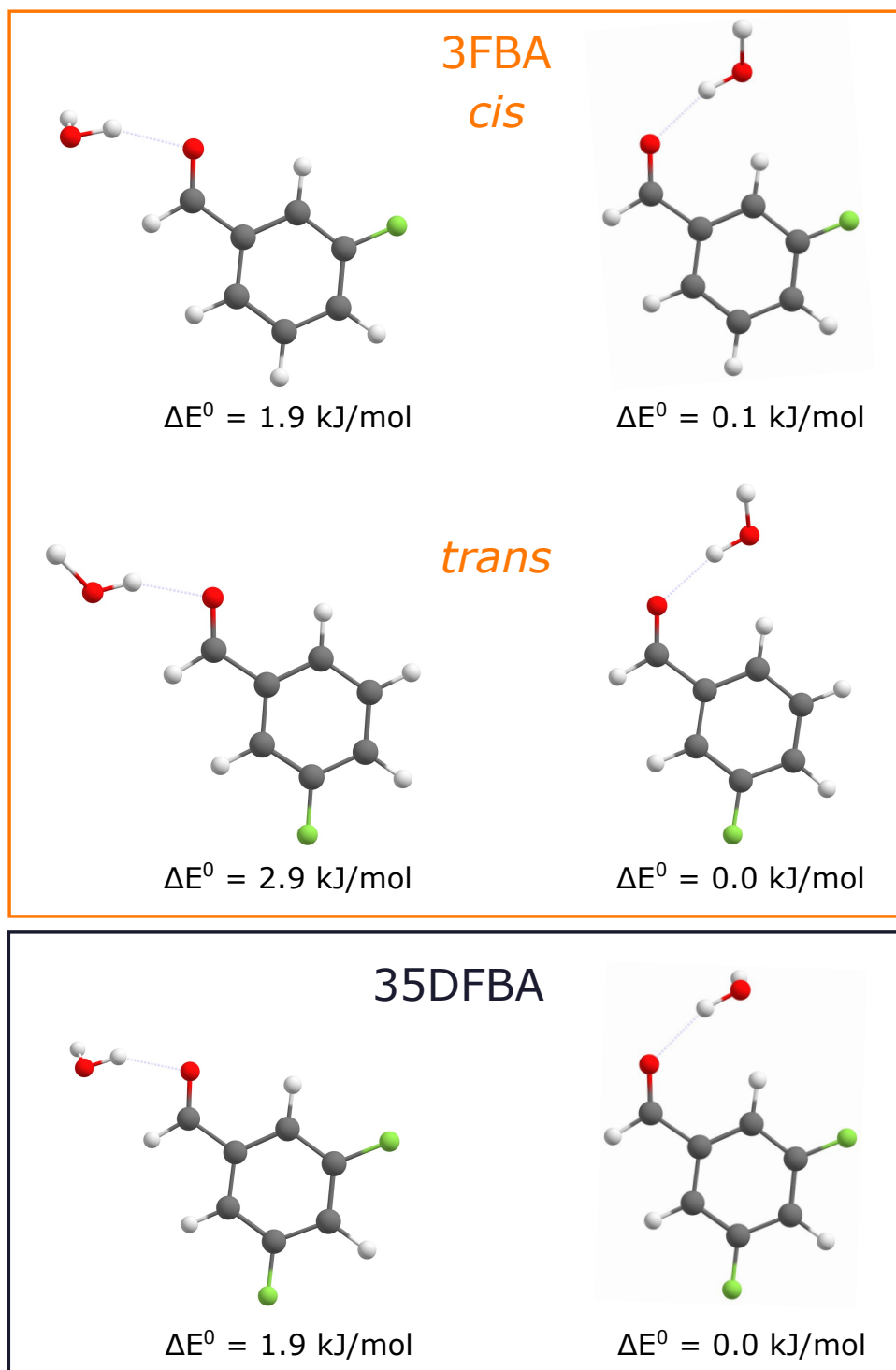


Fig. 6.2: Further minimum structures of investigated benzaldehyde water complexes and the energy difference compared to the most stable conformer within one group. The minimum structures were determined using CREST and later optimized on B3LYP-D3(BJ)/def2-TZVP level on ORCA 4.2.1. 3-Fluorobenzaldehyde is shortened as 3-FBA (with *cis/trans* isomerism of the aldehyde oxygen relative to the fluorine) and 3,5-difluorobenzaldehyde as 35DFBA.

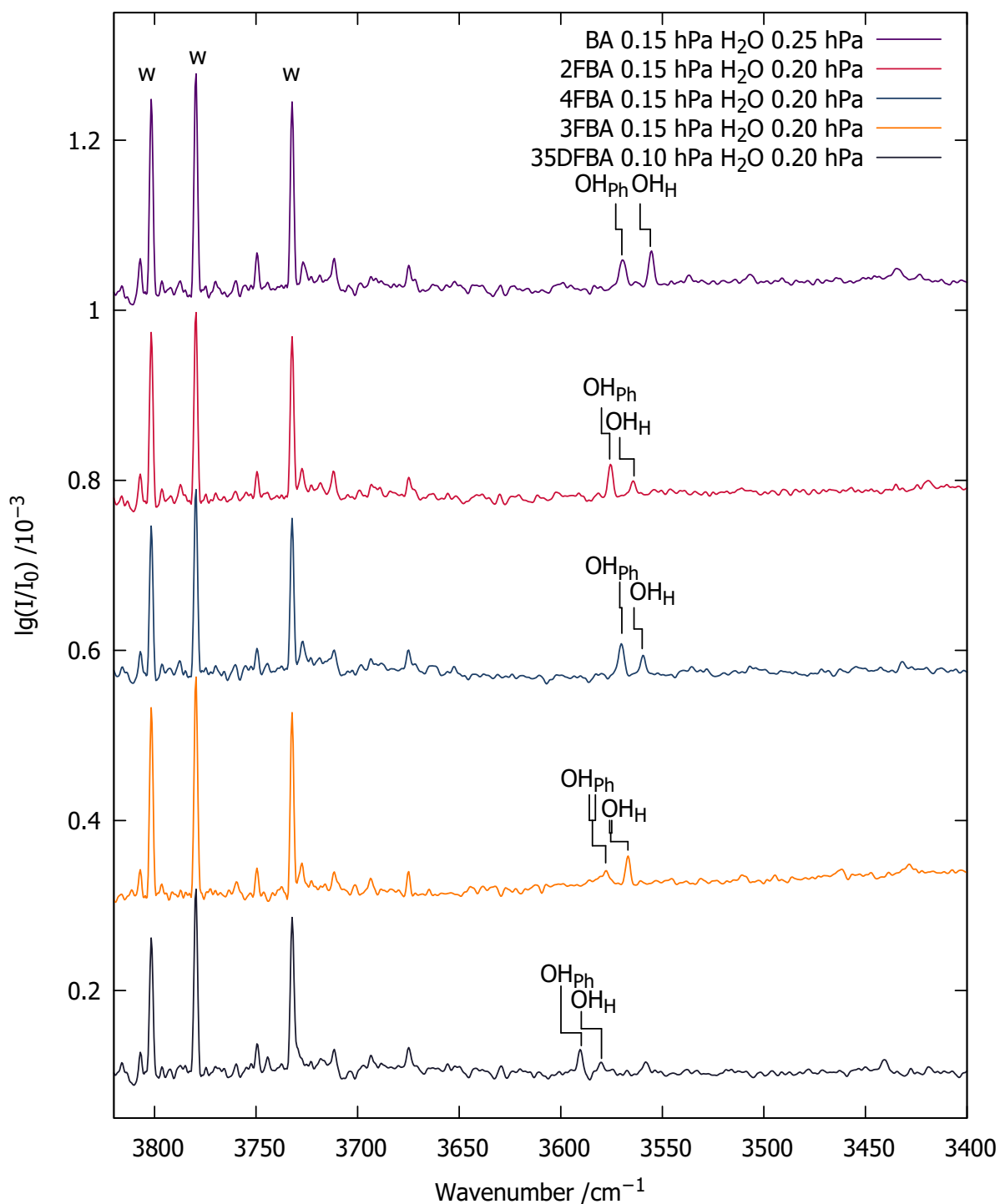


Fig. 6.3: Jet cooled infrared spectra of monohydrates of different benzaldehyde derivatives. The molecules were expanded using helium as carrier gas and a stagnation pressure of 750 mbar. The concentration of the benzaldehyde derivative and the corresponding water concentration used is given in hPa in the title. The hetero dimer signals are labeled OH_{Ph} and OH_{H} and water monomer signals with w.

Tab. 6.2: Theoretical predictions featuring the energy differences between different conformers of a variety of hydrated benzaldehyde species using the energies corrected by the zero point vibrational energy (ΔE^0) on B3LYP-D3(BJ)/def2-TZVP level. Additionally the predicted wavenumber (ω) of bound OH-stretching vibration (unscaled and scaled by a factor of 0.98)) and their infrared intensities are given.

Structure	ΔE^0	ω	ω^{scaled}	IR Int	$\Delta\omega^{\text{scaled}}$
	/kJ mol ⁻¹	/cm ⁻¹	/cm ⁻¹		/ km mol ⁻¹
BA _H	2.4	3634	3561	510	0
BA _{Ph}	0.0	3646	3573	360	12
2FBA _H	3.6	3644	3571	480	0
2FBA _{Ph}	0.0	3653	3580	340	9
4FBA _H	3.2	3637	3564	500	0
4FBA _{Ph}	0.0	3644	3571	350	7
<i>cis</i> -3FBA _H	1.9	3648	3575	440	0
<i>cis</i> -3FBA _{Ph}	0.1	3659	3586	310	11
<i>trans</i> -3FBA _H	2.9	3649	3576	440	1
<i>trans</i> -3FBA _{Ph}	0.0	3656	3583	339	8
35DFBA _H	1.9	3663	3590	380	0
35DFBA _{Ph}	0.0	3673	3600	270	10

positions between the conformer signals were taken into account. In all cases the signal labeled OH_{Ph} corresponds to the conformers where the water approaches the benzaldehyde lone pair from the side of the phenyl ring and OH_H to the conformer where water binds from the less sterically hindered side of the H atom. The scaled value of the theory prediction is given in Figure 6.3 as vertical line towards the label.

For the BA spectrum the predicted scaled wavenumbers and the experimental signals are in good agreement (compare to Table 6.3) as well as the predicted wavenumber difference between the signals. The same holds true for 2FBA and 4FBA.

If one moves to a more complicated candidate where the benzaldehyde itself not only have one stable conformer present in the expansion, the assignment is not as secure. For 3FBA, the benzaldehyde monomer has two different conformers. For both benzaldehyde conformers two conformers with water are possible. All four conformers are close in energy and the differences of the OH shifts are small. For the OH_H conformers the predicted wavenumber difference amounts only 1 cm⁻¹, so the signal in Figure 6.3 might correspond to two conformers. The OH_b signals have a predicted wavenumber difference of 3 cm⁻¹ and the signal in the spectrum is broader. To assign the signals in the 3FBA spectrum, 35DFBA was measured, as it only has one stable conformer in the expansion (for the monomer), but should provide a similar sterical environment as the 3FBA_{Ph}. Unfortu-

Tab. 6.3: Signal assignment using the experimental wavenumbers and the scaled frequencies from the theoretical predictions from table 6.2. The experimental wavenumbers for 3FBA are left open as the cannot be assigned securely.

Structure	$\tilde{\nu}_{\text{exp}}$ /cm ⁻¹	ω^{scaled} /cm ⁻¹	Signal
BA _H	3556	3561	OH _{b2}
BA _{Ph}	3570	3573	OH _b
2FBA _H	3564	3571	OH _{b2}
2FBA _{Ph}	3576	3580	OH _b
4FBA _H	3560	3564	OH _{b2}
4FBA _{Ph}	3570	3571	OH _b
<i>cis</i> -3FBA _H		3575	OH _{b2}
<i>cis</i> -3FBA _{Ph}		3586	OH _b
<i>trans</i> -3FBA _H		3576	OH _{b2}
<i>trans</i> -3FBA _{Ph}		3583	OH _b
35DFBA _H	3580	3590	OH _{b2}
35DFBA _{Ph}	3590	3600	OH _b

Tab. 6.4: All values needed to calculate the ratio between the two conformers $c(\text{OH}_H)/c(\text{OH}_{Ph})$ for BA, 2FBA, and 4FBA.

Structure	$\sigma(\text{OH}_{Ph})/\sigma(\text{OH}_H)$	$I(\text{OH}_H)/I(\text{OH}_{Ph})$	$c(\text{OH}_H)/c(\text{OH}_{Ph})$	H:Ph
BA	0.7	1.2 ± 0.2	0.87	1:1
2FBA	0.7	0.4 ± 0.1	0.26	1:4
4FBA	0.7	0.5 ± 0.1	0.36	1:3

nately 35DFBA is not as volatile as the other benzaldehydes and seems to form higher clusters more easily which is why the spectrum in Figure 6.3 is not helpful in assigning the 3FBA signals. As a possible continuation of the project, further concentration series of 35DFBA could be measured and a 3FBA+water spectrum with Ne as carrier gas, to obtain a stronger cooling, and hopefully only observe one of the 3FBA conformers. But as the conformers are very close in energy this plan might not be realistic. One could also try measuring with a higher spectral resolution, but this would require much more time and scans as tests with the spectrometer have shown 2.2.5.

6.2.1 Signal Integration

In order to evaluate the abundance of the different benzaldehyde monohydrates, the signal intensities of OH_{Ph} and OH_{H} for BA, 2FBA and 4FBA were integrated using integration method D (introduced in Chapter 1.1.3). The intensity ratio was formed ($I(\text{OH}_{\text{Ph}})/I(\text{OH}_{\text{H}})$) as well as the corresponding ratio of the harmonically computed absorption cross sections ($\sigma(\text{OH}_{\text{H}})/\sigma(\text{OH}_{\text{Ph}})$).

$$\frac{c(\text{OH}_{\text{H}})}{c(\text{OH}_{\text{Ph}})} = \frac{I(\text{OH}_{\text{H}}) \sigma(\text{OH}_{\text{Ph}})}{I(\text{OH}_{\text{Ph}}) \sigma(\text{OH}_{\text{H}})} \quad (6.1)$$

The abundance between the two conformers is then estimated using Equation 6.1 and the results are listed in Table 6.4.

For the integration method D the simulation was run 50 000 times and the standard deviation of the signal intensity ratio was formed. The results of the signal integration, the corresponding error and the ratio of the absorption cross section as well as the corresponding abundance ratios of the monohydrate conformers are give in Table 6.4.

While for the hydrates of BA the two conformers appear in an 1:1 ratio in the expansion, the conformer where the water is binding from the phenyl rings side is favored in 2FBA and 4FBA hydrates. The energy difference between the two conformers is smaller for BA+H₂O than for the two other species, but is larger than one would expect for a 1:1 distribution between the conformers in the expansion. The most probable explanation is that the theoretical method (B3LYP-D3(BJ)/def2-TZVP) is overestimating the energy differences. Future work including higher level methods may solve this case.

7 Summary and Outlook

In this work with the goal to obtain benchmarking data, first the novel *gratin* jet spectroscopy setup was introduced and some tests were performed. The new setup has the advantage that the gas mixture can be recycled and is not lead to the exhaust what reduces the substance consumption by at least one order of magnitude and allows the use of pricier chemicals and carrier gasses. But the recycling concept of the setup leads to a problem, water is desorbing from the walls and traces of water monomer become visible after some gas cycles. Once hydrate clusters are investigated, this is no longer a disadvantage.[2] Even though hydrates have a lot to offer, like the b2lib resonance [14], we aim to at least reduce the amount of water inside the jet in the future. First steps will be the usage of a pump that can fully be evacuated. Another project is to test the heatable nozzle and the heating of the whole system. Other interesting projects would be to investigate warmer expansions by lowering the stagnation pressure and trying to create nano matrices by using heavier and/or more electron rich carrier gasses.

A lot of benchmarking suited data was produced, ranging from neutral hydrate cluster from the HyDRA blind challenge [84] to more complex systems as the jet cooled gas phase spectra of hydrates of stable radicals [20] or the b2lib resonance [14]. For many of the systems also isotopic data is available. All 44 published OH_b stretching wavenumbers and vibrational shifts $\Delta\tilde{\nu}_{\text{OH}}$ are given in Table 7.1 and 7.2 sorted by the name of the acceptor molecule and water isotopes. For HDO an underscore is marking the binding hydrogen isotope. For candidates with a b2lib resonance the deperturbed values are given and they are marked with *. If the OH_b stretching vibration couples with an alcohol, the OH stretching vibration with more water character is listed. For substances with more than one conformer, the most stable one is listed first, followed by the others.

Tab. 7.1: Experimental IR wavenumbers of all substances measured for this work giving the substance, CAS registry number, the water species and the OH_b and $\Delta\tilde{\nu}_{\text{OH}}$ (relative to 3657 cm^{-1}). For candidates with a b2lib resonance the perturbed wavenumber is given and the substance is marked with a *.

Substance	CAS No	Water species	OH_b cm^{-1}	$\Delta\tilde{\nu}_{\text{OH}}$ cm^{-1}
acetone[14]*	67-64-1	H_2O	3538	119
acetone[14]*	67-64-1	H_2^{18}O	3528	
acetone D_6 [14]*	666-52-4	H_2O	3537	120
acetone-2- ^{13}C [14]*	3881-06-9	H_2O	3537	120
acetophenone[14]*	98-86-2	H_2O	3536	121
			3567	90
cyclobutanone[14]	1191-95-3	H_2O	3548	109
cycloheptanone[14]*	502-42-1	H_2O	3512	145
cyclohexanone[14]*	108-94-1	H_2O	3532	125
cyclooctanone[84]	502-49-8	H_2O	3503	154
			3525	132
cyclooctanone[84]	502-49-8	D_2O	2573	
			2583	
4,4-dimethylcyclohexanone[14]*	4255-62-3	H_2O	3513	144
1,3-dimethyl-2-imidazolidinone[84]	80-73-9	H_2O	3492	165
(-)-fenchone[14]*	7787-20-4	H_2O	3511	146
2-fluoroacetophenone[14]	445-27-2	H_2O	3545	112
	445-27-2	H_2O	3576	81
formaldehyde[84]	50-00-0	H_2O	3591	66
formaldehyde[84]	50-00-0	D_2O	2629	
1-hydroxy-2,2,6,6-tetramethyl-piperidine[79]	7031-93-8	H_2O	3534	123
methyl lactate[84]	547-64-8	H_2O	3524	133
methyl lactate[84]	547-64-8	H_2^{18}O	3516	
1-phenylcyclohexan-cis-1,2-diol[84]	125132-75-4	H_2O	3597	60
1-phenylcyclohexan-cis-1,2-diol[84]	125132-75-4	H_2^{18}O	3589	68
pinacolone[14]*	75-97-8	H_2O	3533	124
pyridine[84]	110-86-1	H_2O	3454	203
pyridine[84]	110-86-1	D_2O	2541	
pyridine[84]	110-86-1	$\underline{\text{H}}\text{OD}$	3464	
pyridine[84]	110-86-1	$\underline{\text{D}}\text{OH}$	2549	
tetrahydrofuran[84]	109-99-9	H_2O	3491	166
tetrahydrofuran[84]	109-99-9	D_2O	2568	
tetrahydrofuran[84]	109-99-9	$\underline{\text{H}}\text{OD}$	3503	
tetrahydrofuran[84]	109-99-9	$\underline{\text{D}}\text{OH}$	2579	
tetrahydrothiophene[84]	110-01-0	H_2O	3507	150

Tab. 7.2: Experimental IR wavenumbers of all substances measured for this work giving the substance, CAS registry number, the water species and the OH_b and $\Delta\tilde{\nu}_{\text{OH}}$ (relative to 3657 cm^{-1}). For candidates with a b2lib resonance the perturbed wavenumber is given and the substance is marked with a *.

Substance	CAS No	Water species	OH_b cm^{-1}	$\Delta\tilde{\nu}_{\text{OH}}$ cm^{-1}
2,2,6,6-tetramethylcyclohexanone[20]*	1195-93-3	H_2O	3550	107
3,3,5,5-tetramethylcyclohexanone[14]*	14376-79-5	H_2O	3510	147
(2,2,6,6-tetramethylpiperidin-1-yl)oxyl[20]*	2564-83-2	H_2O	3497	160
(2,2,6,6-tetramethylpiperidin-1-yl)oxyl[20]*	2564-83-2	H_2^{18}O	3486	
(2,2,6,6-tetramethylpiperidin-1-yl)oxyl[20]	2564-83-2	D_2O	2572	
(2,2,6,6-tetramethylpiperidin-1-yl)oxyl[20]	2564-83-2	$\underline{\text{H}}\text{OD}$	3514	
(2,2,6,6-tetramethylpiperidin-1-yl)oxyl[20]	2564-83-2	$\underline{\text{D}}\text{OH}$	2556	
2,2,2-trifluoroacetophenone[84]	434-45-7	H_2O	3611	46
2,2,2-trifluoroethan-1-ol[84]	75-89-8	H_2O	3649	8

In total a number of 25 substances (counting all acetone derivatives) was investigated and 44 OH/OD shifts could be reported. The data will be made available for the benchmarking community on the qmbench.net website.

We hope that the BENCH RTG2455 will kick start more benchmarking projects and blind challenges after the first HyDRA blind challenge was a success with 11 participating groups providing 20 data sets for comparison with the experimental values. We were happy to be able to provide the experimental data for all 10 systems and hope to add even more hydrates to the data base.

8 Supplement

8.1 Energy Consumption *Gratin* Jet Spectroscopy Setup

Tab. 8.1: Energy consumption of some of the components of the *gratin* jet spectroscopy setup.

Component	Energy Consumption /W
ACP dry pump	630
Edwards nXDS dry pump	300
external light source (W150) on	200
Cooling of light source	40
Spectrometer (no measurement running)	70
Computer	40
Turbomolecular pump (with ACP)	150
Turbomolecular pump (starting + gas load)	1250

8.2 Experimental Details

8.2.1 A Rather Universal Resonance

Tab. 8.2: Details on the recorded spectra in Chapter 3 giving the number of collected pulses # and the dates dd/mm/yyyy of record and used optical filter F (F20: $< 4000 \text{ cm}^{-1}$, F13: 2500 cm^{-1} – 4100 cm^{-1}).[14]

Code	#	dd/mm/yyyy	F
C4	700	10/02/2020	F20
2FAph	900	25/04/2019	F13
Aph	900	09/04/2019	F13
		+ 16/04/2019	
Ace	850	11/12/2020	F13
Pin	700	03/04/2019	F13
C6	900	12/02/2020	F20
Fen	700	20/05/2020	F20
44C6	800	06/05/2020	F20
3355C6	690	24/04/2020	F20
C7	850	21/04/2020	F20
D6Ace	900	12/12/2019	F13
13CAce	1100	17/06/2020	F20
Ace with 18OHH	900	23/07/2020	F20

8.2.2 Radicals

Tab. 8.3: Experimental details of the spectra shown in Chapter 4.1.1 Figure 4.2 giving the number of averaged gas pulses # and the date the spectrum was recorded dd/mm/yyyy and expanded and the He:Ne gas mixture used as carrier gas.[20]

Spectrum	He:Ne	#	dd/mm/yyyy	Figure
TEMCO + H ₂ O	1:0	900	14/09/2020	S2
TEMCO + H ₂ O	1:0	800	17/09/2020	2 A; S2
TEMPO + H ₂ O	1:0	900	23/09/2020	S2
TEMPO + H ₂ O	1:0	900	24/09/2020	2 C; S2
TEMPO + H ₂ O	1:1	1200	20/10/2020	2 D
TEMPO + H ₂ ¹⁸ O	1:1	750	03/11/2020	2 F
<i>minus</i> TEMPO + H ₂ O (20/10/2020)				
TEMPO + D ₂ O	1:0	800	10/11/2020	2 H, 2 J
450 scans (10/11/2020) <i>plus</i>			11/11/2020	
350 scans (11/11/2020)				

Tab. 8.4: Experimental details on the spectra shown in Chapter 4.1.3 Figure 4.9 and 4.10. The spectroscopic data was obtained by averaging # scans of 133 ms He gas pulses with a stagnation pressure of 0.75 bar. The date on which the spectrum was recorded is given as dd/mm/yyyy. The partial pressures for TEMPO-H (p_{TH}), TEMPO (p_{T}), and water (p_{w}) are also given in Figures 4.9 and 4.10.[79]

p_{TH}/hPa	p_{T}/hPa	p_{w}/hPa	#	dd/mm/yyyy
0.05	0.00	0.00	1000	01/11/2021
0.10	0.00	0.00	1000	20/10/2020
0.05	0.00	0.05	1000	19/08/2022
0.05	0.00	0.00	1000	01/11/2021
0.05	0.10	0.00	1000	13/05/2022
0.05	0.05	0.00	1000	04/11/2021
0.10	0.05	0.00	1000	22/08/2022

8.3 Unpublished Hydrate Spectra

8.3.1 Additional Data on Acetophenone Hydrates

Acetophenone + ^{18}O -water

In order to further investigate the b2lib resonance, which is described in Chapter 3, Acetophenone (APh in the following) was not only investigated using ^{16}O -water, but also with ^{18}O -water. As acetone with ^{18}O -water was the easier example, the data on APh was not included in the publication and spared for the HyDRA blind challenge (described in Chapter 5). It was not included in the end, as other molecular clusters seemed better suited. As isotopic data were not included in the theory submissions it would not have been a good addition anyway.

Tab. 8.5: Experimental details of the spectra shown in Figur 8.1 giving the number of averaged gas pulses # and the spectral identifiers [yyyymmdd]-[averaged spactra]. In all measurements helium was used as carrier gas with a stagnation pressure of 750 mbar.

Spectrum	Molecule	#	Identifier
violet	Acetophenone + ^{18}O -water	500	24/07/2020-abcdefg
red	Acetophenone + ^{16}O -water	1600	09/04/2019-abcdefg 17/04/2019-abcdefgh

The spectra are shown in Figure 8.1 and more details on the experiment are given in Table 8.5. The upper violet spectrum containing APh, ^{18}O -water and traces of ^{16}O -water is subtracted by the scaled (scaling factor=0.6) spectrum of APh with ^{16}O -water, resulting in the blue spectrum. As expected the difference spectrum is revealing 3 signals similar to the APh+ H_2^{16}O . The signals labelled $^{18}\text{OH}_{\text{Ph}}$ correspond to the OH_b stretching vibration of water docking to the APh from the side of the phenyl ring and $^{18}\text{OH}_{\text{Me}}$ to the docking from the direction of the methyl side. $^{18}\text{b2lib}$ labels the b2lib resonance. All wavenumbers are listed in Table 8.6.

Tab. 8.6: Wavenumbers of all assigned OH signals in Figure 8.1 for APh with ^{16}O - and ^{18}O -water.

assignment	$\text{H}_2^{16}\text{O} / \text{cm}^{-1}$	$\text{H}_2^{18}\text{O} / \text{cm}^{-1}$
$^{(18)}\text{OH}_{\text{Ph}}$	3567	3558
$^{(18)}\text{OH}_{\text{Me}}$	3536	3526
$^{(18)}\text{b2lib}$	3515	3504

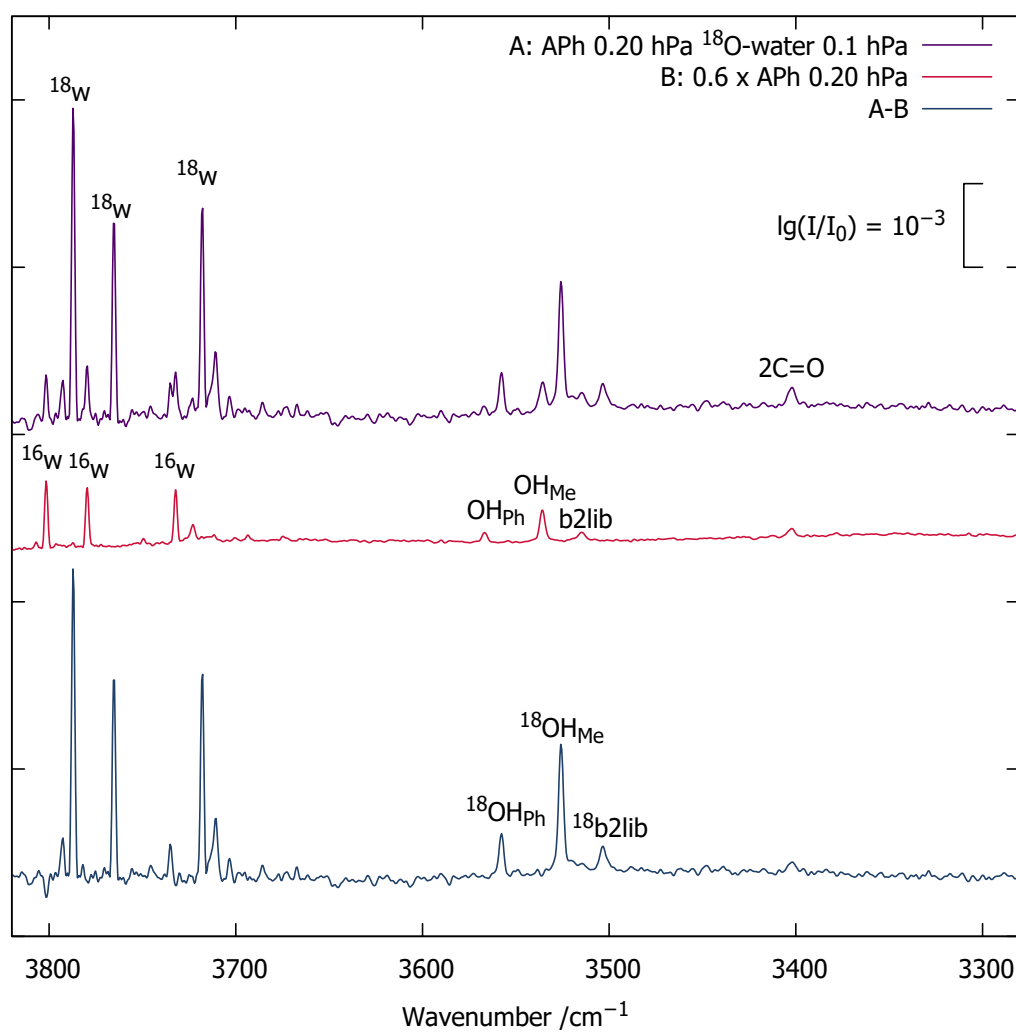


Fig. 8.1: FTIR spectra of APh with ^{18}O (violet) and ^{16}O -water (red). The red spectrum is scaled by a factor of 0.6 and is subtracted from the purple spectrum to obtain a more clear spectrum of APh with ^{18}O water. Details on the spectra can be found in Table 8.5. All spectra were recorded using a 750 mbar expansion of helium.

4-Fluoroacetophenone Hydrates

Another potential candidate for the b2lib resonance was 4-fluoroacetophenone (4FAPh; 99%, Acros Organics, Lot:A0382614). As shown in Figure 8.2 the OH_{Ph} and OH_{Me} can be assigned easily to the signals at 3568 and 3540 cm^{-1} respectively. In the red and violet spectrum the OH_{Me} signal may be overlapped by signals of larger clusters and therefore scale different compared to OH_{Ph} . If a b2lib resonance is present or not is difficult to tell as there is no clear assignment possible. The OH shift of OH_{Me} is close enough to 3510 cm^{-1} to show a resonance and a potential b2lib resonance would be assigned to the small signal at 3512 cm^{-1} . Another measurement with a small 4FAPh concentration with more water might solve the issue, but due to the insecure assignment the spectrum was not included in the b2lib publication [14]. More information on the experimental conditions can be found in Table 8.7.

Tab. 8.7: Experimental details of the spectra shown in Fig 8.5 giving the number of averaged gas pulses # and the dates on which they were recorded (dd/mm/yyyy). In all measurements helium was used as carrier gas with a stagnation pressure of 750 mbar.

Spectrum	#	dd/mm/yyyy
Fig 8.2 violet	700	16/07/2019
Fig 8.2 red	500	17/07/2019
Fig 8.2 blue	900	19/07/2019
Fig 8.2 orange	800	18/07/2019
Fig 8.2 black	400	17/07/2019

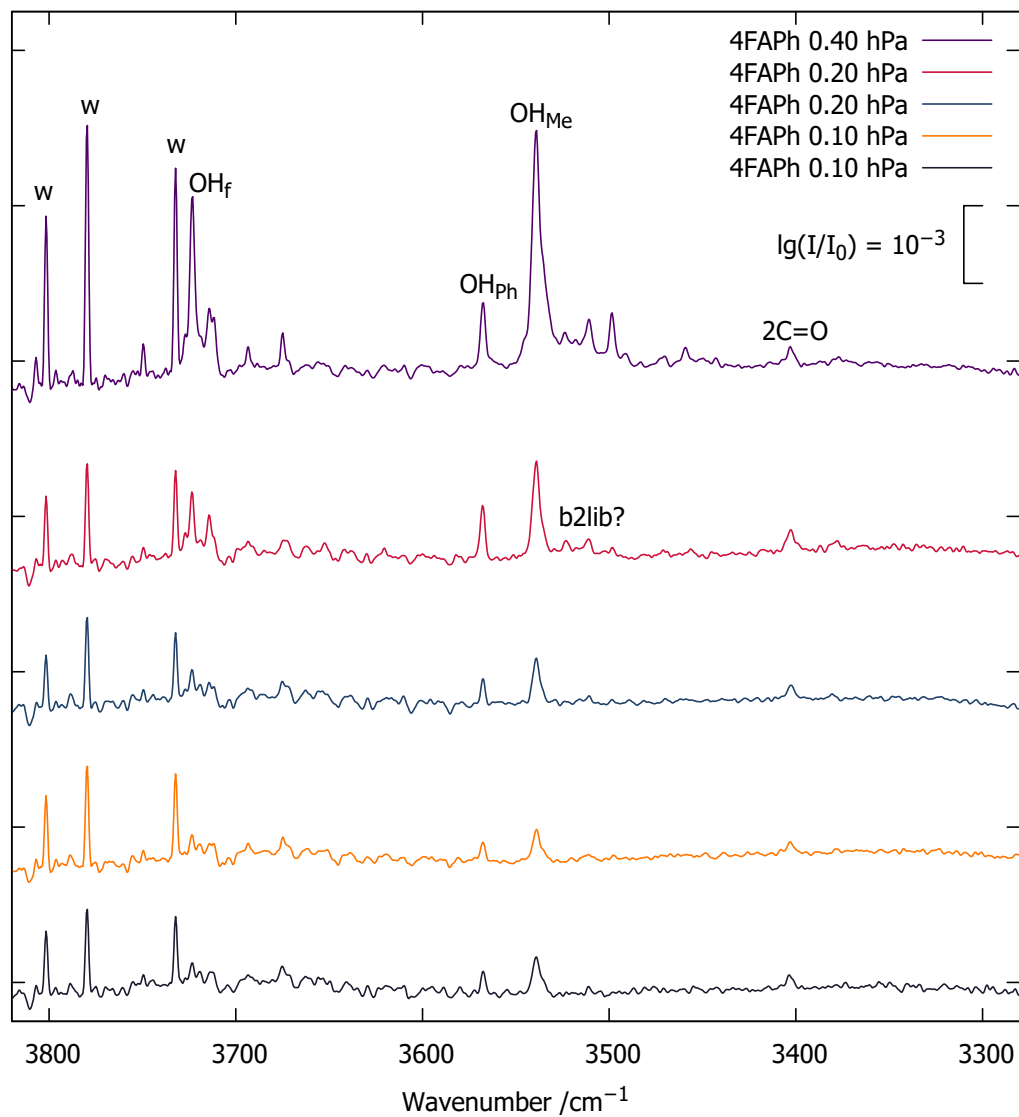


Fig. 8.2: FTIR spectra of 4FAPh hydrates. Details on the spectra can be found in Table 8.7. All spectra were recorded using a 750 mbar expansion of helium.

All Acetophenone Hydrates

Tab. 8.8: Experimental details of the spectra shown in Figur 8.3 giving the number of averaged gas pulses # and the spectral identifiers [dd/mm/yyyy]-[averaged spectra]. In all measurements helium was used as carrier gas with a stagnation pressure of 750 mbar.

Spectrum	Molecule	Abbreviation	#	Identifier
violet	Trifluoroacetophenone	TFAPh	1500	02/06/2021-abcdefg
red	2-Fluoroacetophenone	2FAPh	1600	02/06/2021-abcdef
blue	4-Fluoroacetophenone	4FAPh	1400	24/04/2019-abcdefg 26/04/2019-abcdefgh 17/07/2019-abcde
orange	Acetophenone	APh	1600	19/07/2019-abcdefgh 09/04/2019-abcdefg 17/04/2019-abcdefgh

In this work many hydrates of different acetophenone derivatives were investigated, namely trifluoroacetophenone (TFAPh), 2-fluoroacetophenone (2FAPh), 4-fluoroacetophenone (4FAPh) and acetophenone (APh). In Figure 8.3 an overview of the hydrates of the four investigated acetophenones can be found and further details on the recorded spectra are listed in Table 8.8. The spectra are sorted by the OH shift of water, the stronger the OH shift, the lower they are shown in the figure. More spectra of TFAPh can be found in Chapter 5.2.3, APh and 2FAPh are also shown in Chapter3 and 4FAPh can be found in Chapter 8.3.1.

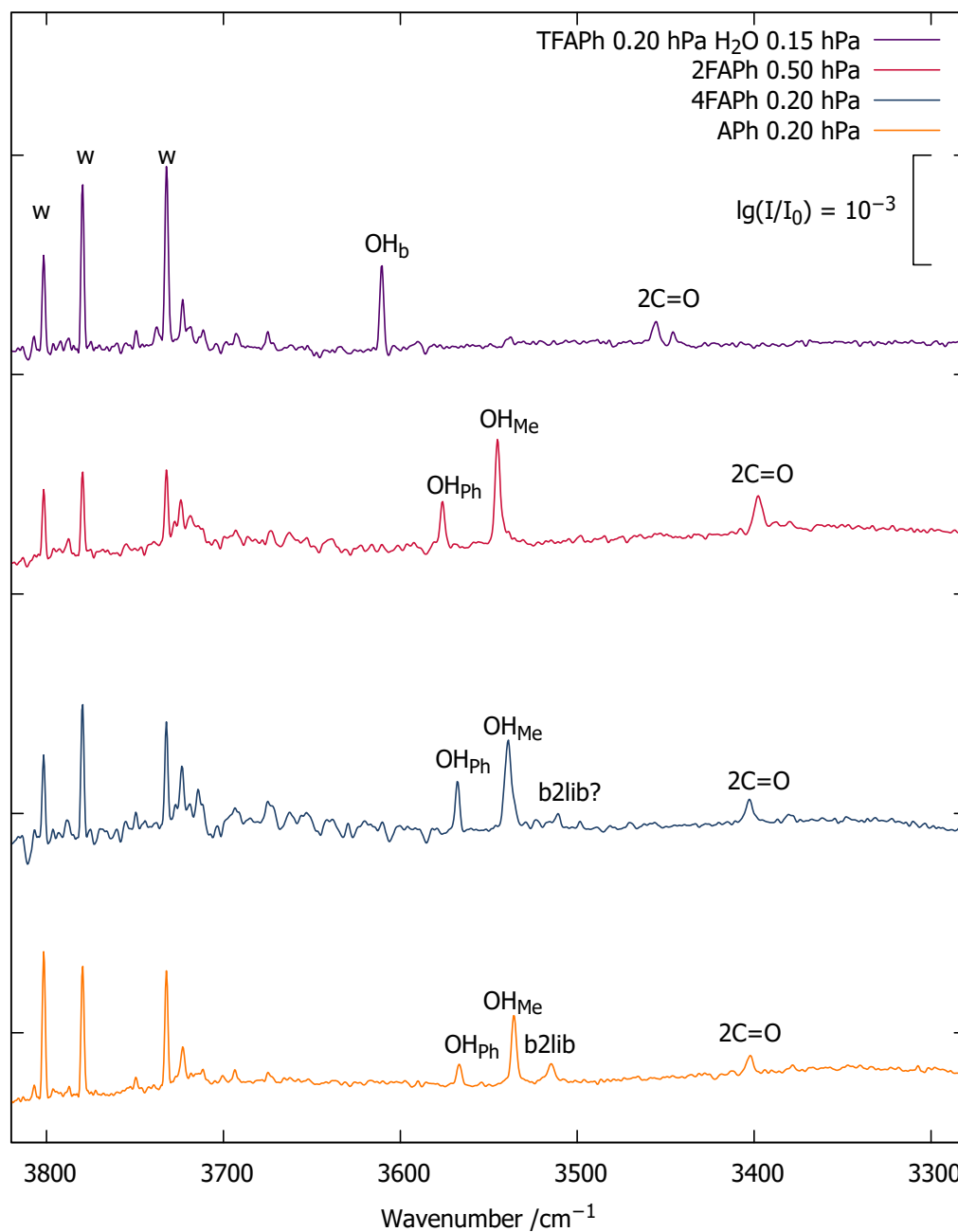


Fig. 8.3: FTIR spectra of all investigated hydrates of acetophenone derivatives. Details on the spectra can be found in Table 8.8. All spectra were recorded using a 750 mbar expansion of helium.

8.3.2 1,4-diazabicyclo[2.2.2]octane (DABCO) Hydrate

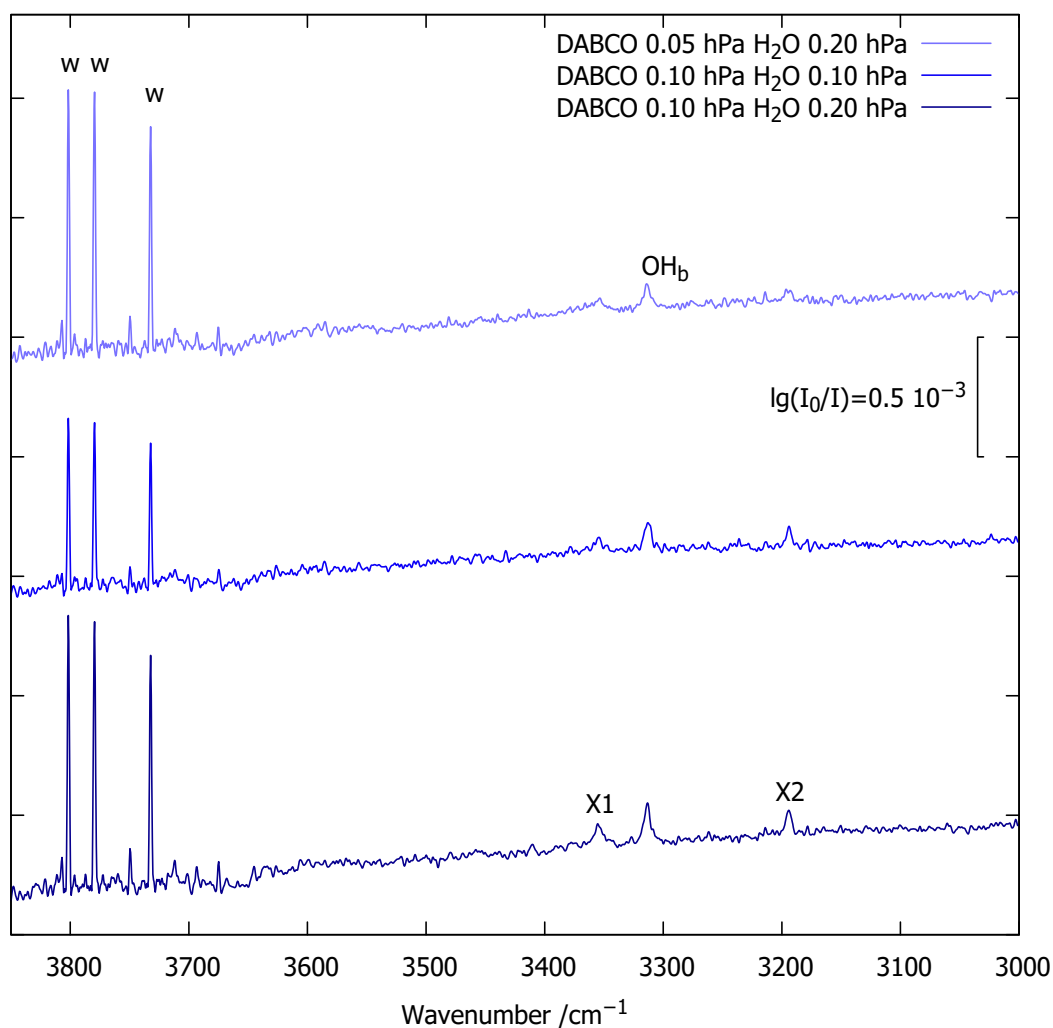


Fig. 8.4: FTIR spectrum of DABCO (99.93%, BLDpharm, Cat.#BD54566-5g) in 750 mbar He. The water is offered two equivalent binding sites, making the distinction between a potential resonance and higher clusters challenging without size selective methods. Further experimental and theory work is needed before the spectrum can fully be understood.

8.3.3 Cyclopentanone

Cyclopentanone Hydrate

Tab. 8.9: Experimental details of the spectra shown in Figure 8.5 giving the number of averaged gas pulses # and the date the spectrum was recorded dd/mm/yyyy. All substances were expanded in 750 mbar helium.

Spectrum	#	dd/mm/yyyy
Fig 8.5 violet	600	04/05/2020
Fig 8.5 red	400	16/03/2020
Fig 8.5 blue	750	29/04/2020
Fig 8.6 violet	800	29/07/2020

In order to investigate the resonance described in Chapter 3 the hydrates of cyclopentanone (99%, abcr, Lot:1022060) were investigated. The resulting FTIR spectra are shown in Figure 8.5. Cyclopentanone is abbreviated as C5 in the following. Unfortunately the results were not conclusive as the spectra show at least 3 overlapping signals in the OH region. The largest signal at 3516 cm^{-1} is most likely to correspond to the OH_b stretching vibration. If a b2lib resonance is present or not cannot be determined precisely as the signals overlap and probably larger clusters are formed. For the measurements no additional water was added, because we were hoping to get rid of the jet water at some stage, but a measurement with additional water could solve the question, whether a b2lib resonance is present or not. The position of the OH_b vibration makes it very likely to be present. Probably the formation of higher clusters can be suppressed and the resulting hetero dimer signals evaluated.

To get more insights a spectrum with ^{18}O water was recorded. The result is shown in Figure 8.6 as violet spectrum. When all C5 spectra are averaged, multiplied by 1.25 (red spectrum in Figure 8.6) and subtracted from the violet spectrum the blue spectrum is obtained, which mostly contains ^{18}O -water signals. They are labeled ^{18}X and the two signals at 3521 and 3503 cm^{-1} could correspond to the $^{18}\text{OH}_b$ stretching vibration and a b2lib resonance. The signal at 3450 cm^{-1} cannot be explained yet. Further investigations are needed to understand this hydration process and is why the data is not included in [14].

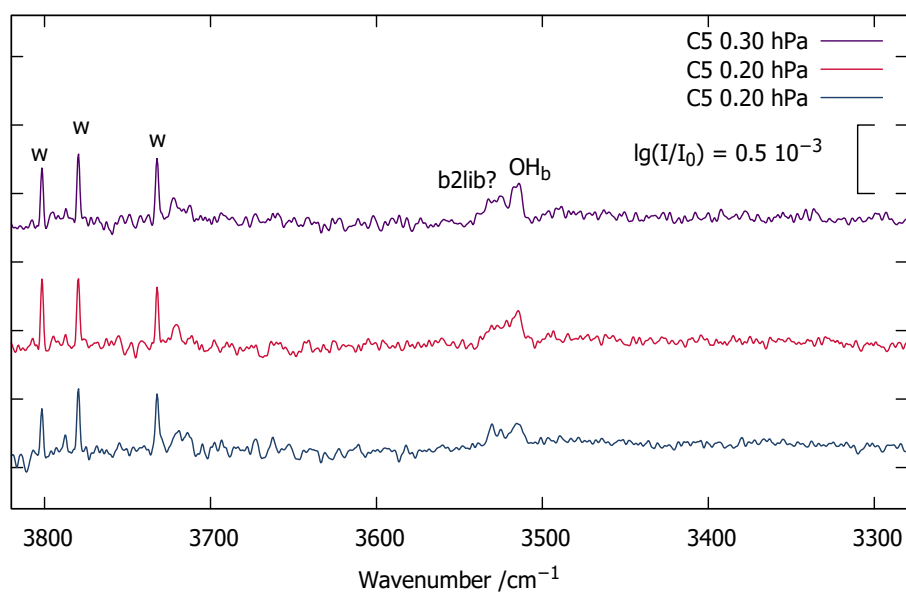


Fig. 8.5: Recorded infrared spectra of cyclopentanone with water. The water concentration is unknown because back in 2020 no water was added to spectra. Additional data on the used spectra can be found in Table 8.9.

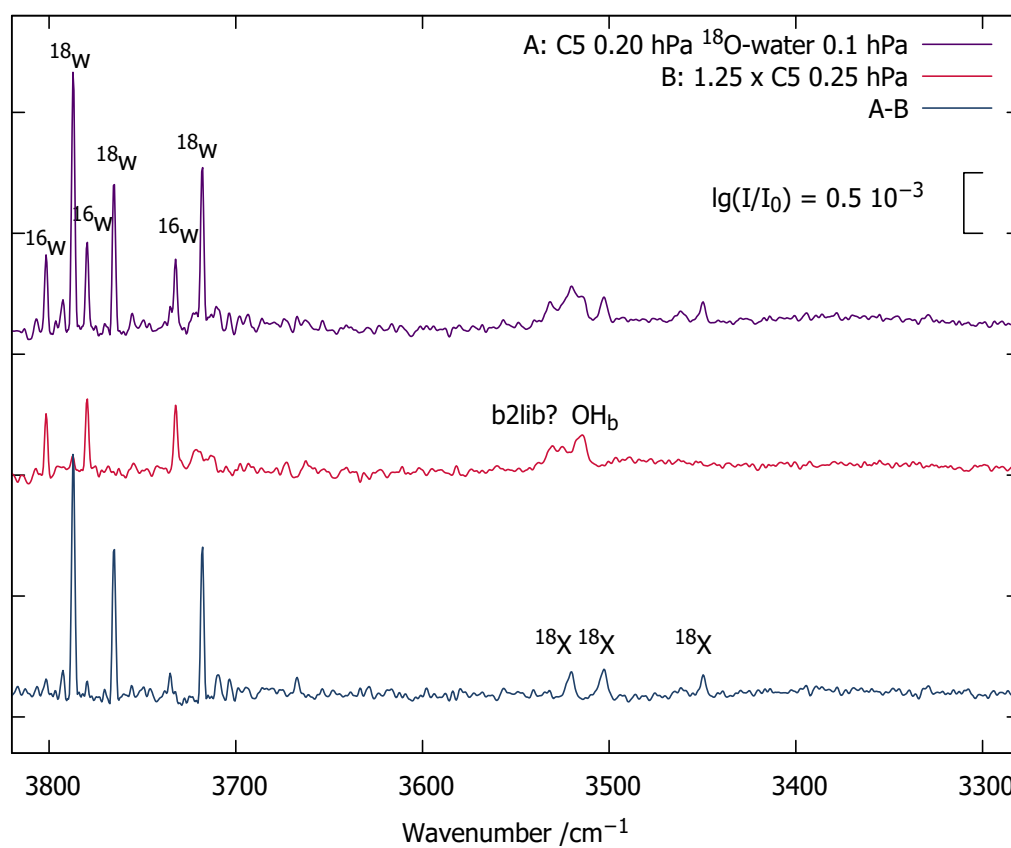


Fig. 8.6: Recorded infrared spectra of cyclopentanone with ^{18}O -water (violet), the averaged spectrum of all C5 measurements (red) multiplied by 1.25 and the subtraction spectrum between the two (blue). Additional data on the used spectra can be found in Table 8.9.

Cyclo-n-none Hydrates

Tab. 8.10: Experimental details of the spectra shown in Figure 8.7 giving the number of averaged gas pulses # and the dates used for the spectral identifier [dd/mm/yyyy]-[averaged spectra] and expanded in helium.

Spectrum	Molecule	Abbreviation	#	Identifier
violet	Cyclobutanone	C4	700	10/02/2020-abcd
red	Cyclopentanone	C5	1750	16/03/2020-cdefg 29/04/2020-abcdefgh 04/05/2020-abcdef
blue	Cyclohexanone	C6	1700	12/02/2020-abcdef 13/02/2020-abcde
orange	Cycloheptanone	C7	500	16/03/2020-abc
black	Cyclooctanone	C8	1500	19/08/2021-abcde 15/10/2021-abcd

Tab. 8.11: Theory predictions of the most stable cyclo-n-nones (n=4–8) hydrate conformer on B3LYP-D3(BJ)/def2-TZVP level of theory. The predicted OH_b wavenumber is given unscaled and scaled (scaling factor 0.98) and is compared to the perturbed experimental wavenumber.

Molecule	$\text{OH}_b^{\text{theo}} / \text{cm}^{-1}$	$\text{OH}_b^{\text{theo, scaled}} / \text{cm}^{-1}$	$\text{OH}_b^{\text{exp, perturbed}} / \text{cm}^{-1}$
C4	3635	3563	3548
C5	3605	3533	3516
C6	3601	3529	3532
C7	3593	3521	3512
C8	3581	3509	3503

In this work the hydrates of a lot of different donors molecules were investigated. The cyclopentanone (C5) nicely fits into a series of cyclic ketones, namely cyclobutanone (C4), cyclohexanone (C6), cycloheptanone (C7) and cyclooctanone (C8). The spectra of all cyclo-n-none hydrates are shown in Figure 8.7 (more data on the recorded spectra can be found in Table 8.10). One can observe that the OH_b stretching vibration is shifted to lower wavenumbers with increasing ring size. C5 is the only outlier in this series, but the signal assignment is not secure, and the signal at 3516 cm^{-1} may not correspond to OH_b . The shift of the OH_b vibration is predicted by quantum chemical calculations on B3LYP-D3(BJ)/def2-TZVP level of theory (see Table 8.11) and they show the same trend as the experimental data, the larger the ring size, the stronger the predicted OH shift.

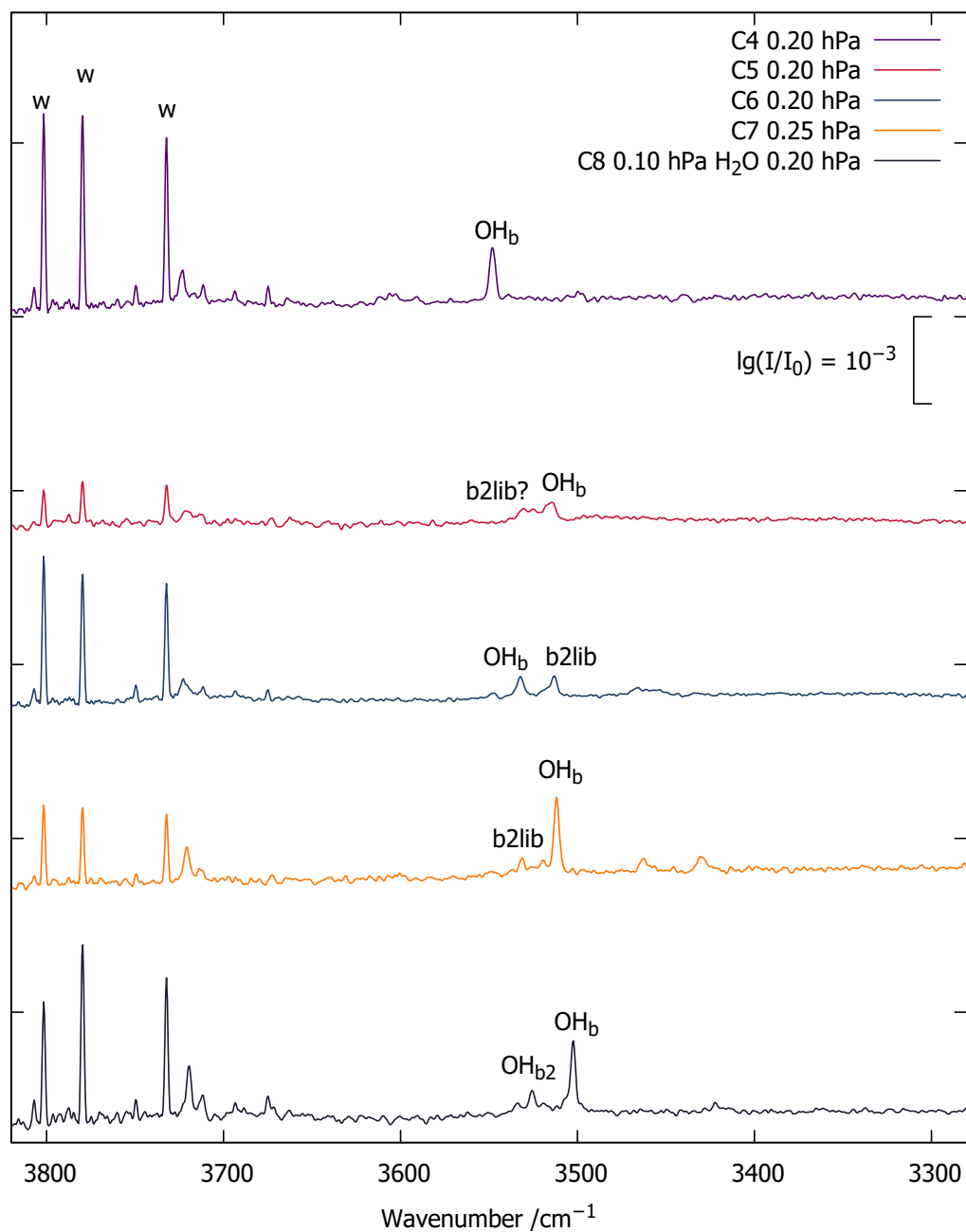


Fig. 8.7: FTIR spectra of C4–8 hydrates. Details on the spectra can be found in Table 8.10. All spectra were recorded using a 750 mbar expansion of helium.

Hydrates of Acetaldehyde and Propylene Oxide

Tab. 8.12: Experimental details of the spectra shown in Figure 8.8 giving the number of averaged gas pulses #, and the spectral identifiers giving the dates on which the spectrum was recorded (dd/mm/yyyy) and the spectra used for the averaged spectrum. In all measurements helium was used as carrier gas with a stagnation pressure of 750 mbar.

Spectrum	Molecule	Abbreviation	#	Identifier
Fig 8.8 violet	Acetaldehyde	AA	700	30/06/2021-abcdefg
Fig 8.8 red	Propylene oxide	PO	800	27/07/2021-abcde

Before the final decision on the test set of the HyDRA blind challenge (further in formation in Chapter 5) was made, a lot of test experiments with different substances were performed to increase the success rate in having a secure signal assignment without theory predictions. Two potential candidates were acetaldehyde (AA; acetaldehyde, $\geq 99.5\%$, Sigma Aldrich, Lot#SHBL3064) and propylene oxide (PO; propylene oxide, $> 99\%$, TCI, Lot.UVEUG-ZX). The measured hydrates are shown in Figure 8.8 and further details on the experimental conditions can be found in Table 8.12. Both spectra show one broad signal, which in both cases may be explained by two possible conformers which have a very similar shift and are overlapping. The band center for the AA hydrate(s) (violet) lies at 3561 cm^{-1} and for the PO hydrate (red) at 3533 cm^{-1} . The two dimer signals may be resolved by using a higher resolution in the measurement and/or looking whether the less stable conformer relaxes into the minimum structure when adding neon to the expansion. Both molecular clusters are interesting for benchmarking purposes as they are small, so further investigations may be of interest.

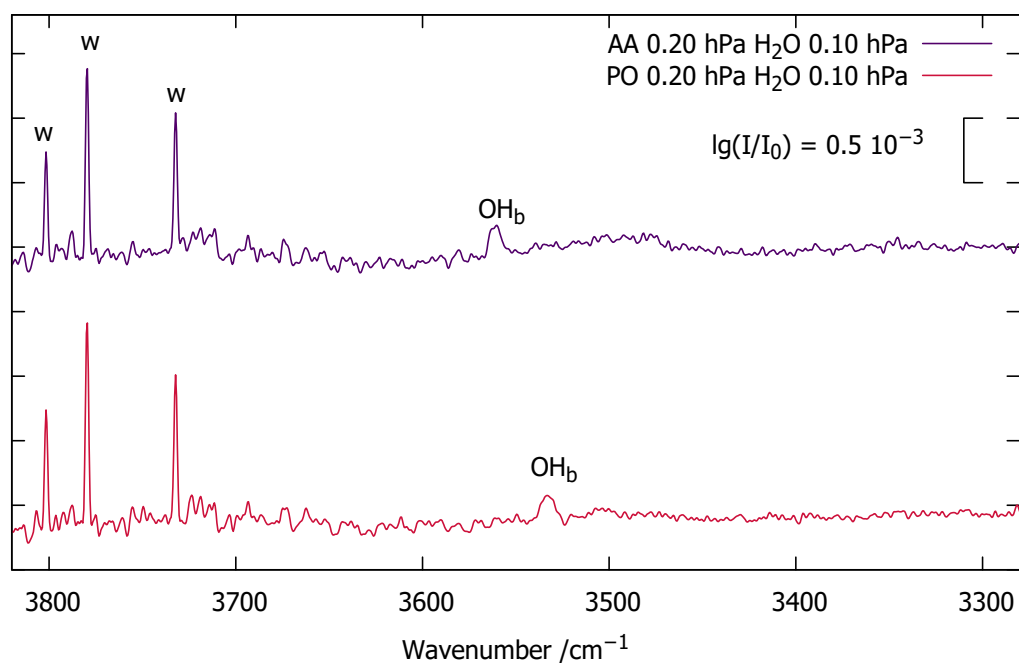


Fig. 8.8: Recorded infrared spectra of the hydrates of acetaldehyde (AA, violet) and propylene oxide (PO, red). Additional data on the recorded spectra can be found in Table 8.12. In all measurements helium was used as carrier gas and a stagnation pressure of 750 mbar was applied.

8.3.4 Methyl 2-Hydroxyacetate Hydrate

Tab. 8.13: Experimental details of the spectra shown in Figure 8.9 giving the number of averaged gas pulses # and the spectral identifiers consisting of the spectrum was recorded dd/mm/yyyy and which individual spectra were used. For all measurements helium was used as carrier gas at a stagnation pressure of 750 mbar helium.

Spectrum	#	dd/mm/yyyy
Fig 8.9 violet	800	24/08/2021-abcdef
Fig 8.9 red	800	23/08/2021-abcde
Fig 8.9 blue	800	20/08/2021-abcdef

To secure the signal assignment of the (–)methyl L-lactate (MLA) hydrate for the HYDRA blind challenge the hydrate of methyl 2-hydroxyacetate (MHA; 98%, BLDpharm, Lot No:BTL542) was also investigated. The spectra were not shown in the final publication [84] as for MLA also Raman measurements were performed and ^{18}O -water was used to secure the assignment, so the MHA measurements were no longer needed. They are shown in Figure 8.9 and more details on the used measurement conditions can be found in Table 8.13. The spectra are sorted by the amount of added water. When moving from blue to red to violet, the amount of water is increased, while the amount of MHA is kept constant. The signals labeled OH_b and $\text{OH}_{b_2}?$ are increasing proportional with the amount of water and are most likely to be assigned to water clusters. The size of the cluster can not be securely determined at this stage. By comparing the spectral information of MHA and MLA, the signal at 3542 cm^{-1} is most likely to be assigned to the OH_b stretching vibration of the 1:1 complex. The broad signal at 3484^{-1} , labeled $\text{OH}_{b_2}?$, cannot be assigned securely yet. It may be another 1:1 conformer or a higher cluster.

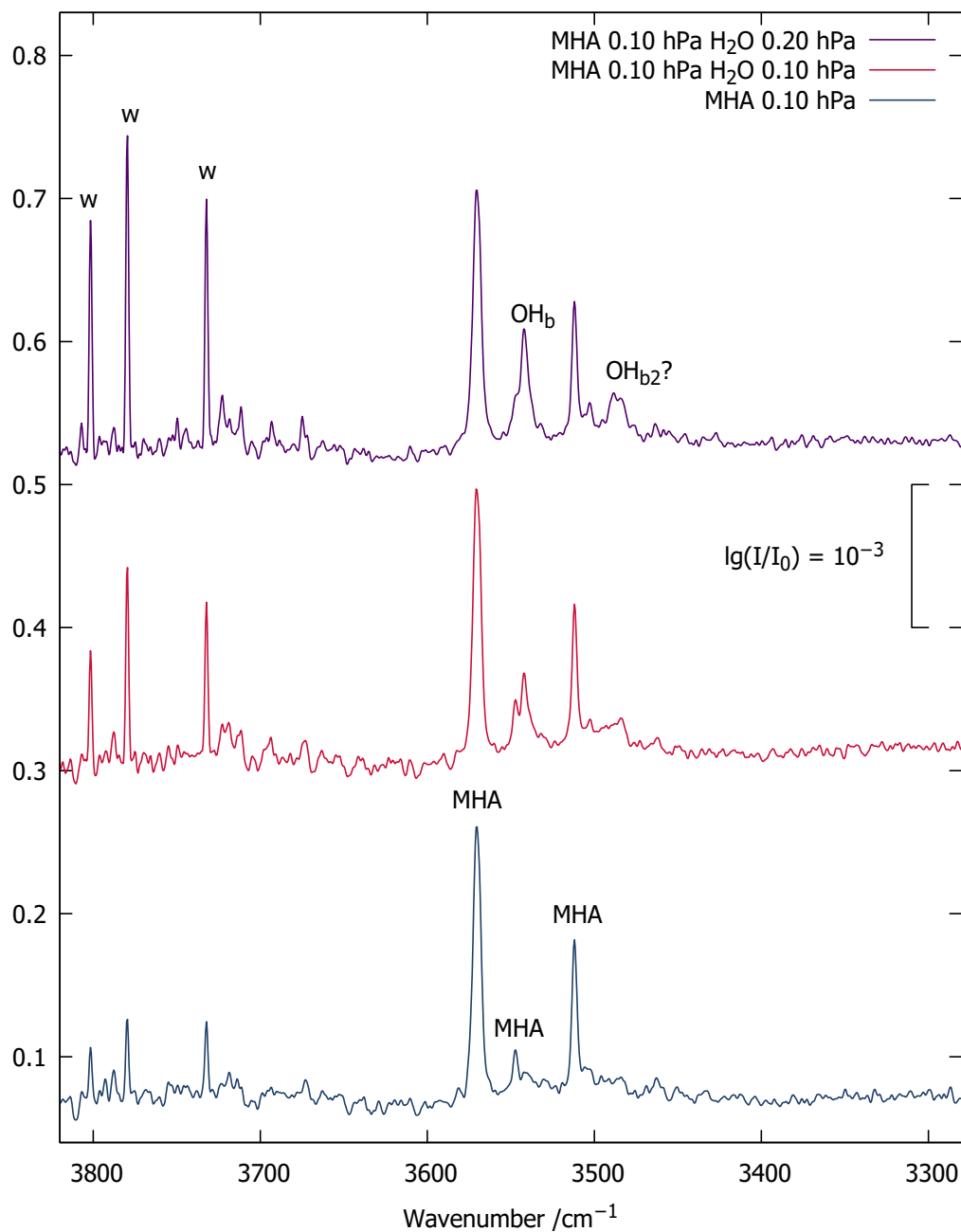


Fig. 8.9: Recorded infrared spectra of methyl-2-hydroxyacetate with water. Additional data on the used spectra can be found in Table 8.13. For all spectra a 750 mbar expansion with helium was used.

8.3.5 *tert*-Butylalcohol Hydrate

Tab. 8.14: Experimental details of the spectra shown in Figur 8.10 giving the number of averaged gas pulses # and the date the spectrum was recorded dd/mm/yyyy. All substances were expanded in 750 mbar helium.

Spectrum	#	dd/mm/yyyy
Fig 8.10 violet	800	05/10/2022
Fig 8.10 red	700	04/01/2022
Fig 8.10 blue	800	29/09/2022
Fig 8.10 orange	800	02/11/2022
Fig 8.10 black	600	28/09/2022
Fig 8.11 violet	600	29/11/2022
Fig 8.11 red	800	02/11/2022

In order to prove that the b2lib resonance (described in Chapter 3) is not only visible in hydrates of ketones, other groups of compounds were investigated. One of them is *tert*-butyl alcohol (*t*BuOH; $\geq 99\%$, Carl Roth GmbH, Charge 012180819). The recorded spectra with ^{16}O -water are shown in Figure 8.10 and an additional one with ^{18}O -water in Figure 8.11. The experimental data on the spectra can be found in Table 8.14. The complexes purely containing *t*BuOH are labeled *t*Bu in case of the monomer and (*t*Bu) $_2$ for the homodimer. The position of the homodimer signals are 3642 and 3497 cm^{-1} and are reported in a lot of publications like [134]. The OH_b stretching vibration of the hydrate can be found at 3530 cm^{-1} for ^{16}O -water and at 3512 cm^{-1} for ^{18}O -water. In Figure 8.10 the OH_b signals are rather small compared to the (*t*Bu) $_2$ signal, making it hard to evaluate if a b2lib resonance is present. The spectrum with ^{18}O -water does not give new insights in solving the question, whether a resonance is present or not. Even with a high ^{18}O -water concentration the OH_b signal remains small. Maybe a measurement with a high concentration of *t*BuOH and water give more insights, but it might be tricky to evaluate, as higher clusters might form.

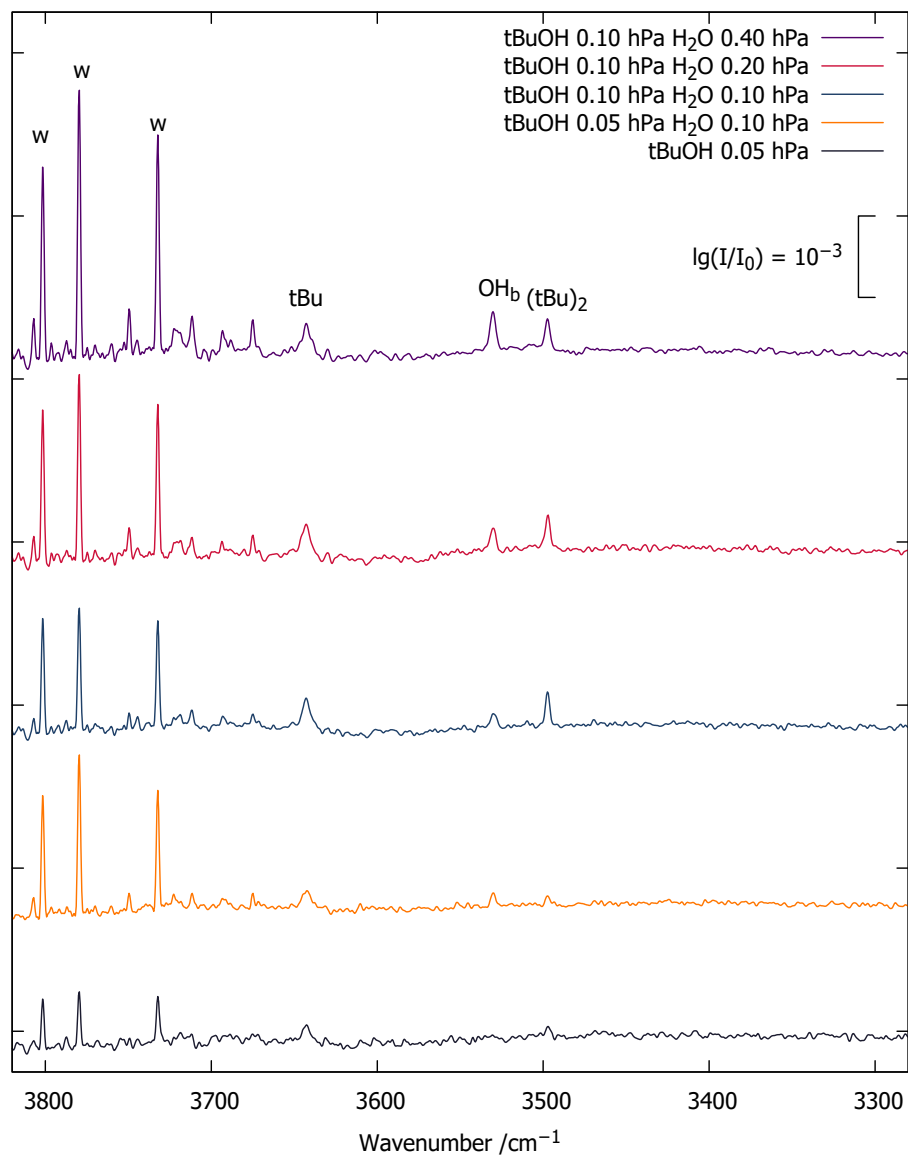


Fig. 8.10: Recorded infrared spectra of *tert*-butyl alcohol with water. Additional data on the used spectra can be found in Table 8.14. For all spectra a 750 mbar expansion with helium was used.

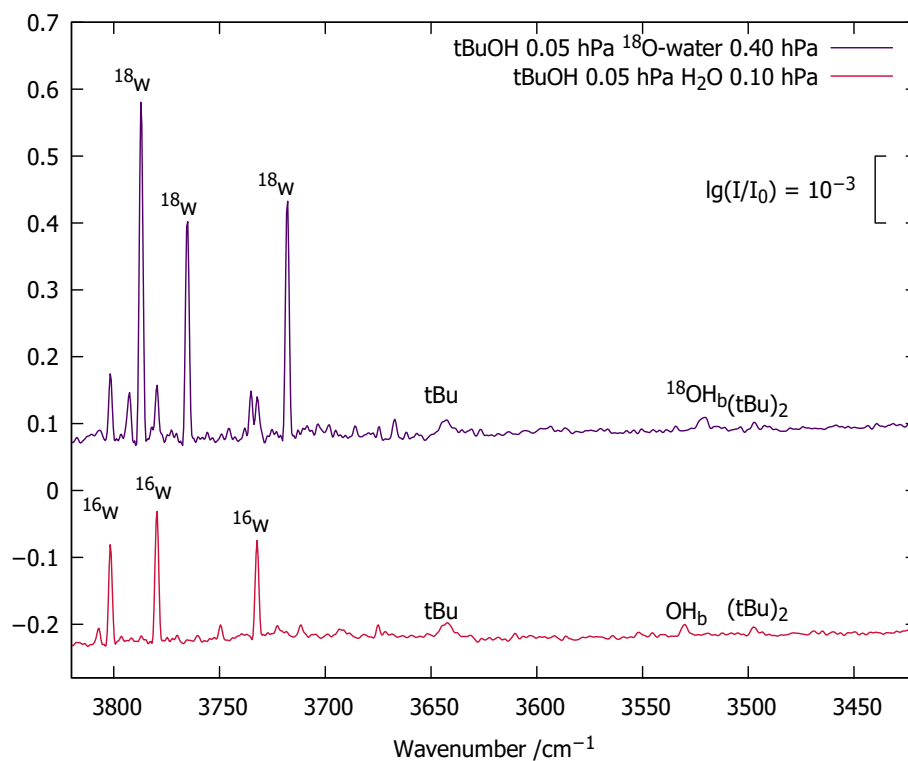


Fig. 8.11: Recorded infrared spectra of *tert*-butyl alcohol with different isotopes of water (^{16}O and ^{18}O). Additional data on the used spectra can be found in Table 8.14. For all spectra a 750 mbar expansion with helium was used.

8.3.6 2,2,4,4-Tetramethyl-3-pentanone Hydrate

Tab. 8.15: Experimental details of the spectra shown in Fig 8.12 giving the number of averaged gas pulses # and the date the spectrum was recorded dd/mm/yyyy and which individual spectra were used. For all measurements helium was used as carrier gas at a stagnation pressure of 750 mbar helium.

Spectrum	#	dd/mm/yyyy
Fig 8.12 violet	800	10/06/2021-abcdefg
Fig 8.12 red	800	22/06/2021-abcdefg
Fig 8.12 blue	800	17/06/2021-abcdefg
Fig 8.12 orange	700	11/06/2021-abcdefg
Fig 8.12 black	800	21/06/2021-abcdefg

Another potential acceptor molecule candidate for the HyDRA blind challenge (described in Chapter 5) was 2,2,4,4-Tetramethyl-3-pentanone (98%, Alfa Aesar, Lot:N10G009), which is shortened as TMP in the following. While a structural search using CREST and a later optimization on B3LYP-D3(BJ)/def2-TZVP level of theory predict one stable conformer for the TMP hydrate, the Figure 8.12 shows two signals, that scale similarly with the water and TMP concentration and are labeled OH_{b1} and OH_{b2} . More data on the measurements can be found in Table 8.15. The larger signal at 3564 cm^{-1} can be assigned to the most stable conformer, which theory predicts at 3658 cm^{-1} (scaled with 0.98: 3585 cm^{-1}) even though the prediction is comparably far away. Maybe the theory predictions are failing on this molecule and it would be worth to try out other functionals. From the spectra it cannot be distinguished whether the minor signal at 3534 cm^{-1} is caused by another conformer or a resonance. Future work with water isotopes and/or neon, and other theory approaches may solve the signal assignment.

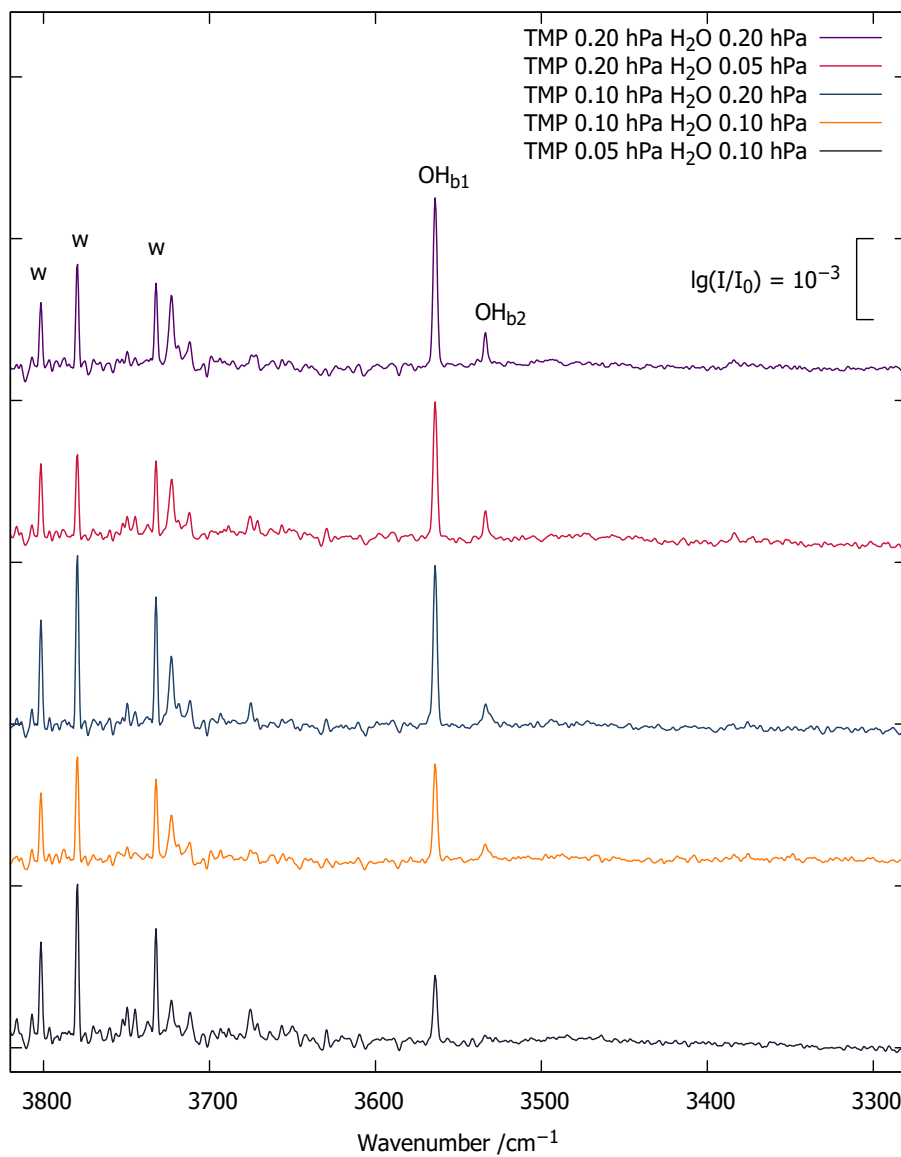


Fig. 8.12: Recorded infrared spectra of 2,2,4,4-tetramethyl-3-pentanone with water. Additional data on the used spectra can be found in Table 8.15. For all spectra a 750 mbar expansion with helium was used.

8.4 Data Collected for the HyDRA Blind Challenge

All measured substances:

Tab. 8.16: All potential donor molecules that have been measured for the HyDRA blind challenge. The chemical name, with the CAS registry number are given and if a spectrum is shown in this work the corresponding chapter is given.

Donor molecule	CAS No.	Chapter	Comment
Acetaldehyde	75-07-0	8.3.3	
Aniline	62-53-3		measured for training set
Benzaldehyde	100-52-7		signal assignment not conclusive, discussion in [29]
2'-Bromoacetophenone	2142-69-0		not volatile enough for experiment
Cyclooctanone	502-49-8	5.2.5	
1,3-Dimethyl-2-imidazolidinone	80-73-9	5.2.6	
4'-Fluorobenzaldehyde	459-57-4	8.3.1	
Formaldehyde	50-00-0	5.2.1	
Furan	110-00-9		no hetero dimer formed in expansion
Hexafluoro-2-propanol	920-66-1		measured at curry
4-Methoxy-2,2,6,6-tetramethyl-piperidine 1-oxyl radical	95407-69-5		not volatile enough for experiment
Methyl lactate	547-64-8	5.2.8	
1-Phenylcyclohexane-cis-1,2-diol	125132-75-4	5.2.9	
Propylene oxide	75-56-9	8.3.3	
Pyridine	110-86-1	5.2.2	
Tetrahydrofuran	109-99-9	5.2.4	
Tetrahydrothiophene	110-01-0	5.2.7	
2,2,4,4-Tetramethyl-3-pentanone	815-24-7	8.3.6	
Thiophene	110-02-1		no hetero dimer formed in expansion
Trifluoroacetophenon	434-45-7	5.2.3	
2,2,2-Trifluoroethanol	75-89-8	5.2.10	

Considered substances:

Tab. 8.17: All donor molecules that were considered, but have not even been experimentally probed for the HyDRA blind challenge. The chemical name and its the CAS registry number are given.

Donor molecule	CAS No.
Acetone oxime	127-06-0
2-Adamantanol	700-57-2
2'-Chloracetophenone	2142-68-9
2-Chlorocyclopentanone	694-28-0
Cyclohexanone oxime	100-64-1
2,6-Dimethylacetophenone	2142-76-9
N,N-Dimethylaniline	121-69-7
Dioxirane	157-26-6
Furfuryl alcohol	98-00-0
Furfuryl mercaptan	98-02-2
Benzonitrile	100-47-0
2'-Iodacetophenon	2142-70-3
4'-Methylacetophenon	122-00-9
Perfluoro(2-methyl-3-pentanone)	756-13-8
Perfluoro- <i>tert</i> -butyl alcohol	2378-02-1
2-Thiophenemethanol	636-72-6
2-Thiophenemethanethiol	6258-63-5
2-Thiophenemethanethiol	6258-63-5

Literature

- [1] F. Franks, R. S. of Chemistry (Great Britain), *Water: A Matrix of Life*, Royal Society of Chemistry, **2000**.
- [2] H. C. Gottschalk, T. L. Fischer, V. Meyer, R. Hildebrandt, U. Schmitt, M. A. Suhm, “A Sustainable Slit Jet FTIR Spectrometer for Hydrate Complexes and Beyond”, *Instruments* **2021**, *5*, 12.
- [3] A. Kryshtafovych, T. Schwede, M. Topf, K. Fidelis, J. Moult, “Critical assessment of methods of protein structure prediction (CASP)—Round XIII”, *Proteins: Structure Function and Bioinformatics* **2019**, *87*, 1011–1020.
- [4] C. R. Groom, A. M. Reilly, “Sixth blind test of organic crystal-structure prediction methods”, *Acta Crystallogr. B* **2014**, *70*, 776–777.
- [5] P. M. Felker, A. H. Zewail, “Stepwise solvation of molecules as studied by picosecond-jet spectroscopy: dynamics and spectra”, *Chem. Phys. Lett.* **1983**, *94*, 454–460.
- [6] R. D. Knochenmuss, D. E. Smith, “Time and internal energy dependent fluorescence spectra of naphtholwater clusters”, *J. Chem. Phys* **1994**, *101*, 7327–7336.
- [7] R. Bombach, E. Honegger, S. Leutwyler, “Solute-solvent interactions in microhydrate clusters: Carbazole-(H₂O)_n”, *Chem. Phys. Lett.* **1985**, *118*, 449–454.
- [8] C. Puzzarini, J. Bloino, N. Tasinato, V. Barone, “Accuracy and interpretability: the devil and the holy grail. New routes across old boundaries in computational spectroscopy”, *Chem. Rev.* **2019**, *119*, 8131–8191.
- [9] H. C. Gottschalk, A. Poblitzki, M. A. Suhm, M. M. Al-Mogren, J. Antony, A. A. Auer, L. Baptista, D. M. Benoit, G. Bistoni, F. Bohle, *et al.*, “The furan microsolvation blind challenge for quantum chemical methods: First steps”, *J. Chem. Phys* **2018**, *148*, 14301.
- [10] H. C. Gottschalk, A. Poblitzki, M. Fatima, D. A. Obenchain, C. Pérez, J. Antony, A. A. Auer, L. Baptista, D. M. Benoit, G. Bistoni, *et al.*, “The first microsolvation step for furans: New experiments and benchmarking strategies”, *J. Chem. Phys* **2020**, *152*, 164303.

- [11] M. Nedić, T. N. Wassermann, R. W. Larsen, M. A. Suhm, “A combined Raman- and infrared jet study of mixed methanol-water and ethanol-water clusters”, *Phys. Chem. Chem. Phys.* **2011**, *13*, 14050–14063.
- [12] C. Camy-Peyret, J. M. Flaud, G. Guelachvili, C. Amiot, “High resolution Fourier transform spectrum of water between 2930 and 4255 cm^{-1} ”, *Mol. Phys.* **1973**, *26*, 825–855.
- [13] B. Zhang, Y. Yu, Y.-Y. Zhang, S. Jiang, Q. Li, H.-S. Hu, G. Li, Z. Zhao, C. Wang, H. Xie, W. Zhang, D. Dai, G. Wu, D. H. Zhang, L. Jiang, J. Li, X. Yang, “Infrared spectroscopy of neutral water clusters at finite temperature: Evidence for a noncyclic pentamer”, *Proc. Natl. Acad. Sci. U.S.A.* **2020**, *117*, 15423–15428.
- [14] T. L. Fischer, T. Wagner, H. C. Gottschalk, A. Nejad, M. A. Suhm, “A rather universal vibrational resonance in 1:1 hydrates of carbonyl compounds”, *J. Phys. Chem. Lett.* **2021**, *12*, 138–144.
- [15] G. Karir, N. O. B. Lüttschwager, M. A. Suhm, “Phenylacetylene as a gas phase sliding balance for solvating alcohols”, *Phys. Chem. Chem. Phys.* **2019**, *21*, 7831–7840.
- [16] N. Lüttschwager, “NoisySignalIntegration. jl: A Julia package for uncertainty evaluation of numeric integrals.”, *J. Open Source Softw.* **2021**, *6*, 3526.
- [17] V. Meyer, S. Eisermann, H. C. Gottschalk, R. Hildebrandt, B. Langer, U. Schmitt, M. Zippert, M. A. Suhm, “Gratin Jet Figures: Version 1.0”, **2020**, DOI 10.25625/6V6KSN.
- [18] H. C. Gottschalk, “IR-Untersuchung von schwach gebundenen Molekülaggregaten im Überschallstrahl”, <https://hdl.handle.net/21.11130/00-1735-0000-0005-14EE-9>, Georg-August-Universität Göttingen, **2020**.
- [19] M. A. Suhm, F. Kollipost, “Femtosecond single-mole infrared spectroscopy of molecular clusters”, *Phys. Chem. Chem. Phys.* **2013**, *15*, 10702–10721.
- [20] E. M. Brás, T. L. Fischer, M. A. Suhm, “The hydrates of TEMPO: Water vibrations reveal radical microsolvation”, *Angew. Chem.* **2021**, *60*, 19013–19017.
- [21] M. Heger, “Diagonal and Off-Diagonal Anharmonicity in Hydrogen-Bonded Systems”, <https://ediss.uni-goettingen.de/handle/11858/00-1735-0000-0028-874B-E>, Georg-August-Universität Göttingen, **2016**.
- [22] J. B. Paul, C. P. Collier, R. J. Saykally, J. J. Scherer, A. O’Keefe, “Direct Measurement of Water Cluster Concentrations by Infrared Cavity Ringdown Laser Absorption Spectroscopy”, *J. Phys. Chem. A* **1997**, *101*, 5211–5214.

-
- [23] A. Moudens, R. Georges, M. Goubet, J. Makarewicz, S. E. Lokshantov, A. A. Vigasin, “Direct absorption spectroscopy of water clusters formed in a continuous slit nozzle expansion”, *J. Chem. Phys.* **2009**, *131*, 204312.
- [24] K. E. Otto, Z. Xue, P. Zielke, M. A. Suhm, “The Raman spectrum of isolated water clusters”, *Phys. Chem. Chem. Phys.* **2014**, *16*, 9849–9858.
- [25] B. Lucas, F. Lecomte, B. Reimann, H.-D. Barth, G. Grégoire, Y. Bouteiller, J.-P. Schermann, C. Desfrancois, “A new infrared spectroscopy technique for structural studies of mass-selected neutral polar complexes without chromophore”, *Phys. Chem. Chem. Phys.* **2004**, *6*, 2600–2604.
- [26] F. Huisken, M. Kaloudis, A. Kulcke, “Infrared spectroscopy of small size-selected water clusters”, *J. Chem. Phys.* **1996**, *104*, 17–25.
- [27] K. Kuyanov-Prozument, M. Y. Choi, A. F. Vilesov, “Spectrum and infrared intensities of OH-stretching bands of water dimers”, *J. Chem. Phys.* **2010**, *132*, 14304.
- [28] I. León, R. Montero, F. Castaño, A. Longarte, J. A. Fernández, “Mass-Resolved Infrared Spectroscopy of Complexes without Chromophore by Nonresonant Femtosecond Ionization Detection”, *J. Phys. Chem. A* **2012**, *116*, 6798–6803.
- [29] M. Bödecker, “Mitgestaltung eines Blindwettbewerbs zur Vorhersagbarkeit von Hydratclusterschwingungen”, Georg-August-Universität Göttingen, **2021**.
- [30] M. Banno, K. Ohta, S. Yamaguchi, S. Hirai, K. Tominaga, “Vibrational Dynamics of Hydrogen-Bonded Complexes in Solutions Studied with Ultrafast Infrared Pump–Probe Spectroscopy”, *Acc. Chem. Res.* **2009**, *42*, 1259–1269.
- [31] E. T. J. Nibbering, J. Dreyer, O. Kuhn, J. Breidenbeck, P. Hamm, T. Elsaesser, *Vibrational dynamics of hydrogen bonds*, Springer, **2007**, pp. 619–687.
- [32] M. Grechko, T. Hasegawa, F. D’Angelo, H. Ito, D. Turchinovich, Y. Nagata, M. Bonn, “Coupling between intra- and intermolecular motions in liquid water revealed by two-dimensional terahertz-infrared-visible spectroscopy”, *Nat. Commun.* **2018**, *9*, 1–8.
- [33] K. M. Hunter, F. A. Shakib, F. Paesani, “Disentangling coupling effects in the infrared spectra of liquid water”, *J. Phys. Chem. B* **2018**, *122*, 10754–10761.
- [34] D. Laage, H. Demirdjian, J. T. Hynes, “Intermolecular vibration–vibration energy transfer in solution: Hydrogen fluoride in water”, *Chem. Phys. Lett.* **2005**, *405*, 453–458.
- [35] T. S. Zwier, “Laser spectroscopy of jet-cooled biomolecules and their water-containing clusters: Water bridges and molecular conformation”, *J. Phys. Chem. A* **2001**, *105*, 8827–8839.

- [36] F. Kollipost, A. V. Domanskaya, M. A. Suhm, “Microscopic roots of alcohol–ketone demixing: infrared spectroscopy of methanol–acetone clusters”, *J. Phys. Chem. A* **2015**, *119*, 2225–2232.
- [37] J. A. Stride, P. H. Dallin, U. A. Jayasooriya, “Intermolecular Fermi resonance”, *J. Chem. Phys.* **2003**, *119*, 2747–2752.
- [38] M. Miyazaki, J. Saikawa, H. Ishizuki, T. Taira, M. Fujii, “Isomer selective infrared spectroscopy of supersonically cooled cis- and trans-N-phenylamides in the region from the amide band to NH stretching vibration”, *Phys. Chem. Chem. Phys.* **2009**, *11*, 6098–6106.
- [39] J. Pochert, M. Quack, J. Stohner, M. Willeke, “Ab initio calculation and spectroscopic analysis of the intramolecular vibrational redistribution in 1,1,1,2-tetrafluoroiodoethane CF₃CHF₂I”, *J. Chem. Phys.* **2000**, *113*, 2719–2735.
- [40] H. K. Shin, “Inter- and Intramolecular Vibrational Energy Flow in a Formamide–Water Complex”, *J. Phys. Chem. A* **2020**, *124*, 3031–3037.
- [41] E. Fermi, “Über den Ramaneffekt des Kohlendioxyds”, *Zeitschrift für Physik* **1931**, *71*, 250–259.
- [42] I. Plastinin, S. Burikov, S. Dolenko, T. Dolenko, “Contribution of Fermi and Darling–Dennison resonances to the formation of Raman spectra of water and water–ethanol solutions”, *J. Raman Spectrosc* **2017**, *48*, 1235–1242.
- [43] S. J. Daunt, H. Shurvell, “The gas phase infrared band contours of s-triazine and s-triazine-d₃: The fundamentals of C₃N₃H₃ and C₃N₃D₃ and some overtone and combination bands of C₃N₃H₃”, *J. Mol. Spectrosc.* **1976**, *62*, 373–395.
- [44] J. M. L. Martin, P. R. Taylor, “Accurate ab initio quartic force field for trans-HNNH and treatment of resonance polyads”, *Spectrochim. Acta Part A* **1997**, *53*, 1039–1050.
- [45] A. M. Rosnik, W. F. Polik, “VPT2+ K spectroscopic constants and matrix elements of the transformed vibrational Hamiltonian of a polyatomic molecule with resonances using Van Vleck perturbation theory”, *Mol. Phys.* **2014**, *112*, 261–300.
- [46] K. Mackeprang, H. G. Kjaergaard, T. Salmi, V. Hänninen, L. Halonen, “The effect of large amplitude motions on the transition frequency redshift in hydrogen bonded complexes: A physical picture”, *J. Chem. Phys.* **2014**, *140*, 184309.
- [47] P. R. Rablen, J. W. Lockman, W. L. Jorgensen, “Ab initio study of hydrogen-bonded complexes of small organic molecules with water”, *J. Phys. Chem. A* **1998**, *102*, 3782–3797.

-
- [48] A. Poblitzki, H. C. Gottschalk, M. A. Suhm, “Tipping the scales: Spectroscopic tools for intermolecular energy balances”, *J. Phys. Chem. Lett.* **2017**, *8*, 5656–5665.
- [49] S. Grimme, “Exploration of Chemical Compound, Conformer, and Reaction Space with Meta-Dynamics Simulations Based on Tight-Binding Quantum Chemical Calculations”, *J. Chem. Theory Comput.* **2019**, *15*, 2847–2862.
- [50] P. Pracht, F. Bohle, S. Grimme, “Automated exploration of the low-energy chemical space with fast quantum chemical methods”, *Phys. Chem. Chem. Phys.* **2020**, *22*, 7169–7192.
- [51] S. Grimme, C. Bannwarth, P. Shushkov, “A Robust and Accurate Tight-Binding Quantum Chemical Method for Structures, Vibrational Frequencies, and Noncovalent Interactions of Large Molecular Systems Parametrized for All spd-Block Elements ($Z = 1-86$)”, *J. Chem. Theory Comput.* **2017**, *13*, 1989–2009.
- [52] C. Bannwarth, S. Ehlert, S. Grimme, “GFN2-xTB—An Accurate and Broadly Parametrized Self-Consistent Tight-Binding Quantum Chemical Method with Multipole Electrostatics and Density-Dependent Dispersion Contributions”, *J. Chem. Theory Comput.* **2019**, *15*, 1652–1671.
- [53] J. G. Brandenburg, C. Bannwarth, A. Hansen, S. Grimme, “B97-3c: A revised low-cost variant of the B97-D density functional method”, *J. Chem. Phys.* **2018**, *148*, 064104.
- [54] P. A. M. Dirac, R. H. Fowler, “Quantum mechanics of many-electron systems”, *Proc. R. Soc. London Ser. A* **1929**, *123*, 714–733.
- [55] J. C. Slater, “A Simplification of the Hartree-Fock Method”, *Phys. Rev.* **1951**, *81*, 385–390.
- [56] A. D. Becke, “Density-functional exchange-energy approximation with correct asymptotic behavior”, *Phys. Rev. A* **1988**, *38*, 3098–3100.
- [57] C. Lee, W. Yang, R. G. Parr, “Development of the Colle-Salvetti correlation-energy formula into a functional of the electron density”, *Phys. Rev. B* **1988**, *37*, 785–789.
- [58] A. D. Becke, “Density-functional thermochemistry. I. The effect of the exchange-only gradient correction”, *J. Chem. Phys.* **1992**, *96*, 2155–2160.
- [59] TURBOMOLE V7.4 2019, a development of University of Karlsruhe and Forschungszentrum Karlsruhe GmbH, 1989-2007, TURBOMOLE GmbH, since 2007; available from <http://www.turbomole.com>.
- [60] F. Furche, R. Ahlrichs, C. Hättig, W. Klopper, M. Sierka, F. Weigend, “Turbo-mole”, *WIREs Comput. Mol. Sci.* **2014**, *4*, 91–100.

- [61] J. Tennyson, N. F. Zobov, R. Williamson, O. L. Polyansky, P. F. Bernath, “Experimental energy levels of the water molecule”, *J. Phys. Chem. Ref. Data* **2001**, *30*, 735–831.
- [62] A. Mukhopadhyay, W. T. S. Cole, R. J. Saykally, “The water dimer I: Experimental characterization”, *Chem. Phys. Lett.* **2015**, *633*, 13–26.
- [63] R. Schwan, M. Kaufmann, D. Leicht, G. Schwaab, M. Havenith, “Infrared spectroscopy of the ν_2 band of the water monomer and small water clusters $(\text{H}_2\text{O})_n=2,3,4$ in helium droplets”, *Phys. Chem. Chem. Phys.* **2016**, *18*, 24063–24069.
- [64] Y. Bouteiller, B. Tremblay, J. P. Perchard, “The vibrational spectrum of the water dimer: Comparison between anharmonic ab initio calculations and neon matrix infrared data between 14,000 and 90cm^{-1} ”, *Chem. Phys.* **2011**, *386*, 29–40.
- [65] P. K. Verma, A. Kundu, M. S. Puretz, C. Dhoonmoon, O. S. Chegwiddden, C. H. Londergan, M. Cho, “The Bend+Libration Combination Band Is an Intrinsic, Collective, and Strongly Solute-Dependent Reporter on the Hydrogen Bonding Network of Liquid Water”, *J. Phys. Chem. B* **2017**, *122*, 2587–2599.
- [66] A. B. McCoy, “The role of electrical anharmonicity in the association band in the water spectrum”, *J. Phys. Chem. B* **2014**, *118*, 8286–8294.
- [67] J. Ceponkus, P. Uvdal, B. Nelander, “Far-Infrared Band Strengths in the Water Dimer: Experiments and Calculations”, *J. Phys. Chem. A* **2008**, *112*, 3921–3926.
- [68] J. B. Paul, R. A. Provencal, C. Chapo, K. Roth, R. Casaes, R. J. Saykally, “Infrared cavity ringdown spectroscopy of the water cluster bending vibrations”, *J. Phys. Chem. A* **1999**, *103*, 2972–2974.
- [69] T. Wagner, “Environmental and Resonance Effects on the Infrared Spectra of Hydrogen Bonded Complexes”, Georg-August-Universität Göttingen, **2020**.
- [70] K. Halbmaier, J. Seikowski, I. Tkach, C. Höbartner, D. Sezer, M. Bennati, “High-resolution measurement of long-range distances in RNA: pulse EPR spectroscopy with TEMPO-labeled nucleotides”, *Chemical science* **2016**, *7*, 3172–3180.
- [71] B. Keoshkerian, M. K. Georges, D. Boils-Boissier, “Living free-radical aqueous polymerization”, *Macromolecules* **1995**, *28*, 6381–6382.
- [72] L. Tebben, A. Studer, “Nitroxides: applications in synthesis and in polymer chemistry”, *Angew. Chem.* **2011**, *50*, 5034–5068.
- [73] A. De Mico, R. Margarita, L. Parlanti, A. Vescovi, G. Piancatelli, “A versatile and highly selective hypervalent iodine (III)/2,2,6,6-tetramethyl-1-piperidinyloxy-mediated oxidation of alcohols to carbonyl compounds”, *The J. Org. Chem.* **1997**, *62*, 6974–6977.

-
- [74] J. Guin, S. De Sarkar, S. Grimme, A. Studer, “Biomimetic Carbene-Catalyzed Oxidations of Aldehydes Using TEMPO”, *Angew. Chem.* **2008**, *47*, 8727–8730.
- [75] I. Kaminker, R. Barnes, S. Han in *Methods in enzymology*, Vol. 564, Elsevier, **2015**, pp. 457–483.
- [76] J. Hunold, J. Eisermann, M. Brehm, D. Hinderberger, “Characterization of aqueous lower-polarity solvation shells around amphiphilic 2,2,6,6-tetramethylpiperidine-1-oxyl radicals in water”, *The Journal of Physical Chemistry B* **2020**, *124*, 8601–8609.
- [77] A. Wilting, M. Kuegler, I. Siewert, “Copper Complexes with NH-Imidazolyl and NH-Pyrazolyl Units and Determination of Their Bond Dissociation Gibbs Energies”, *Inorg. Chem.* **2016**, *55*, 1061–1068.
- [78] P. Franchi, M. Lucarini, P. Pedrielli, G. F. Pedulli, “Nitroxide radicals as hydrogen bonding acceptors. An infrared and EPR study.”, *ChemPhysChem* **2002**, *3*, 789–793.
- [79] T. L. Fischer, M. Tepaske, M. A. Suhm, “Hydrogen sharing between two nitroxyl radicals in the gas phase and other microsolvation effects on the infrared spectrum of a bulky hydroxylamine”, *Phys. Chem. Chem. Phys.* **2023**, 11324–11330.
- [80] N. A. Giffin, M. Makramalla, A. D. Hendsbee, K. N. Robertson, C. Sherren, C. C. Pye, J. D. Masuda, J. A. C. Clyburne, “Anhydrous TEMPO-H: reactions of a good hydrogen atom donor with low-valent carbon centres”, *Org. Biomol. Chem.* **2011**, *9*, 3672–3680.
- [81] E. A. Mader, E. R. Davidson, J. M. Mayer, “Large Ground-State Entropy Changes for Hydrogen Atom Transfer Reactions of Iron Complexes”, *J. Am. Chem. Soc.* **2007**, *129*, 5153–5166.
- [82] D. Luckhaus, “The rovibrational spectrum of hydroxylamine: A combined high resolution experimental and theoretical study”, *J. Chem. Phys.* **1997**, *106*, 8409–8426.
- [83] T. L. Fischer, M. Bödecker, A. Zehnacker-Rentien, R. A. Mata, M. A. Suhm, “Setting up the HyDRA blind challenge for the microhydration of organic molecules”, *Phys. Chem. Chem. Phys.* **2022**, *24*, 11442–11454.
- [84] T. L. Fischer, M. Bödecker, S. M. Schweer, J. Dupont, V. Lepère, A. Zehnacker-Rentien, M. A. Suhm, B. Schröder, T. Henkes, D. M. Andrada, *et al.*, “The first HyDRA challenge for computational vibrational spectroscopy”, *ChemRxiv* **2023**.

- [85] T. L. Fischer, M. Bödecker, S. M. Schweer, J. Dupont, V. Lepère, A. Zehnacker-Rentien, M. A. Suhm, “Experimental Supplement to the HyDRA blind challenge”, *GRO.data*, Version 2 **2022**.
- [86] “QMbench – challenges for numerical quantum chemistry, <https://qmbench.net/>”, **2021**.
- [87] K. C. Fischer, S. L. Sherman, E. Garand, “Competition between solvation and intramolecular hydrogen-bonding in microsolvated protonated glycine and β -alanine”, *J. Phys. Chem. A* **2020**, *124*, 1593–1602.
- [88] I. León, P. F. Arnáiz, I. Usabiaga, J. A. Fernández, “Mass resolved IR spectroscopy of aniline–water aggregates”, *Phys. Chem. Chem. Phys.* **2016**, *18*, 27336–27341.
- [89] D. Bernhard, M. Fatima, A. Poblitzki, A. L. Steber, C. Pérez, M. A. Suhm, M. Schnell, M. Gerhards, “Dispersion-controlled docking preference: Multi-spectroscopic study on complexes of dibenzofuran with alcohols and water”, *Phys. Chem. Chem. Phys.* **2019**, *21*, 16032–16046.
- [90] J. Zischang, J. J. Lee, M. A. Suhm, “Communication: Where does the first water molecule go in imidazole?”, *J. Chem. Phys.* **2011**, *135*, 61102.
- [91] M. Broquier, F. Lahmani, A. Zehnacker-Rentien, V. Brenner, P. Millié, A. Pere-mans, “Hydrogen-bonded bridges in complexes of o-cyanophenol: Laser-induced fluorescence and IR/UV double-resonance studies”, *J. Phys. Chem. A* **2001**, *105*, 6841–6850.
- [92] K. L. Barbu, F. Lahmani, M. Mons, M. Broquier, A. Zehnacker, “IR–UV investigation of the structure of the 1-phenylethanol chromophore and its hydrated complexes”, *Phys. Chem. Chem. Phys.* **2001**, *3*, 4684–4688.
- [93] V. Venkatesan, A. Fujii, T. Ebata, N. Mikami, “A direct experimental evidence for an aromatic C–HO hydrogen bond by fluorescence-detected infrared spectroscopy”, *Chem. Phys. Lett.* **2004**, *394*, 45–48.
- [94] M. Becucci, S. Melandri, “High-resolution spectroscopic studies of complexes formed by medium-size organic molecules”, *Chem. Rev.* **2016**, *116*, 5014–5037.
- [95] S. E. Novick, “Bibliography of rotational spectra of weakly bound complexes; https://wesfiles.wesleyan.edu/home/snovick/SN_webpage/vdw.pdf.”, **2019**.
- [96] W. Caminati, J.-U. Grabow, *Chapter 15, Section 4.2*, (Ed.: J. Laane), Elsevier, **2011**.
- [97] P. Pinacho, D. A. Obenchain, M. Schnell, “New findings from old data: A semi-experimental value for the eQq of the nitrogen atom”, *J. Chem. Phys.* **2020**, *153*, 234307.

-
- [98] E. Burevschi, I. Peña, M. E. Sanz, “Medium-sized rings: Conformational preferences in cyclooctanone driven by transannular repulsive interactions”, *Phys. Chem. Chem. Phys.* **2019**, *21*, 4331–4338.
- [99] E. Burevschi, I. Peña, M. E. Sanz, “Geminal diol formation from the interaction of a ketone with water in the gas phase: Structure and reactivity of cyclooctanone-(H₂O) 1, 2 clusters”, *J. Phys. Chem. Lett.* **2021**, *12*, 12419–12425.
- [100] E. Vrolix, M. Goethals, T. Zeegers-Huyskens, “Infrared study of hydrogen bond complexes involving 1, 3-dimethyl, 2-imidazolidinone and hydroxylic derivatives”, *Spectrosc. Lett.* **1993**, *26*, 497–507.
- [101] A. Vigorito, L. Paoloni, C. Calabrese, L. Evangelisti, L. B. Favero, S. Melandri, A. Maris, “Structure and dynamics of cyclic amides: The rotational spectrum of 1, 3-dimethyl-2-imidazolidinone”, *J. Mol. Spectrosc.* **2017**, *342*, 38–44.
- [102] B. Nelander, “A matrix isolation study of the water-formaldehyde complex. The far-infrared region”, *Chemical Physics* **1992**, *159*, 281–287.
- [103] F. J. Lovas, C. L. Lugez, “The microwave spectrum and structure of CH₂O–H₂O”, *J. Mol. Spectrosc.* **1996**, *179*, 320–323.
- [104] J. Thomas, O. Sukhorukov, W. Jäger, Y. Xu, “Direct spectroscopic detection of the orientation of free OH groups in methyl lactate–(water)_{1,2} clusters: Hydration of a chiral hydroxy ester”, *Angew. Chem.* **2014**, *53*, 1156–1159.
- [105] S. A. Katsyuba, S. Spicher, T. P. Gerasimova, S. Grimme, “Revisiting conformations of methyl lactate in water and methanol”, *J. Chem. Phys.* **2021**, *155*, 24507.
- [106] E. Galántay, “1-phenylcyclohexane-1,2-diols and their geometry”, *Tetrahedron* **1963**, *19*, 319–321.
- [107] P. Nieto, M. Letzner, T. Endres, G. Schwaab, M. Havenith, “IR spectroscopy of pyridine–water structures in helium nanodroplets”, *Phys. Chem. Chem. Phys.* **2014**, *16*, 8384–8391.
- [108] R. B. Mackenzie, C. T. Dewberry, R. D. Cornelius, C. J. Smith, K. R. Leopold, “Multidimensional large amplitude dynamics in the pyridine–water complex”, *J. Phys. Chem. A* **2017**, *121*, 855–860.
- [109] D. G. Melnik, S. Gopalakrishnan, T. A. Miller, F. C. D. Lucia, “The absorption spectroscopy of the lowest pseudorotational states of tetrahydrofuran”, *J. Chem. Phys.* **2003**, *118*, 3589–3599.
- [110] P. K. Sahu, S.-L. Lee, “Hydrogen-bond interaction in 1:1 complexes of tetrahydrofuran with water, hydrogen fluoride, and ammonia: A theoretical study”, *J. Chem. Phys.* **2005**, *123*, 44308.

- [111] M. E. Sanz, J. C. López, J. L. Alonso, A. Maris, P. G. Favero, W. Caminati, “Conformation and stability of adducts of sulfurated cyclic compounds with water: Rotational spectrum of tetrahydrothiophene–water”, *J. Phys. Chem. A* **1999**, *103*, 5285–5290.
- [112] J. Lei, S. Alessandrini, J. Chen, Y. Zheng, L. Spada, Q. Gou, C. Puzzarini, V. Barone, “Rotational spectroscopy meets quantum chemistry for analyzing substituent effects on non-covalent interactions: The case of the trifluoroacetophenone–water complex”, *Molecules* **2020**, *25*, 4899.
- [113] M. Heger, T. Scharge, M. A. Suhm, “From hydrogen bond donor to acceptor: The effect of ethanol fluorination on the first solvating water molecule”, *Phys. Chem. Chem. Phys.* **2013**, *15*, 16065–16073.
- [114] B. Hartwig, M. A. Suhm, “Subtle hydrogen bonds: benchmarking with OH stretching fundamentals of vicinal diols in the gas phase”, *Phys. Chem. Chem. Phys.* **2021**, *23*, 21623–21640.
- [115] A. Sen, A. Bouchet, V. Lepère, K. L. Barbu-Debus, D. Scuderi, F. Piuzzi, A. Zehnacker-Rentien, “Conformational analysis of quinine and its pseudo enantiomer quinidine: A combined jet-cooled spectroscopy and vibrational circular dichroism study”, *J. Phys. Chem. A* **2012**, *116*, 8334–8344.
- [116] B. Nelander, “Infrared spectrum of the water formaldehyde complex in solid argon and solid nitrogen”, *J. Chem. Phys.* **1980**, *72*, 77–84.
- [117] T. K. Ha, J. Makarewicz, A. Bauder, “Ab initio study of the water-formaldehyde complex”, *The Journal of Physical Chemistry* **1993**, *97*, 11415–11419.
- [118] Y. Dimitrova, S. D. Peyerimhoff, “Theoretical study of hydrogen-bonded formaldehyde–water complexes”, *The Journal of Physical Chemistry* **1993**, *97*, 12731–12736.
- [119] T. A. Ramelot, C.-H. Hu, J. E. Fowler, B. J. DeLeeuw, H. F. Schaefer, “Theoretical study of hydrogen-bonded formaldehyde–water complexes”, *J. Chem. Phys.* **1994**, *100*, 4347–4354.
- [120] D. J. Millen, G. W. Mines, “Hydrogen bonding in the gas phase. Part 5.—Infrared spectroscopic investigation of O–HN complexes formed by water: Ammonia monohydrate and amine and pyridine monohydrates”, *Journal of the Chemical Society Faraday Transactions 2: Molecular and Chemical Physics* **1977**, *73*, 369–377.
- [121] M. Y. Choi, R. E. Miller, “Infrared laser spectroscopy of imidazole complexes in helium nanodroplets: Monomer, dimer, and binary water complexes”, *J. Phys. Chem. A* **2006**, *110*, 9344–9351.

-
- [122] A. Destexhe, J. Smets, L. Adamowicz, G. Maes, “Matrix isolation FT-IR studies and ab initio calculations of hydrogen-bonded complexes of molecules modeling cytosine or isocytosine tautomers. 1. Pyridine and pyrimidine complexes with water in argon matrixes”, *J. Phys. Chem.* **1994**, *98*, 1506–1514.
- [123] J.-Y. Feng, Y.-P. Lee, H. A. Witek, P.-J. Hsu, J.-L. Kuo, T. Ebata, “Structures of Pyridine-Water Clusters Studied with Infrared-Vacuum Ultraviolet Spectroscopy”, *J. Phys. Chem. A* **2021**, *125*, 7489–7501.
- [124] R. Meyer, J. C. López, J. L. Alonso, S. Melandri, P. G. Favero, W. Caminati, “Pseudorotation pathway and equilibrium structure from the rotational spectrum of jet-cooled tetrahydrofuran”, *J. Chem. Phys.* **1999**, *111*, 7871–7880.
- [125] N. Borho, M. A. Suhm, K. L. Barbu-Debus, A. Zehnacker, “Intra- vs. intermolecular hydrogen bonding: dimers of alpha-hydroxyesters with methanol”, *Phys. Chem. Chem. Phys.* **2006**, *8*, 4449–4460.
- [126] N. Borho, M. A. Suhm, “Self-organization of lactates in the gas phase”, *Organic & Biomolecular Chemistry* **2003**, *1*, 4351–4358.
- [127] P. Zielke, M. A. Suhm, “Concerted proton motion in hydrogen-bonded trimers: A spontaneous Raman scattering perspective”, *Phys. Chem. Chem. Phys.* **2006**, *8*, 2826–2830.
- [128] R. N. Pribble, T. S. Zwier, “Size-specific infrared spectra of benzene-(H₂O)_n clusters (n= 1 through 7): Evidence for noncyclic (H₂O)_n structures”, *Science* **1994**, *265*, 75–79.
- [129] S. Tanabe, T. Ebata, M. Fujii, N. Mikami, “OH stretching vibrations of phenol-(H₂O)_n (n= 1–3) complexes observed by IR-UV double-resonance spectroscopy”, *Chem. Phys. Lett.* **1993**, *215*, 347–352.
- [130] W. Li, C. Pérez, A. L. Steber, M. Schnell, D. Lv, G. Wang, X. Zeng, M. Zhou, “Evolution of Solute–Water Interactions in the Benzaldehyde-(H₂O)_{1–6} Clusters by Rotational Spectroscopy”, *J. Am. Chem. Soc.* **2023**, DOI <https://doi.org/10.1021/jacs.2c11732>.
- [131] T. L. Fischer, “Schwingungsspektroskopie von zwischenmolekularen Waagen”, Georg-August-Universität Göttingen, **2019**.
- [132] C. Zimmermann, “Investigation of Intermolecular Ketone-Alcohol Balances via FTIR Spectroscopy”, <https://ediss.uni-goettingen.de/handle/11858/14362>, Georg-August-Universität Göttingen, **2022**.

- [133] C. Zimmermann, H. C. Gottschalk, M. A. Suhm, “Three-dimensional docking of alcohols to ketones: an experimental benchmark based on acetophenone solvation energy balances”, *Phys. Chem. Chem. Phys.* **2020**, *22*, 2870–2877.
- [134] D. Bernhard, F. Dietrich, M. Fatima, C. Perez, A. Poblitzki, G. Jansen, M. A. Suhm, M. Schnell, M. Gerhards, “Multi-spectroscopic and theoretical analyses on the diphenyl ether–tert-butyl alcohol complex in the electronic ground and electronically excited state”, *Phys. Chem. Chem. Phys.* **2017**, *19*, 18076–18088.